

ASTARTE

Assessment, Strategy And Risk Reduction for Tsunamis in Europe

Grant Agreement no: 603839
 Organisation name of lead contractor: IPMA
 Coordinator: Maria Ana Baptista

DELIVERABLE D8.14

Methods to assess exposure and vulnerability to tsunamis: application in the NEAM region and in the ASTARTE test sites

Leading partner organisation name: NATIONAL OBSERVATORY OF ATHENS (NOA)

Leading partner number: 12

Lead scientist (PI): Dr. Gerassimos Papadopoulos

Creation date: 2015-02-20

Last change: 2015-06-25

Dissemination level: PU

Date of Delivery: Month 18

Actual Date of Delivery: June 2015

Contributors

Partner	Contributors
1 – IPMA	Maria Ana Baptista, Rachid Omira
2 – FFCUL	André Trindade, Cristina Catita
3 – METU	Ceren Cankaya, Betul Aytore, Nilay Dogulu, Ahmet Cevdet
7 – UNIBO	Gianluca Pagnoni, Stefano Tinti, Alberto Armigliato
10 – UB	Miquel Canals, Galdéric Lastras
12 – NOA	Gerassimos Papadopoulos, Tatyana Novikova, Anna Fokaefs
21 – SRB RAS	Andrey Zaytsev
22 – CNRST	Sabah Benchkroun, Azelarab El Mouraouah

Revision history

Revision	Date	Issued by	Description
0.1.0	2015-02-20	UNIBO – Alberto Armigliato	Created template
0.2.0	2015-06-10	NOA – Anna Fokaefs	Compiled partner's reports
0.2.1	2015-06-24	NOA – Gerassimos Papadopoulos	Reviewed the entire report
0.2.2	2015-06-25	NOA – Anna Fokaefs	Edited the entire report

Table of contents

1.	Introduction and glossary	9
1.1	References.....	11
2.	Review of the methods in place: qualitative and quantitative approaches for tsunami vulnerability Assessment	13
2.1	Early studies and the PTVA model.....	13
2.2	Post-2004 developments: new versions of the PTVA model and other approaches	14
2.3	Tsunami vulnerability assessment based on fragility functions and damage curves....	15
2.4	The role of environmental factors	18
2.5	Time-dependent vulnerability	19
2.6	Summary and evaluation	20
2.7	References.....	20
3.	Vulnerability Assessment for the ASTARTE Test Sites	24
3.1	Sines.....	24
3.1.1	Description of the site.....	24
3.1.2	SCHEMA	25
3.1.3	References	34
3.2	Tanger	35
3.2.1	Description of the site.....	35
3.2.2	SCHEMA	36
3.2.3	Comparison of the results.....	43
3.2.4	References	44
3.3	Colonia Sant Jordi	46
3.3.1	Description of the site.....	46
3.3.2	PTVA-3.....	51
3.3.3	SCHEMA	57
3.3.4	Comparison of the results.....	60
3.3.5	References	60
3.4	Siracusa-Augusta	62
3.4.1	Description of the site.....	62
3.4.2	PTVA-3.....	64
3.4.3	SCHEMA	71
3.4.4	Comparison of the results.....	77
3.4.5	References	81

3.5	Heraklion, Crete Island	83
3.5.1	Description of the site.....	83
3.5.2	PTVA-3.....	84
3.5.3	SCHEMA	85
3.5.4	Comparison of the results.....	93
3.5.5	References	94
3.6	Haydarpasa	97
3.6.1	Description of the site.....	97
3.6.2	References	99
4.	Guidelines for tsunami vulnerability assessment in the NEAM region	101
5.	Conclusions	102

List of figures

Figure 2.3.1. Example of fragility functions for damage states DS_i ($i=1, 2, 3, 4, 5$) (Leone et al. 2011)	15
Figure 2.3.2. Example of the damage curves published by Reese et al. (2007).	16
Figure 2.3.3. The mean damage curves developed by Valencia et al. (2011).	17
Figure 3.1.1. Sines test-site. (A) Regional overview; (B) Sines Test-site, (C) global image of the Sines harbour and coastal city (Adapted from: http://www.portodesines.pt/pls/portal/go).	25
Figure 3.1.2 . Tsunami fragility curves developed for masonry/brick buildings located within the inundation area at Sines test-site.	27
Figure 3.1.3. Main core of the tsunami vulnerability mapping.	28
Figure 3.1.4. Digram of the “Data Preparation” submodel.	28
Figure 3.1.5. Diagram for inundation value extraction	29
Figure 3.1.6. Diagram for Buildings Attributes Reclassification	29
Figure 3.1.7. Diagram of Damage Level Classification model.	30
Figure 3.1.8. Diagram for Brick Buildings Damage Level Classification.	30
Figure 3.1.9. Building tsunami vulnerability maps for Sines test-site with 20% probability of occurrence	31
Figure 3.1.10. 3D view of the vulnerability map	31
Figure 3.1.11. Building tsunami vulnerability maps for Sines test-site with 50% probability of occurrence	32
Figure 3.1.12. 3D view of the vulnerability map	32
Figure 3.1.13. Building tsunami vulnerability maps for Sines test-site with 80% probability of occurrence	33
Figure 3.1.14. 3D view of the vulnerability map	33
Figure 3.1.15. (A) zoom on the building tsunami vulnerability map of Sines, (B) Effect of considering the building number of floors on tsunami vulnerability	34
Figure 3.2.1. Geographical map and airphoto of the Tangier harbor	35
Figure 3.2.2. The Tangier harbor: Before / After	35
Figure 3.2.3. Damage functions for buildings classes A, B, C, D, and E1 as a function of water elevation in meters (After Gardi et al. 2009)	37
Figure 3.2.4. High-resolution DTM (Digital Terrain Model) of 10 m used in inundation modelling.	39
Figure 3.2.5. Inundation map considering the Cadiz Wedge scenario as the most credible earthquake tsunami source.	39
Figure 3.2.6. Examples of constructions indicating different building vulnerability classes at the city of Tangier.	41
Figure 3.2.7. Spatial distribution of buildings vulnerability at the coastal zone of Tangier	42
Figure 3.2.8. Number of buildings according to different classes of vulnerability.	42
Figure 3.2.9. Map displaying the level of damage to buildings caused by the most credible earthquake tsunami impact	43
Figure 3.3.1. Colònia Sant Jordi test site: Location in the northwestern Mediterranean and satellite view (Google Earth image) of the site and its two main populations (Colònia Sant Jordi and Cala Santanyí).	47
Figure 3.3.2. Topo-bathymetric map of Colònia Sant Jordi test site.	48
Figure 3.3.3. Location of urban areas, buildings and roads in Colònia Sant Jordi test site. Zooms to Colònia Sant Jordi and Cala Santanyí towns are provided, only indicating the location of buildings.	48

Figure 3.3.4. Storey height of each of the buildings within Colònia Sant Jordi test site.	49
Figure 3.3.5. Number of basement levels of the buildings within Colònia Sant Jordi test site. Buildings with no basement are not depicted.	49
Figure 3.3.6. Minimum distance to coastline of each plot of land within Colònia Sant Jordi test site.	50
Figure 3.3.7. Minimum topographic height of each plot of land within Colònia Sant Jordi test site. ...	50
Figure 3.3.8. Location of special buildings in Colònia Sant Jordi test site.	51
Figure 3.3.9. Scaled building vulnerability for Colònia Sant Jordi test site. Higher values indicate an increase of the average building vulnerability.....	53
Figure 3.3.10. Scaled protection level of each building within Colònia Sant Jordi test site. Higher values indicate a lesser level of protection.....	53
Figure 3.3.11. Scaled building exposure to a tsunami height of 4 m. Note that buildings above a topographic height of 4 m are not exposed.	54
Figure 3.3.12. Scaled building vulnerability to water intrusion taking into account a tsunami height of 4 m.	54
Figure 3.3.13. Scaled building vulnerability to water intrusion taking into account a tsunami height of 1m.	55
Figure 3.3.14. Scaled building vulnerability to water intrusion taking into account a tsunami height of 4m.	55
Figure 3.3.15. Scaled building vulnerability to water intrusion taking into account a tsunami height of 8m.	56
Figure 3.3.16. Scaled building vulnerability to water intrusion taking into account a tsunami height of 10m.	56
Figure 3.3.17. Building typology in a limited area within Colònia Sant Jordi test site.	57
Figure 3.3.18. Damage level calculated for a limited area within Colònia Sant Jordi test site and a tsunami height of 2 m.	58
Figure 3.3.19. Damage level calculated for a limited area within Colònia Sant Jordi test site and a tsunami height of 4 m.	59
Figure 3.3.20. Damage level calculated for a limited area within Colònia Sant Jordi test site and a tsunami height of 8 m.	59
Figure 3.3.21. Damage level calculated for a limited area within Colònia Sant Jordi test site and a tsunami height of 10 m.	60
Figure 3.4.1. Google Earth view of the Siracusa areas involved in the vulnerability assessment.	63
Figure 3.4.2. Google Earth view of the Augusta areas involved in the vulnerability assessment.	64
Figure 3.4.3. Results of vulnerability classification. The number of buildings and the percentage is specified for each class.	66
Figure 3.4.4. Map of building vulnerability (BV) calculated by means of the PTVA-3 model for Siracusa.	67
Figure 3.4.5. Damage level for Siracusa obtained through the PTVA-3 approach.	68
Figure 3.4.6. Geographical distribution of the damage level for Siracusa obtained through the PTVA-3 approach.	68
Figure 3.4.7. Results of vulnerability classification. The number of buildings and the percentage are specified for each class.	69
Figure 3.4.8. Map of building vulnerability (BV) provided by PTVA-3 model for Augusta.	70
Figure 3.4.9. Damage level for Augusta obtained through the PTVA-3 approach.	70

Figure 3.4.10. Geographical distribution of the damage level for Augusta obtained through the PTVA-3 approach.	71
Figure 3.4.11. SCHEMA vulnerability classes for Siracusa.	72
Figure 3.4.12. Geographical distribution of the SCHEMA vulnerability classes for Siracusa.	73
Figure 3.4.13. Damage level for Siracusa estimated through the SCHEMA approach.	73
Figure 3.4.14. Geographical distribution of the SCHEMA damage level for Siracusa.....	74
Figure 3.4.15. SCHEMA vulnerability classes for Augusta.....	75
Figure 3.4.16. Geographical distribution of the SCHEMA vulnerability classes for Augusta.	75
Figure 3.4.17. SCHEMA damage level for Augusta.	76
Figure 3.4.18 Geographical distribution of the SCHEMA damage level for Augusta.....	77
Figure 3.4.19. Histograms of the difference between damage levels, computed as SCHEMA - PTVA-3 for Siracusa.....	78
Figure 3.4.20. Geographical distribution of the difference between damage levels, computed as SCHEMA - PTVA-3.	79
Figure 3.4.21. Histograms of the difference between damage levels, computed as SCHEMA - PTVA-3 for Augusta.....	80
Figure 3.4.22. Geographical distribution of the difference between damage levels, computed as SCHEMA - PTVA-3 for Augusta.....	81
Figure 3.5.1. The coastal area of Gazion. Malevizion, Crete, marked by red rectangular.....	83
Figure 3.5.2. Airphoto of the Pancritio Stadium in Gazion, Crete.	83
Figure 3.5.3. Typical picture of Ammoudara during summer in Gazion, Crete.	84
Figure 3.5.4. Crete Inundation depth for the realistic scenario.....	89
Figure 3.5.5. Inundation depth for the worst scenario.....	90
Figure 3.5.6. Spatial distribution of building blocks vulnerability classes A and E at Gazion, Heraklion area.	91
Figure 3.5.7. Distribution of building blocks vulnerability classes.	91
Figure 3.5.8. Spacial distribution of buildings' blocks damage level at Gazion, Crete caused by the Minoan eruption.....	92
Figure 3.5.9. Spacial distribution of buildings' blocks damage level at Gazion, Crete caused by pyroclastic flow of the 17th century BC.....	93
Figure 3.5.10. Number of buildings' blocks according to different damage level for the pyroclastic flow of the 17th century BC.....	93
Figure 3.6.1. The study area: Yenikapı, Istanbul.	98
Figure 3.6.2. The tsunami source YAN (top) (Ayca, 2012)and the resulting inundation (flow depth) map (bottom) (Cankaya, 2015).	98
Figure 3.6.3. The final map of the locational vulnerability.....	99
Figure 3.6.4. The final map of the evacuation vulnerability.	99

List of tables

Table 3.1.1. Damage levels, their classification, description and corresponding observed tsunami effects on buildings after the Tohoku-oki 2011 tsunami (adapted from Supasri et al., 2013).....	26
Table 3.1.2. Summary of building field survey at Sines	27
Table 3.2.1. Standardized building typology based on structural characteristics of resistance of the constructions (SCHEMA project)	36
Table 3.2.2. Damage matrix adopted in SCHEMA project	37
Table 3.2.3. Fault parameters of the source tsunamigenic scenario. L: fault length in kilometers; W: fault width in kilometers; D: depth from the sea bottom to the top of the fault in kilometers and Mw: the moment magnitude	38
Table 3.3.1. Attributes influencing the structural vulnerability of a building (Bv).	52
Table 3.3.2. Attributes influencing the level of protection of a building (Prot).	52
Table 3.3.3. Damage matrix adapted for Colònia Sant Jordi test site. Values of the flow depth are given in meters.....	58
Table 3.4.1. Attributes influencing the structural vulnerability of a building “BV”. Positive values indicate an increase of the average building vulnerability given by the attribute	64
Table 3.4.2. Building classes depending on the resistance characteristics of the constructions.	71
Table 3.4.3. Damage matrix obtained by discretizing the damage functions. Yellow boxes indicate the modified level of the new damage matrix with respect to the damage matrix presented by Valencia et al. (2011).	71
Table 3.4.4. Buildings in Siracusa classified according to the vulnerability approaches of the PTVA-3 and SCHEMA methods	77
Table 3.4.5. Frequency distribution of damage levels of PTVA-3vs. SCHEMA for Siracusa. The color palette shows the differences calculated as SCHEMA-RVI (purple=+2, red=+1, yellow=0, green=-1, cyan=-2, blue=-3.....	78
Table 3.4.6. Buildings in Augusta classified according to the vulnerability approaches of the PTVA-3 and SCHEMA methods	80
Table 3.4.7. Frequency distribution of damage levels of PTVA-3vs. SCHEMA for Augusta. The color palette shows the differences calculated as SCHEMA-RVI (purple=+2, red=+1, yellow=0, green=-1, cyan=-2, blue=-3.....	80
Table 3.5.1. Parameters of pyroclastic flow	86
Table 3.5.2. Building Vulnerability classification (Leone et al 2010.)	90
Table 3.5.3. Expected Damage Level depending on Building Vulnerability Class and inundation depth (SCHEMA report D2.1)	91

1. Introduction and glossary

Coastal communities are exposed to hazards due to sea level changes while the associated risks increase as the communities become more and more developed. In the case of tsunamis, the hazard, vulnerability and risk modeling and assessments are essential to develop effective tsunami risk mitigation and management systems that may offer appropriate guidelines for emergency planners and decision makers.

In the European-Mediterranean region, sporadic tsunami studies and publications were undertaken since the 1950's. Coordinated tsunami research was put forward since 1992 with several projects funded by the European Commission. However, only after the big Indian Ocean tsunami of 26 December 2004 a systematic effort has been made to develop actions aiming to reduce tsunami risk. The main initiative is the North-East Atlantic and Mediterranean Tsunami Warning System (NEAMTWS) operating under the coordination of the country members affiliated with the IOC/UNESCO. Collateral actions include education and preparedness projects, some of them coordinated by the NEAMTIC, that is the Tsunami Information Center in the NEAM region, as well as by parallel national actions.

In this report we focus on the tsunami vulnerability issue, particularly as regards in the NEAM region. The aim of the report is to review the several methods and techniques that are in place for the tsunami vulnerability assessment and to suggest prospects for further progress particularly in the frame of the ongoing research project ASTARTE. In our review, however, the international experience obtained beyond NEAM is not ignored since it is quite useful for better understanding the current status in this field of research in the NEAM region.

It is noteworthy that a puzzling issue is the very different ways that terms such as hazard, exposure, vulnerability, risk, impact, damage, resilience and the similar are in use by different authors or listed in glossaries prepared by several organizations. Therefore, this review starts with a critical discussion of terminologies.

In the science of natural hazards a variety of terms are in use to express the level of exposure to this or that type of hazard as well as the level of impact that could be produced. Although there is a general consensus on the need to discriminate between hazard and risk, often confusion prevails for these terms as well as for other terms in use, such as exposure, vulnerability, resilience, damage and intensity. Therefore, it is useful to look after definitions suggested for such terms and indicate what are the most appropriate according to our judgments and experience.

A comprehensive report relevant to the issue of guidelines and definitions related to natural hazards and risks is the "Commission Staff Working Paper" produced by the EC (2010), hereafter called EC-Working Paper (2010) for reasons of brevity. For the purpose of these guidelines, international standards developed by the International Organization for Standardisation, in particular ISO 31000, ISO 31010, and the corresponding ISO guide 73 for terminology were used, in combination with the more targeted UNISDR terminology on disaster risk reduction.

According to the EC-Working Paper (2010) natural hazard is a natural process or phenomenon that may cause loss of life, injury, or other health impacts, property damage, loss of livelihoods and services, social and economic disruption, or environmental damage. The term is used to describe actual hazard events as well as the latent hazard conditions that may give rise to future events. Natural hazard events can be characterized by their magnitude or intensity, speed of onset, duration, and area of extent (UNISDR, 2009).

In the tsunami glossary coordinated and published by IOC (2013) tsunami hazard is the probability that a tsunami of a particular size will strike a particular section of coast, while the tsunami hazard assessment includes an identification of populations and assets at risk and definition of the level of that risk. However, since the hazard assessment regardless if it concerns tsunami, earthquakes or other natural phenomena, could be performed either on a qualitative way or quantitatively from probabilistic models or other approaches, e.g. deterministic ones, we feel that the definition of the term hazard should not rely on the possible method(s) in use (e.g. probabilistic) for the hazard

assessment but on the fact that hazard is an expression only of a phenomenon that potentially may have some impact.

On the basis of the previous analysis we do prefer to define tsunami hazard as a qualitative or quantitative expression of the possibility that potentially tsunami impact may take place in a particular coastal segment, area or region within a given time window. The assessment of the tsunami hazard level can be based either on descriptive, or probabilistic (stochastic) or deterministic approaches.

In relation to this considerations, and by taking into account definitions of terms proposed by UNISDR (2009) the term exposure to tsunami hazard may express people, property, systems or other elements present in tsunami hazard zones that are thereby subject to potential losses. As a consequence, the characteristics and circumstances of a community, system or asset that make it susceptible to the damaging effects of tsunami hazard is termed tsunami vulnerability. To make it fully understandable two examples are given in the next lines.

Vulnerability Example 1, Buildings: Suppose that two houses, one of reinforced concrete frame and another rural, are lying at exactly the same point of a coastal zone and are attacked by a powerful tsunami. In this case all natural conditions are the same for both houses but their physical features, that is their characteristics. It becomes obvious that the houses are not characterized by the same degree of vulnerability, the one of reinforced concrete frame being more tsunami resistant than the rural one. As an alternative, let us assume that the second house is lying significantly further inland with respect to the first one. The characteristics of both buildings remain unchanged. What changes is the degree of exposure which is much higher at distance of only 5 m from a fixed point of the seashore and much less at distance of 1000 m inland from the same seashore point. In other words, the circumstances under which the two buildings are exposed are quite different and increase the relative vulnerability of the first building with respect to that of the second.

Vulnerability Example 2, Humans: Suppose that a father and his daughter are standing in a particular point of a coastal segment at the time that a powerful tsunami attacks the coast. As soon as they realize the tsunami threat they need to counteract. A realistic option is to run in higher ground. In this realization the daughter becomes more vulnerable compared to her father. In fact, because of her natural features she is not able to understand immediately the danger, as his father does, and she is unable to run as quickly as her father. However, one may argue that the father is more vulnerable by considering that his daughter got school lessons about the correct personal behavior against tsunamis but his father didn't. From this point of view education plays important role. The father's physical vulnerability is still less than that of her daughter but he is more exposed to the tsunami hazard due to that he is uneducated.

The consequence of the above definition of the term vulnerability is that keeping exactly the same features for the potentially destructive natural phenomenon, here tsunami is meant, two or more assets of the same type (human beings, houses or other engineered structures, vessels etc.) have different overall vulnerability, not only because of their different physical features but also due to the different degree of exposure which is controlled by a variety of factors.

In the present discussion, according to the EC-Working Paper (2010) human impacts due to natural hazards are defined as the quantitative measurement of the number of deaths, severely injured or ill people and permanently displaced people. On the other hand, economic impacts can be quantified in terms of immediate or long-term sum of costs, while political, social and environmental impacts usually are difficult to quantify and, therefore, they are expressed qualitatively or semi-quantitatively.

A relevant term is the one of tsunami damage which is the loss or harm caused by a destructive tsunami (IOC, 2013), while tsunami intensity is the degree of tsunami impact on the anthropogenic and the natural environment estimated in a certain scale (see review and introduction of a new 12-point intensity scale in Papadopoulos and Imamura, 2001). A more general definition of tsunami intensity considers it as a measure of strength, force or energy (IOC, 2013) but such terms are respective rather to physical hydrodynamic tsunami features than to the impact itself.

Another important concept is that of resilience, which according to the IPCC (Intergovernmental Panel on Climate Change), is the capacity of social, economic, and environmental systems to cope with a hazardous event or trend or disturbance, responding or reorganizing in ways that maintain their

essential function, identity, and structure, while also maintaining the capacity for adaptation, learning, and transformation. The term resilience was seen from a similar point of view by the UNISDR (2009) and adopted by the EC-Working Paper (2010): resilience is the ability of a system, community or society exposed to hazards to resist, absorb, accommodate to and recover from the effects of a hazard in a timely and efficient manner, including through the preservation and restoration of its essential basic structures and functions.

A remarkable approach was presented by Flood and Schechtman (2014) who examined the value of resilience as a concept in planning and policy in the USA and Ireland associated with climate change. Three alternative approaches were put forward: engineering, ecological and psychological resilience, while the resilience of each of these systems is sometimes at odds with each other. In that study the authors argue that “becoming more resilient” requires strengthening all three systems in a reinforcing manner rather than championing one to the detriment of the others.

As regards tsunamis, a more compact definition could be read as: tsunami resilience is the ability to withstand to, and recover from, the impact caused by tsunami action.

To discriminate between hazard and risk, the EC-Working Paper (2010) adopted that according to ISO 31010 risk is a combination of the consequences of an event (hazard) and the associated likelihood/probability of its occurrence. Mathematically this may be expressed as a convolution of two terms:

$$\text{risk} = \text{hazard impact} * \text{probability of occurrence} \quad (1)$$

Such a perception of risk is not new. For example, a similar expression was introduced by Smith (1992). However, with the aim to get quantitative results reflecting a wide range of the potential impact, we may consider that risk could be expressed as the convolution of three main factors, thus taking the form

$$\text{risk} = \text{hazard} * \text{vulnerability} * \text{value} \quad (2)$$

In this sense, we see that vulnerability is a critical quantifiable factor in the overall risk assessment. Then, risk is expressed in a descriptive, qualitative or quantitative way depending on how the three factors composing it are expressed. If the term hazard incorporates the percentage probability and at the same time vulnerability and value are quantified, then we may define tsunami risk as a quantitative description of the expected impact of tsunami action in a particular coastal segment, area or region within a given time window. One may realize that in this sense risk is dependent on the level of the physical process or phenomenon, that is on tsunami hazard, on the vulnerability of the several elements or assets exposed to the tsunami action, as well as on the economic (or other) value(s) exposed to hazard.

From the previous analysis it comes out that the increase of resilience results to the decrease of risk and vice versa. Then, for reasons of simplicity we may mathematically express it as

$$\text{resilience} = 1/\text{risk} \quad (3)$$

Combining (2) and (3) we see that keeping constant the level of hazard, then both risk and resilience are directly dependent on vulnerability and value, that is practically speaking on a variety of social, economic and environmental parameters.

1.1 References

Flood S. and Schechtman J. 2014, The rise of resilience: Evolution of a new concept in coastal planning in Ireland and the US, *Ocean & Coastal Management*, 102, 19-31.

IOC (Intergovernmental Oceanographic Commission), 2013. Tsunami Glossary, Technical Series 85, UNESCO, 1-42.

Papadopoulos G. A., Imamura F.: A proposal for a new tsunami intensity scale, in: Proceedings International Tsunami Symposium 2001, Seattle, Session 5(5–1), 569–577, 2001.

Smith K. 1992. Environmental Hazards- Assessing Risk and Reducing Disaster, Routledge, (1st ed.), pp 324.

UNISDR (International Strategy for Disaster Reduction) 2009. Terminology on Disaster, Risk Reduction, 35pp.

2. Review of the methods in place: qualitative and quantitative approaches for tsunami vulnerability Assessment

Post-event collections of tsunami impact data are of critical importance for the development and validation of vulnerability and risk assessment methodologies. However, earlier methodologies initially focused mainly on damage assessment, the concept of vulnerability being rather neglected, while vulnerability was approached in more recent studies which included the physical and socio-economic dimensions of tsunami impacts. In particular, after mainly the Indian Ocean tsunami on 26 December 2004 and the 11 March 2011 Tohoku-oki tsunami in Japan several studies focusing particularly on the vulnerability of buildings to tsunamis were published.

There are two chief classes of vulnerability analysis currently applied to tsunamis and other geo-hazards that can be grossly denoted as qualitative and quantitative approaches. Typically a qualitative method characterizes the exposed elements by means of attributes, uses territorial element inventories, assigns scores to each element according to some subjective criteria, and combines scores (usually through a weighted average) to determine the vulnerability class of each element. On the other hand, a quantitative method defines damage through fragility curves (for buildings/structures) and defines losses through mortality curves (for persons), that link damage and losses to values of tsunami parameters, uses territorial inventories and determines vulnerability classes.

In the next sections we summarize the available methods for tsunami vulnerability assessment.

2.1 *Early studies and the PTVA model*

One of the earliest studies was that of Reese et al. (1968) who presented the results of the damage survey performed after the 1960 tsunami at Hilo, Hawaii. They included observations on the height of wave, the structural damage caused and the pressures acted on structures from the hydrodynamic force of the wave. The effect of floated and washed away timbers as well as oil spread due to tsunamis was investigated by Goto (1990) who developed and applied numerical models for the Miyako Bay in Japan. The maximum impulsive force on structures was examined by Matsutomi (1991). For that purpose, variations of the apparent inertia coefficient and the impact duration time of timbers due to the opening ratio and the size of timbers were examined experimentally. The study concluded that the impulsive force of timbers is not negligible compared with that of bores themselves.

Shuto (1991) provided a summary of some old approaches for tsunami vulnerability assessment pointing out the strong connection of structural effects on the resistance against tsunamis. Namely, the author examined the relation between losses of lives and residences based on observations of big past tsunami events in Japan and the damage percentage of houses over tsunami height and the drag force, and the damage percentage of fishing boats over tsunami height.

In his study for Grays Harbor, Washington, and Lima, Peru, Preuss (1991) defined vulnerability by considering tsunami as a system rather than a single physical process. In that study the author introduced the assumption that the physical threat, including inundation, strong currents and the potential for ground subsidence, should be correlated with land use characteristics. The methodology used consisted by four components: 1. Define characteristics and dimensions of direct tsunami threat (direction of energy, wave height run-up and arrival time), 2. Define vulnerability patterns, i.e. land use and population distribution patterns) 3. Identify secondary hazards, i.e. subsidence/ground failure, battering, fire, potential toxic release, 4. Determine microzonation of risk reduction, which includes land use zonation and preparedness and evacuation district.

In the European-Mediterranean region, one of the first relevant studies performed within the frame of the GITEC-TWO EC Tsunami Project (1996-1998), considered tsunami risk as expressed in formula (2), where vulnerability is one of the main three parameters involved (Papadopoulos and Dermentzopoulos, 1998). With an application in a 6-km-long coastal segment of the test-site of Heraklion, the capital city of Crete Isl., Greece, vulnerability was considered and mapped in a series of thematic maps in a semi-quantitative way for a variety of assets, such as soil foundation conditions, land use/land cover types, road network, functions and lifelines, socioeconomic and population parameters. The worse case scenario, based on past tsunami history, predicted a 6-m-high tsunami

attacking the coastal zone of Heraklion. The approach developed by those authors included also assessments of tsunami impact and recommendations for reducing tsunami vulnerability and finally risk.

Looking back from a considerable time distance, the study of Papadopoulos and Dermentzopoulos (1998) was a premature realization of the vulnerability analysis recommended later by the EC-Working Paper (2010) which includes: identification of elements and people potentially at risk (exposure), identification of vulnerability factors/impacts (physical, economic, environmental, social/political), assessment of likely impacts, analysis of self-protection capabilities reducing exposure or vulnerability).

Some years later after the Heraklion pilot study by Papadopoulos and Dermentzopoulos, (1998), the approach was further developed as described in the publications of Papathoma and Dominey-Howes (2003) and Papathoma et al. (2003) based on the PhD Thesis of Papathoma (2003). The main developments included the introduction of the concepts of (a) the Relative Vulnerability Index (BVI), based on several structural criteria for buildings, and (2) the Human Vulnerability (HV) expressed as

$$HV = BV \times P \text{ (BV is Building Vulnerability and P is Population)} \quad (4)$$

The application of the so-called PTVA-1 model (Papathoma Tsunami Vulnerability Assessment, version #1) was performed in Heraklion, Crete, as well as in a part of western Corinth Gulf, Central Greece, with the inundation zone being considered between the coastline and the certain contour based on probability studies of historical tsunamis. For example, the contour of 5 m was selected for the Heraklion test-site. Thematic maps of BV and HV were displayed in a GIS form.

2.2 Post-2004 developments: new versions of the PTVA model and other approaches

The big tsunami of 26 December 2004, that affected directly 16 nations around the Indian Ocean and indirectly the entire globe, influenced drastically the development of tsunami science and engineering. This is also the case of tsunami vulnerability assessment thanks to the post-tsunami damage data that are increasingly available after 2004. Abundant data became available after other recent, destructive tsunamis, such as the ones of July 2006 Java and of February 2010 Chile tsunamis, but mainly after the devastating Tohoku-oki, Japan, tsunami on 11 March 2011. As a consequence, over the past decade, work has increasingly focused on the development of tsunami-building vulnerability assessment models (Tarbotton et al., 2015). It has been realized that the capacity of a building to withstand the forces imposed by a tsunami depends on a variety of attributes, including its structural design, construction material, foundation type and ground floor characteristics (UNESCO-IOC, 2011). For this reason, most recent approaches are based on empirical functions due to the complex nature of buildings. However, the further development of the PTVA-1 model was not neglected.

In fact, a first line of development was the revision and validation of the PTVA-1 model. Douglas (2007) showed how the lack of post-event observations affected the early models. According to Dall'Osso et al. (2009) the PTVA-1 model was developed before 2004 in the absence of robust, well-constructed and validated building fragility models for assessing the vulnerability of buildings to tsunami. In view of this reality, Dominey-Howes and Papathoma (2007) upgraded the model to version #2 (PTVA-2) and validated using data collected from field surveys at the Maldives affected by the 2004 big Indian Ocean tsunami.

The PTVA-2 model was also tested by Dominey-Howes et al. (2010) in the Cascadia subduction zone (Seaside, Oregon, USA) in relation to the large tsunami of AD 1700. In that study the PTVA-2 model was coupled with a probabilistic tsunami hazard assessment and Probable Maximum Losses were calculated for a 1:500 year tsunami inundation.

Dall'Osso et al. (2009) presented an enhanced version (PTVA-3) of the model that took account of a new understanding of the factors that influence BV and significantly, introduced the use of the Analytic Hierarchy Process (AHP) for weighting the various attributes in order to limit concerns about subjective ranking of attributes in the original model. The application was made for Maroubra, Sydney,

Australia. In the frame of the EC-FP6 TRANSFER Tsunami Research Project, the same model (PTVA-3) was applied and validated for the assessment of the vulnerability of buildings to tsunamis in the volcanic archipelago of the Aeolian Islands, Italy, and specifically for the islands of Stromboli and Panarea affected by the 30 December 2002 local but powerful tsunami wave (Dall' Osso et al., 2010). The advantage of the initial PTVA model and its later versions is that it provides estimations of the vulnerability levels for coastal zones in the lack of building damage data from real tsunami attacks. However, the inundation area is only roughly considered from historical data, while tsunami hydrodynamic parameters, such as flow depth or current velocity, are not taken into account.

These problems can be solved with the performance of inundation numerical modeling for tsunami scenarios (Tinti and Armigliato, 2003). This approach was implemented in the tsunami vulnerability study performed by Omira et al. (2010) for the Casablanca harbor and surrounding area in the frame of the EC-FP6 NEAREST Tsunami Research Project. Those authors used a combination of field survey data, GIS and tsunami inundation numerical modeling, thus linking tsunami hazard, expressed by wave flow depths, with tsunami vulnerability. In this case, the large Lisbon tsunami of 1 November 1755 was modeled as the worst case tsunami scenario. In addition, this study deviated from PTVA model in that it distinguished between the “main criteria” and the “intrinsic attributes” that influence the building vulnerability to tsunamis. A similar approach was followed for the tsunami impact and vulnerability assessment in the harbor area of Tangier, Morocco (Bencheikroun et al., 2013).

Other numerical approaches were also tested to investigate the resistance to tsunami attacks of buildings or critical facilities. For example, Koutitas and Karambas (2005) presented a computational model consisting of the nonlinear shallow water equations in the 2DH space, in the presence of an embedded typical building. The normalized integral of the hydrodynamic loads distributed on the building surface in the direction of the wave propagation is plotted against the normalized length of the structure for various building walls configurations. The importance of the building orientation with respect to the wave propagation and the importance of the openings in the walls were revealed by means of a number of numerical experiments. Cruz et al. (2011), employed the JRC tsunami propagation and inundation code HyFlux2 to describe the potential consequences of two historical tsunami scenarios and their impacts on an oil refinery in Sicily.

2.3 Tsunami vulnerability assessment based on fragility functions and damage curves

The utilization of post-tsunami damage data being available over the past decade have contributed greatly to the development of empirical vulnerability functions. In published studies there are two main types of vulnerability functions: the fragility functions and the damage curves. A fragility function, also known as a fragility curve, is a probabilistic vulnerability model that describes the conditional probability (P) that a damage state will be reached or exceeded for a given hazard level (Singhal and Kiremidjian, 1996; Choi et al., 2004, Peiris and Pomonis, 2006) (Fig.2.3.1).

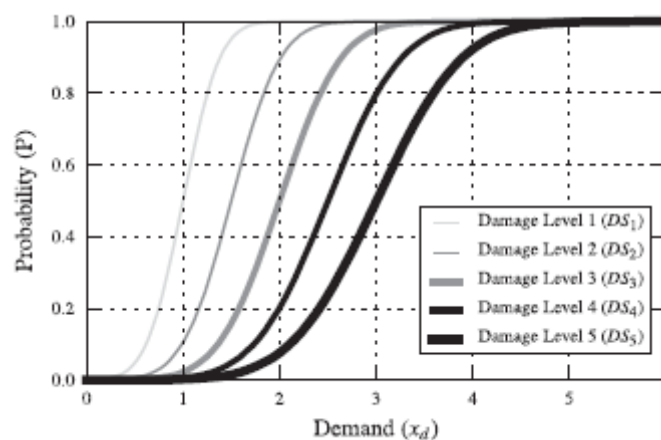


Figure 2.3.1. Example of fragility functions for damage states DS_i ($i=1, 2, 3, 4, 5$) (Leone et al. 2011)

Damage curves typically represent a structure's damage response as an index or a percentage, referring to the overall level of damage that the building would incur (e.g. 80% damaged) (Fig. 2.3.2).

Unlike damage curves, which typically describe the mean/average damage response of a building, fragility functions describe a range of possible damage outcomes and their associated probability of occurrence. This provides the means of describing the damage response of complex structures for which there are large uncertainties in the vulnerability of the components and/or in the loads that are imposed on them (see review in Tarbotton et al., 2015). Reese et al. (2007), Dias et al. (2009), Koshimura et al. (2009a) and Leone et al. (2011) applied such approaches collecting data during post-tsunami field surveys and established the link between observed damage level and tsunami flow depth.

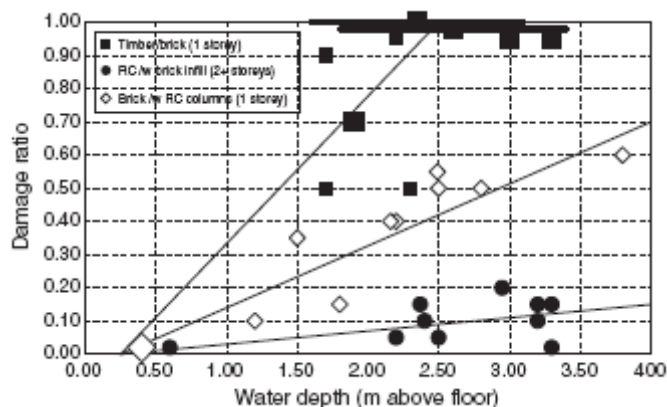


Figure 2.3.2. Example of the damage curves published by Reese et al. (2007).

In the aftermath of the 11 March 2011 Great East Japan tsunami, Suppasri et al. (2013) constructed fragility functions using least-squares regressions derived with the use of data for more than 250,000 structures damaged or destroyed. Extended details upon damage level, structural material, number of stories per building and locations were utilized. They also calculated the cumulative probability of damage occurrence using the statistical method described in Koshimura et al. (2009b). Suppasri et al. (2013) showed probability damage results for different buildings classified by their construction materials and number of stores as a function of the flow depth. The results demonstrated very clearly the effect that the mentioned factors have on building damage level.

In the frame of the EC-FP6 SCHEMA Tsunami Research Project, the DamASCHE GIS tool was developed (Valencia et al., 2011) and applied in several test-sites of the European-Mediterranean coastal zones. The DamASCHE GIS tool was initially based on data from Banda Aceh (Indonesia) after the 2004 Indian Ocean tsunami. The tool overlays damage curves onto an inundation map to estimate the damage level. A combined field-remote survey methodology was used, which was capable of classifying building typology and damage state into multiple categories both on-the-ground (e.g. field surveys) and by inspecting satellite imagery (remote surveys). Building damage was classified into six discrete states ranging from D0 to D5, while building typology was classified into four categories (A, B, C and D). The tsunami demand parameter was determined by fitting a representative flood depth surface onto available field data using 2D interpolation techniques. Damage curves (Fig. 2.3.3) were developed for the four building typologies by aggregating the TIB data into flood depth bins and considering the mean damage response within each bin interval. The damage curves were taken to be the “enveloping curve” that represented the upper confidence range of the mean damage values calculated at each bin.

The same methodology was applied in several test-sites of the SCHEMA Project in Balchik, Bulgarian Black Sea, in the Rabat-Salé, Morocco, as well as in Mandelieu, French Riviera in western Mediterranean Sea, in Setúbal, Portugal and in Catania, Italy (Deliverables 4.1-4.5 in <http://www.schema.project.org/>). Omira et al. (2013) investigated the effectiveness of sea-defense structures in preventing/reducing the tsunami overtopping as well as evaluating the resulting tsunami impact at El Jadida, Morocco.

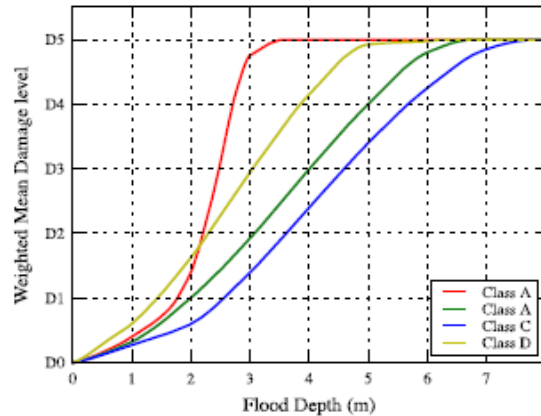


Figure 2.3.3. The mean damage curves developed by Valencia et al. (2011).

For Padang, Indonesia case study, Taubenböck et al. (2008), used high resolution satellite data to assess tsunami vulnerability in urban areas based on building sizes, built-up density, number of buildings and their location and population. It was proven that remote sensing data and methods in combination with GIS enable a highly detailed classification of vulnerability patterns and their quantification.

The potential and limitations of remote sensing techniques (geo-data) in vulnerability assessment were investigated by Römer et al. (2012). Their research showed that remote sensing can be used to spatially extrapolate field data on socio-economic or ecological vulnerability collected in the field, to regionalize exposure elements and assets and to predict vulnerable areas. A similar approach was presented by Mas et al. (2012) for the 2012 Chilean tsunami. In their study, Mas et al. (2012) introduced a practical method suitable when there are limitations on available data for numerical simulation or damage evaluation from surveys: they classified the damage to houses using surveyed data of inundation depth and visual inspection of satellite images of Dichato, Chile and developed tsunami fragility curves.

Gokon et al. (2014), focusing to the areas affected by the 2009 Samoa earthquake and tsunami reproduced the tsunami inundation by numerical modeling and validated the results with field surveys and waveforms from DART gauges. They compared satellite images in order to investigate building damages. Finally they integrated the tsunami features and building damage using GIS and developed fragility functions on statistical analysis as a tool to evaluate structural vulnerability. Those authors pointed out the need to improve their method in terms of taking into consideration floating debris and scourings, building types, as well as age of buildings or floors.

Approaches based on fragility curves and damage curves appear promising for the realistic tsunami vulnerability assessment. However, there are still several problems that make difficult the generalized application of such approaches. One issue is that in most cases such curves are based on empirical data from one location and one event. Also, the structures examined are typically dissimilar to those found in other places. In addition, undamaged structures are often not included which biases the data to damaged structures, which results in overestimating losses.

Such critical problems were considered by Dale and Flay (2006) who described an interesting approach directed at assessing the risk posed by tsunami hazard to Australian communities. They proposed to replace curves based on observed damage from a number of past tsunami events by future curves based on an engineering approach. This requires a generalized hazard definition, an engineering model of the structure of interest, and a costing module to convert damage scenarios to restoration costs. According to Dale and Flay (2006), the generalized hazard definition is a way of generalizing the complex behavior of fluid flow around (and through) a structure and defining the resultant loads on the structure.

Although some design guides exist that contain methods for designing for wave forces, including tsunamis (e.g. the FEMA 55 guide, see FEMA, 2000; the USACE Technical Note III-29, see USACE, 1990), there are a number of reasons it may be problematic to use these guidelines to estimate tsunami wave loads on a structure (Dale and Flay, 2006). Therefore, hazard transfer parameters should be chosen to link between hazard modelling and vulnerability. Water depth and water velocity may be used to describe the hazard at a particular location as an output of the inundation model. Once loads on the structure have been defined an engineering model of a structure can be used to assess damage outcomes. Finally, an automated costing will take the damage outcomes from the engineering model of the structure and cost the repair.

It is of interest that the usefulness of the methodology proposed by Dale and Flay (2006) could be seen from the point of view of the findings reached by Gardi et al. (2011) who examined the uncertainties associated with the process of tsunami damage assessment on buildings. This examination, which was performed within the frame of the EC-FP6 SCHEMA Tsunami Project, concluded that a variety of sources of errors/uncertainties can be introduced at several steps of the damage assessment process. Errors can be introduced when collecting post-disaster observations owing to different types of instruments/methods, water marks considered, tide correction etc. Much uncertainty comes from difficulties in identifying and characterizing the potential tsunami sources as well as from the numerical modelling and Digital Terrain Models employed and the cartographic processes. Another source of uncertainty is that usually damage functions link the mean damage level on buildings with the maximum water elevation measured in the field without considering other tsunami parameters such as flow velocity.

A comparative review and summary of best practice regarding the use of empirical vulnerability functions for buildings against tsunami impact can be found in the recent paper by Tarbotton et al. (2015). It was found that at present, these functions are highly varied with respect to the building typologies and damage states that they represent, making it difficult to apply them effectively in tsunami vulnerability and loss assessments. Categorization and direct comparisons of existing functions showed that the variation in previous work is due to significant differences in the accuracy of the hazard assessment techniques that are used, inconsistent and poorly defined damage state and building typology classification systems, the use of error-prone and incorrectly applied statistical methods and the use of post-event data that is not representative of the building damage occurring in study area. The recommendations of Tarbotton et al. (2015) are discussed in the subsection “Summary and Evaluation”.

2.4 The role of environmental factors

The examination of environmental factors, such as coastal vegetation and topography, has shown the important role that such factors play in assessing tsunami vulnerability. For example, coastal forest may decrease or increase tsunami damage. Shuto (1987) pointed out that coastal forest may increase tsunami damage since when huge tsunamis attack the forest, the trees would be destroyed and washed away. Then, a serious secondary damage effect to buildings could be produced by the floating trees. Harada and Imamura (2005) examined the hydrodynamic effect of coastal forest on tsunami hazard mitigation. From numerical simulations it was found that an increase of forest width can reduce not only inundation depth but also current and hydraulic force behind the coastal forest. On the other hand, Imai and Matsutomi (2005) examined the 1998 Papua New Guinea tsunami and evaluated the reducing efficiency of tsunami energy caused by the coastal vegetation. They showed that the inertia force reaches 50% of the maximum drag force FD at the early stage of inundation flow and that FD , as well as the linear wave making resistance force are dominant at the quasi-steady state after the early stage. Also, it was found that both the drag coefficient and the mass coefficient decrease as vegetation density increases.

The effects of complex topography on tsunami run-up and inundation distance was examined by Sim et al. (2013). They showed that increasing dunes spacing could not significantly affect inundation

distance. However, if the height of sand dunes is of the same order of magnitude as the incoming tsunami wave and the gaps between the dunes are large enough, successful tsunami mitigation could also be possible.

Wong (2009) in his study discussed the implications to the Integrated Coastal Management of issues like the loss of land, the safety zone in conflict with the buffer zone, the need for better integration of livelihoods restoration with the rehabilitation of coastal ecosystems and the inclusion of tsunami mitigation in the larger framework of climate change mitigation.

2.5 Time-dependent vulnerability

From the review presented in the previous lines it comes out that several types of tsunami vulnerability could be considered, depending on the elements exposed to the tsunami hazard. The list is long and among others may include

- Vulnerability of communities (villages, towns, cities) in general.
- Structural and other vulnerabilities of buildings, infrastructures, critical facilities.
- Vulnerability of population/target groups/individuals.
- Indoor/outdoor vulnerability of people and property.
- Vulnerability of vessels of variable size as well as of coastal and offshore facilities (e.g. fisheries etc.)

However, the characteristics of the several elements exposed to tsunamis change with time and, therefore, vulnerability changes too. In a short-term sense, vulnerability varies, for example in a 24-hour mode, due to the social and economic cycle of daily life. On a weekly scale the differences in everyday life between work-days and week-ends are also well known. On a seasonal scale, strong changes in vulnerability are expected, for example due to seasonal variation of tourism. Such time-dependent components of the tsunami vulnerability have been mentioned (e.g. Papathoma et al., 2003) but were not considered in the several models proposed for the tsunami vulnerability assessment. As a consequence, practically speaking vulnerability is not a static, time-independent variable but a dynamic, time-dependent one.

Further, in the long-term sense, the characteristics of the several elements exposed to the tsunami hazard do not remain unchanged. On the contrary, all factors that control the tsunami vulnerability change, e.g. built environment, population, land use/land cover and other environmental factors and so on. For example, as regards the built environment, in earthquake-prone regions, the characteristics of the reinforced concrete buildings change in time with the revision of the antiseismic building codes. This has been taken into account in the seismic vulnerability assessment of building under the assumption that reinforced concrete buildings constructed by following recent versions of the codes are more earthquake resistant as compared to the ones constructed by following earlier versions of the codes. For example, in Greece the earlier version of the national building code was put forward in 1959, while the last one was established in 2000. A similar situation is realized in Italy and elsewhere.

In tsunami vulnerability assessment, reinforced concrete buildings are generally considered as being of low vulnerability as compared to unreinforced buildings (e.g. Papathoma et al., 2003 and later versions of the PTVA model). Although this practice is correct, is still far behind of the practices applied in earthquake engineering mainly due to the fact that so far no building codes against tsunami loads were developed.

The concluding remark here is that the models developed so far for the tsunami vulnerability assessment are time-independent or static models. A challenging prospect is to go ahead with time-dependent or dynamic models that would incorporate factors that make vulnerability to change on a daily, weekly, seasonal or even longer scale of time. Then, respective time-dependent models for tsunami risk assessment will emerge.

2.6 Summary and evaluation

Reviewing in this section the several approaches used to assess tsunami vulnerability we concluded in a number of critical points that should be taken into account as regards applications not only in the ASTARTE test-sites but also in future studies. First is the issue of terminology, and therefore a critical review was presented. It is beyond doubt that as regards the definition of terms such as hazard, vulnerability, risk and the similar there is need to reach at a consensus with the aim to avoid misunderstandings and for reasons of standardization.

A crucial finding is that at present the main effort regards the tsunami vulnerability of buildings. Very little has been done for other types of vulnerabilities, such as the vulnerability of communities in general, the vulnerability of humans, the vulnerability of properties indoor and outdoor and so on. However, some efforts have been made to assess the role that environmental factors play in the tsunami vulnerability. Such factors include coastal forests and other vegetation and coastal topography. From another point of view, the concept of time-dependent tsunami vulnerability practically has been neglected from the studies so far.

As regards the tsunami vulnerability of buildings, the development of computational methods has been rather neglected and only empirical methods, either qualitative or quantitative, were developed. The list of methods include mainly the PTVA model and its revised versions as well as the tsunami vulnerability assessment based on fragility functions (curves) and damage curves.

The advantage of the initial PTVA model (Papathoma et al., 2003) and its later versions is that it provides estimations of the vulnerability levels for coastal zones in the lack of building damage data from real tsunami attacks. However, the inundation area is only roughly considered from historical data, while tsunami hydrodynamic parameters, such as flow depth or current velocity, are not taken into account. The introduction of fragility curves and damage curves, which are based on observational data collected after real tsunami events, improved the characterization of the expected damage level. Relevant tools were developed, such as the DamASCHE GIS tool (SCHEMA approach), to estimate the building damage level from an overlay of damage curves onto an inundation map.

After the experience accumulated in the last 15 years or so but mainly in the post-2004 period, it was realized that the empirical methods in use for the assessment of the building vulnerability to tsunamis suffer from a variety of errors and uncertainties and, therefore, there is need for drastic improvement. In relevance to this realization, Tarbotton et al. (2015) suggested several recommendations for future work.

2.7 References

Benchekrone S., Omira R., Baptista M. A., El Mouraouah A., Iben Brahim A., Toto E. A., 2013. Tsunami impact and vulnerability in the harbor area of Tangier, Morocco, *Geomatics, Natural Hazards and Risk*, DOI: 10.1080/19475705.2013.858373.

Choi E., DesRoches R., Nielson B., 2004. Seismic fragility of typical bridges in moderate seismic zones, *Eng. Struct.*, 26, 187–199

Cruz AM, Krausmann E., Franchello G., 2011. Analysis of tsunami impact scenarios at an oil refinery, *Natural Hazards*, 58, 141-162.

Dale K., Flay S., 2006. Structural vulnerability estimation for tsunami loads, *Earthquake Engineering in Australia*, Canberra 24-26 November 2006, 179-183.

- Dall'Osso F., Gonella M, Gabbianelli G., Withycombe G. and Dominey-Howes D., 2009. A revised (PTVA) model for assessing the vulnerability of buildings to tsunami damage, *Nat. Hazards Earth Syst. Sci.*, 9, 1557-1565.
- Dall'Osso F., Maramai A., Graziani L., Brizuela B., Cavalletti A., Gonella M. and Tinti S., 2010. Applying and validating the PTVA-3 Model at the Aeolian Islands, Italy: assessment of the vulnerability of buildings to tsunamis, *Nat. Hazards Earth Syst. Sci.*, 10, 1547-1562.
- Dias W. P. S., Yapa, H. D., Peiris, L. M. N., 2009. Tsunami vulnerability functions from field surveys and Monte Carlo simulation, *Civ. Eng. Environ. Syst.*, 26,181–194.
- Dominey-Howes D., Papathoma M., 2007. Validating a Tsunami Vulnerability Assessment Model (the PTVA Model) Using Field Data from the 2004 Indian Ocean Tsunami, *Nat. Hazards*, 40(1), 113-136.
- Dominey-Howes D., Dunbar P., Varner J., Papathoma-Kohle M., 2010. Estimating a probable maximum loss from a Cascadia tsunami, *Nat. Hazards*, 53(1), 43-61.
- Douglas, J., 2007. Physical vulnerability modelling in natural hazard risk assessment. *Nat. Hazards Earth Syst. Sci.* 7, 283–288.
- Gardi A., Valencia N., Guillande R. and André C., 2011. Inventory of uncertainties associated with the process of tsunami damage assessment on buildings (SCHEMA FP6 EC co-funded project), *Nat. Hazards Earth Syst. Sci.*, 11, 883-893.
- Gokon H. Koshimura S., Imai K., Matsuoka M., Nameyaga Y. and Nishimura Y., 2014. Developing fragility functions for the areas affected by the 2009 Samoa earthquake and tsunami, *Nat. Hazards Earth Syst. Sci.*, 14, 3231-3241.
- Goto C., 1990. Simulation models of timber and oil spread due to tsunamis, 2nd UJNR Tsunami Workshop, 5-6 November 1990, Honolulu, Hawaii, 63-66.
- Harada K. and Imamura F., 2005. Effects of coastal forest on tsunami hazard mitigation- a preliminary investigation, K. Satake (ed.), *Tsunamis: Case Studies and Recent Developments*, 279-292, 2005 Springer.
- Imai K. and Matsutomi H., 2005. Fluid Force on Vegetation due to tsunami flow on a sand spit, K. Satake (ed.), *Tsunamis: Case Studies and Recent Developments*, 293-304, 2005 Springer.
- IOC (Intergovernmental Oceanographic Commission), 2013. *Tsunami Glossary*, Technical Series 85, UNESCO, 1-42.
- ISDR, 2004. *Living with Risk: A global review of disaster reduction initiatives* UNISDR, Geneva.
- Koshimura S., Oie T., Yanagisawa H. and Imamura F., 2009a. Developing fragility curves for tsunami damage estimation using numerical model and post-tsunami data from Banda Aceh, Indonesia. *Coast. Eng. J.*, 51, 243–273.
- Koshimura S., Namegaya, Y. and Yanagisawa H. 2009b. Tsunami Fragility: a new measure to assess tsunami damage, *J. Disaster Res.*, 4, 479–488.
- Koutitas Ch. and Karambas, Th., 2005. A computational approach to design codes for tsunami-resisting coastal structures, *ISET Journal of Earthquake Technology*, No 461, 42 (4), 137-145.
- Leone F., Lavigne, F., Paris, R., Denain, J. C. and Vinet, F., 2011. A spatial analysis of the December 26th, 2004 tsunami-induced damages: lessons learned for a better risk assessment integrating buildings vulnerability. *Appl. Geogr.*, 31, 363–375.
- Mas E., Koshimura S., Suppasri A., Matsuoka M., Matsuyama M., Yoshii T., Jimenez C., Yamazaki F. and Imamura F., 2012. Developing tsunami fragility curves using remote sensing and survey data of the 2010 Chilean tsunami in Dichato, *Nat. Hazards Earth Syst. Sci.*, 12, 2689-2697.
- Matsutomi H., 1991. Impulsive force of timbers drifted by tsunamis. Brennan A.M. and Lander J.F. (Eds.), 2nd UJNR Tsunami Workshop, 5-6 November 1990, Honolulu, Hawaii.

- Omira R., Baptista M.A. Miranda J.M., Toto E., Catita C. Catalão J.,2010. Tsunami vulnerability assessment of Casablanca Morocco using numerical modelling and GIS tools, *Nat. Hazards Earth Syst. Sci.*, 54, 75-95.
- Omira R., Baptista M.A., Leone F., Matias L., Mellas S., Zourarah B., Miranda J.M., Carrilho F. and Chereil J-P., 2013. Performance of coastal sea-defense infrastructure at El-Jadida (Morocco) against Tsunami threat – lessons learned from the Japanese March 11, 2011 Tsunami, *Nat. Hazards Earth Syst. Sci.*, 13, 1779–1794.
- Papadopoulos G.A. and Dermentzopoulos Th., 1998. A Tsunami Risk Management Pilot Study in Heraklion, Crete, *Natural Hazards*, 18, 91–118.
- Papathoma Thesis,2003. Tsunami vulnerability assessment using a Geographical Information System with special reference to Greece, PhD Thesis, Voventry University, March 2003, pp. 289.
- Papathoma M. and Dominey-Howes D., 2003. Tsunami vulnerability assessment and its implications for coastal hazard analysis and disaster management planning, Gulf of Corinth, Greece, *Nat. Hazards Earth Syst. Sci.*, 3, 733-747.
- Papathoma M., Dominey-Howes D., Zong Y., and Smith D., 2003. Assessing tsunami vulnerability, an example from Herakleio, Crete, *Nat. Hazards Earth Syst. Sci.*, 3, 377-389.
- Peiris N., Pomonis, A. 2006. December 26, 2004 Indian Ocean tsunami: Vulnerability functions for loss estimation in Sri Lanka. In: Chu, J., Phoon, K.K. and Yong, K.Y. (eds.) International Conference on Geotechnical Engineering for Disaster Mitigation and Rehabilitation, World Scientific, pp. 411-416.
- Preuss J., 1991. Urban planning for tsunami hazards Grays harbor, Washington and Lima, Peru, Brennan A.M. and Lander J.F. (Eds.), 2nd UJNR Tsunami Workshop, 5-6 November 1990, Honolulu, Hawaii.
- Reese L.C., Matlock H. and Asce M., 1968. Structural Damage from Tsunami at Hilo, Hawaii, *Journal of the Hydraulics Division*, Vol. 94, No. 4, July/August 1968, 961-982.
- Reese S., Cousins W.J., Power W.L., Palmer N.G., Tejakusuma I.G. and Nugrahadi S., 2007. Tsunami vulnerability of buildings and people in South Java? Field observations after the July 2006 Java tsunami, *Nat. Hazards Earth Syst. Sci.*, 7, 573–589.
- Römer H., Willroth P., Kaiser G., Vafeidis A.T., Ludwig R., Sterr H. and Diez J.R., 2012. Potential od remote sensing techniques for tsunami hazard and vulnerability analysis- a case study from Phang-Nga province, Thailand, *Nat. Hazards Earth Syst. Sci.*, 12, 2103-2126.
- Shuto N., 1987. The effectiveness and limit of tsunami control forests, *Coastal Engineering in Japan*, 30, 143-153.
- Shuto N., 1991. Historical changes in characteristics of tsunami disasters, *Natural Disaster Reduction and Civil Engineering*, 77-86.
- Sim S.Y., Huang Z. , Switzer A.D., 2013. An experimental study on tsunami inundation over complex coastal topography, *Theoretical & Applied Mechanics Letters*, 3(3): 9-03200.
- Singhal A., Kiremidjian A.S., 1996. Method for probabilistic evaluation of seismic structural damage. *J. Struct. Eng.* 122, 1459–1467.
- Suppasri A., Mas E., Charvet I., Gunasekera R., Imai K., Fukutani Y., Abe Y and Imamura F., 2013. Building damage characteristics based on surveyed data and fragility curves of the 2011 Great East Japan tsunami, *Natural Hazards*, 66, 319-341.
- Tarbotton C., Dall'Osso F., Dominey-Howes D. and Goff J., 2015. The use of empirical vulnerability functions to assess the response of buildings to tsunami impact: Comparative review and summary of best practice, *Earth-Science Reviews*, 142, 120-134.

Taubenböck H., Post J., Kiefl R., Roth A., Ismail F.A., Strunz G. and Dech S., 2008. Risk and vulnerability assessment to tsunami hazard using very high resolution satellite data, Carsten Jürgens (Ed.), *Remote Sensing – New challenges of High Resolution*, Bochum 2008, 77-86.

Tinti S., Armigliato A. 2003. The use of scenarios to evaluate the tsunami impact in southern, Italy. *Marine Geology*, 199,221-243.

UNESCO-IOC (Intergovernmental Oceanographic Commission), 2011. Reducing and managing the risk of tsunamis. *IOC Manuals and Guides (IOC/2011/MG/57Rev.2)*, 57-74.

Valencia N., Gardi A., Gauraz A., Leone F. and Guillande R., 2011. New tsunami damage functions developed in the framework of SCHEMA project: application to European-Mediterranean coasts. *Nat. Hazards Earth Syst. Sci.*, 11, 2835–2846.

Wong P.P., 2009. Rethinking post- tsunami integrated coastal management for Asia- Pacific, *Ocean & Coastal Management*, 52, 405-410.

3. Vulnerability Assessment for the ASTARTE Test Sites

3.1 Sines

3.1.1 Description of the site

Sines is located on the west littoral margin of the Iberian Peninsula, about 150 km south of Lisbon, Portugal (Figure 3.1.1). The city of Sines is the main urban centre of the municipality. It has a coastline approximately 7-km long and its surrounding municipality covers an area of 202.7 km² with 30 km coastline. Sines has 14280 inhabitants (Instituto Nacional de Estatística, 2011) and about 5000 floating population due to economic and touristic purposes. Overnight stays varied between 60000 to 80000 in between 2009 and 2012 in Sines municipality (Instituto Nacional de Estatística, 2012).

Sines plays a major role in terms of energy production via coal in the thermoelectric central of EDP as well as renewable energies in two Aeolic wind parks. Gas is delivered and stored in Portugal's unique natural liquefied gas terminal and distributed throughout the country (REN). Further, Sines contains two great production centrals of Oil and Gas industry (GALP refinery and Repsol YPF petrochemical industrial complex). All the industrial sites are connected with necessary infrastructure in order to transport raw materials and products from and to the port of Sines. Infrastructures in form of streets, railways, pipelines and conveyor belts are especially sensible to inundation. Railways might be destroyed, streets may serve as canalisation of tsunami waves, pipelines might be cracked due to high forces and cause heavy pollution of ambient waters. Coal stored in the multipurpose area of Sines port might be transported completely away by an incoming tsunami (Câmara Municipal de Sines, 2007).

The port of Sines is the main economic pole in the area as it is one of the largest deep-water ports (with 28 m depth) in Western Europe, which rises the country's logistical and industrial values and is situated at the intersection of main marine trading routes in the Northeast Atlantic. Sines port consists of 5 terminals: liquid Bulks, liquid natural gas, petrochemical, container, and multipurpose; as well as fishing and leisure ports (see Figure 3.1.1-C). Another advantage of the port is its perfect connection via railway systems with the entire Iberian Peninsula and the capacity to receive bigger cargo ships. As the port of Sines occupies the main lower coastal area, it also represents our main area of interest (Porto de Sines 2014). Tourism is another important aspect of the municipality of Sines: about 63000 overnight stays in 2012, which covers also stays in nearby Porto Covo (Instituto Nacional de Estatística, 2012). In between Sines and Porto Covo there are popular beaches which are used for recreation. Popular beaches included in our study area are: the beach Vasco da Gama near the city centre and the beach of São Torpes near the thermo electric central that is highly populated during the summer season (Câmara Municipal de Sines, 2007).

Due to its openness and exposure to the sea, the impact of tsunamis and other marine hazards like sea level rise are of great interest in the area. Moreover, the fact that different coastal structures are located within the low-lying coastal lands makes them vulnerable to tsunami impact.

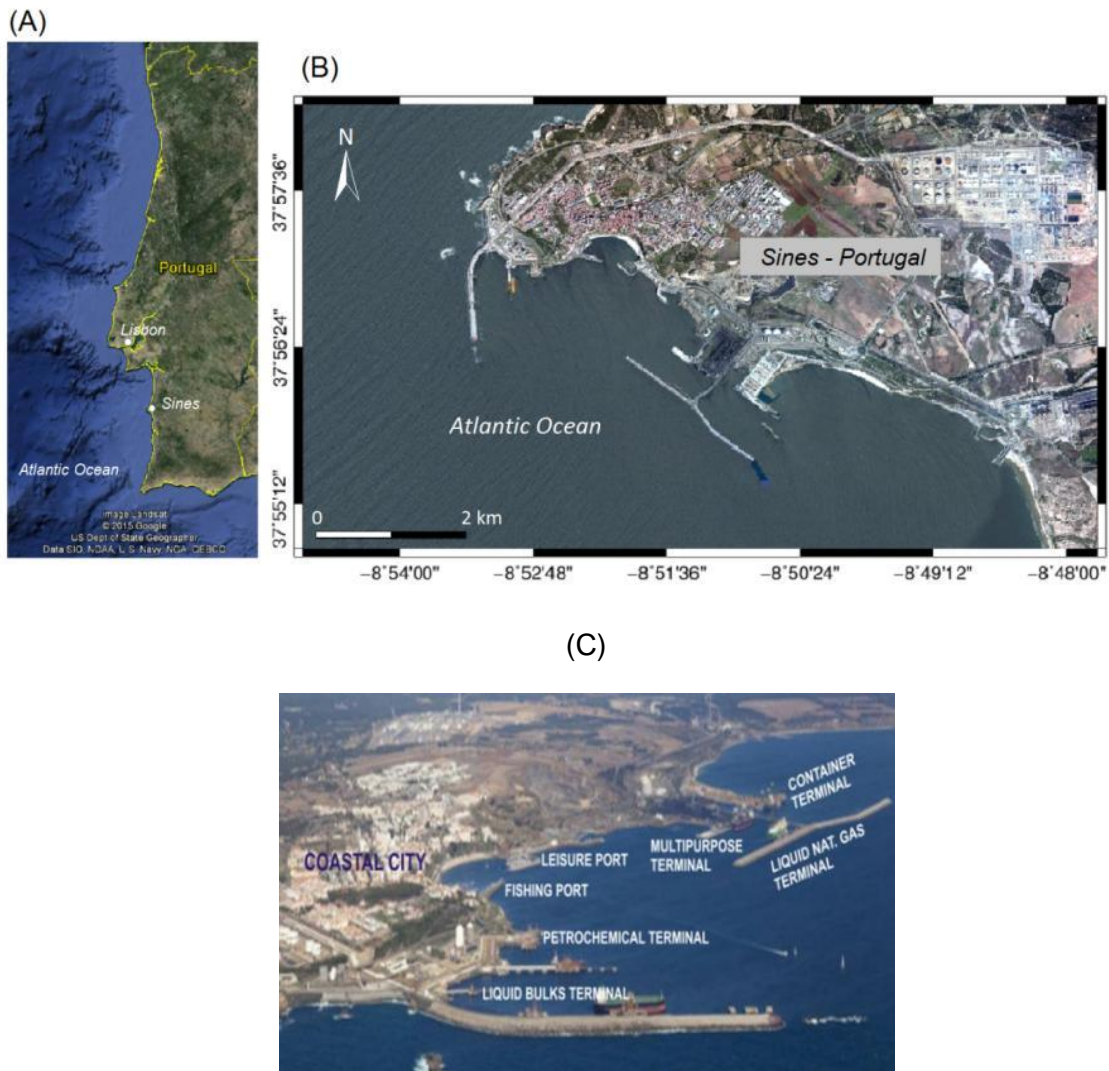


Figure 3.1.1. Sines test-site. (A) Regional overview; (B) Sines Test-site, (C) global image of the Sines harbour and coastal city (Adapted from: <http://www.portodesines.pt/pls/portal/go>).

3.1.2 SCHEMA

The tsunami vulnerability is carried out for coastal buildings located within the inundation prone area along the coast of Sines test-site.

3.1.2.1 Methodology







The building tsunami vulnerability methodology integrates numerical modelling of tsunami inundation (results elaborated in Task 8.2, details can be found in D8.8), field survey data, and post-tsunami building damage data from the Tohoku-oki 2011 event; in a developed GIS toolbox that allows estimating the individual buildings vulnerability to tsunamis. To reach the objectives of this project's task the following steps were conducted:

- 1- Field survey of the existing buildings in the inundation zone of Sines Test-site. Classification of buildings by type taking into account criteria of: construction materials and elevation (number of floors);
- 2- Adaptation of the building fragility curves derived from the 2011 Japanese post-tsunami survey to the sines test-site;
- 3- Development of a GIS toolbox that combines field-survey data, hazard results, and fragility curves in order to automatically estimate the building damage;

4- The tsunami damage of building exposed to tsunami impact is estimated through: i) Vulnerability maps that show the expected level of tsunami damage for each building located within the inundation zone, ii) Probability of occurrence of a given damage level (six levels of damage were considered: D1- Minor, D2- Moderate, D3-Major, D4-Complete, D5- Collapse, and D6-Washed away) for each individual building of Sines test-site.

The damage levels, D1 to D6, considered in this study are the same as the ones defined after the 2011 Tohoku-oki event from post-tsunami field-surveys (Suppasri et al., 2013). In table 3.1.1 we highlight the classification of each damage level, its description and the corresponding observed tsunami damages on structures from the Tohoku-oki event.

Table 3.1.1. Damage levels, their classification, description and corresponding observed tsunami effects on buildings after the Tohoku-oki 2011 tsunami (adapted from Supasri et al., 2013).

Damage Level	Classification	Description	Damaged Building
D1	Minor Damage	No significant structural or non-structural damage, possible to be used immediately after minor floor and wall clean up	
D2	Moderate Damage	Slight damages to non-structural components, possible to be used after moderate reparation	
D3	Major Damage	Heavy damages to some walls but no damages in columns, possible to be used after major reparations	
D4	Complete Damage	Heavy damages to several walls and some columns, possible to be used after complete reparation and retrofitting	
D5	Collapse	Destructive damages to walls and several columns, loss of functionality	
D6	Washed away	Total overturned, Non-repairable	

Field Survey

After identifying, through numerical simulations, the coastal areas of Sines test-site that are prone to tsunami inundation (deliverable D8.8 of ASTARTE project) a field survey was conducted to perform

an inventory of the buildings types. 153 buildings have been identified within the inundation-prone zone of Sines test-site. These buildings have been classified on the basis of their construction materials and number of stories (or elevations).

Within the Sines surveyed zone, four types of construction materials have been identified, namely steel, reinforced-concrete, masonry, and wood, with elevations ranging from 3 m up to 25 m. Among the 153 identified buildings, the dominant construction material is the masonry with more than 100 existing structures in the surveyed area.

In table 3.1.2, we summarize the outcomes of the field survey, highlighting the number of the coastal buildings within the inundation zone, their material of construction and their elevations range.

Table 3.1.2. Summary of building field survey at Sines

Number of buildings	Construction material	Elevation range
18	Steel	3 to 23m
109	Masonry/brick	2.5 to 13.5m
5	Reinforced-concrete	10 to 25m
21	Wood	3 to 15m

Fragility Curves

In this study, where there is no observed tsunami damage for Sines test-site, we use the tsunami fragility curves considering the empirical relationship of Koshimura et al. (2009) and the most recent data set compilation from the 2011 Great East Japan tsunami published by Suppasri et al. (2013) and adapted them to Sines test-site. This set of fragility curves were chosen because of the consistency of the data used (total of 251,301 building data surveyed) detailed on damage level, structural material and number of stories (three level groups: 1, 2 and >=3 stories) per building.

The tsunami fragility curves were rebuilt using the statistical parameters derived from Koshimura et al. (2009) fragility function. The cumulative probability of occurrence of damage was calculated by the normal distribution within a range of every 0.01m (from 0 up to 20m) inundation depth, using the mean and standard deviation values provided by Suppasri et al. (2013) for each damage level. By plotting this cumulative probability values arranged by structural material and number of stories, it was possible to extract the Inundation depth threshold values that could circumscribe the range of each damage level. These thresholds were the key of our building damage probability classification.

Two main buildings criteria are taken into account to develop the tsunami fragility curves for Sines test-site. They are the construction material and the number of building floors. Figure 3.1.2 depicts an example of the computed fragility curves for masonry buildings. The curves in the figure present the probability of damage levels occurrence in function of inundation depths for a given coastal structure.

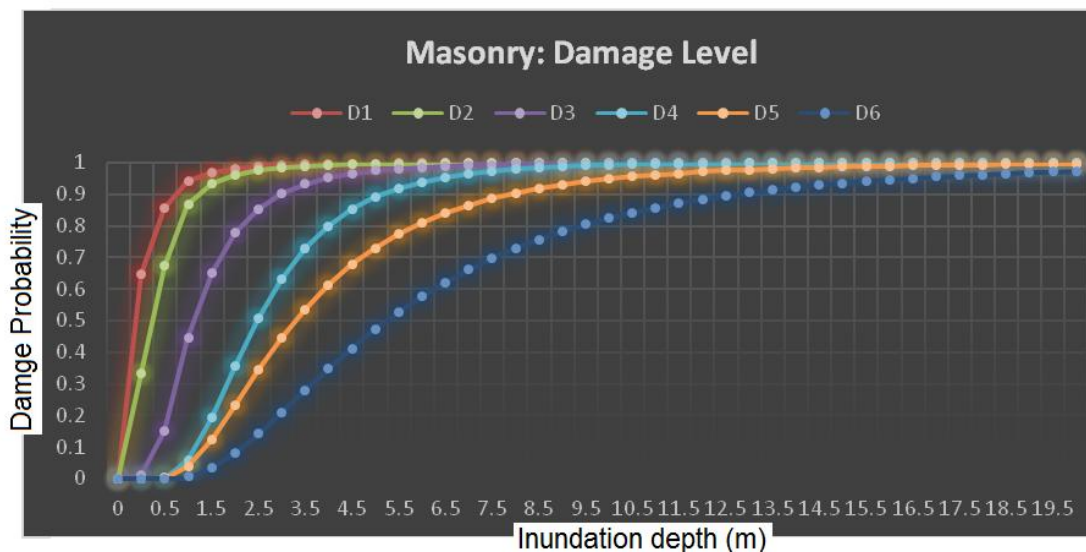


Figure 3.1.2. Tsunami fragility curves developed for masonry/brick buildings located within the inundation area at Sines test-site.

GIS Toolbox development

AGIS-based toolbox has been developed to derive the building tsunami vulnerability maps for the Sines test-site. The latest version 10.2 of ArcGIS has been used. The toolbox was developed with the ability to integrate the different inputs required for tsunami vulnerability mapping (inundation, building types, and fragility curves) in an easy-to-use way cartographic process. In this the work the main development was focused on the ModelBuilder platform, an ArcGIS system dedicated tool that has the capability to perform all the geo-processing functions by a diagrammatic interface in an automated way. Moreover, the developed toolbox has the advantage to be employed to the other test-sites and to different tsunami inundation scenarios.

In the following sections we outline the main core of the toolbox model as well as the submodels used to build the tsunami vulnerability maps.

- o The main core of the toolbox

The toolbox was built from a three-tier model (model within a model). Within the first tier of the model (Figure 3.1.3) there are the main process flow composed of two submodels (Data preparation and Damage level classification), the input features and the output feature.

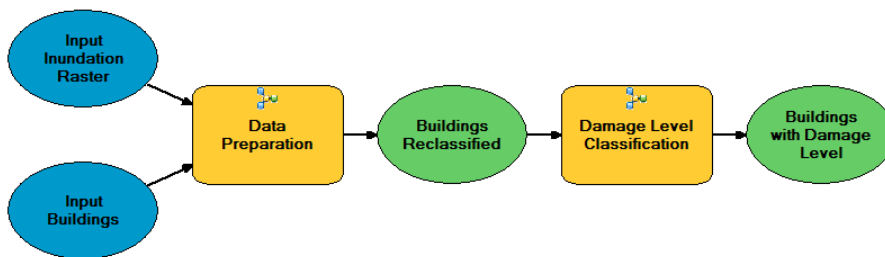


Figure 3.1.3. Main core of the tsunami vulnerability mapping.

Running the model will open the model process dialog window, where the input files can be inserted and the name and save path of the output map.

- o Data Preparation submodel

The “Data Preparation” submodel (Figure3.1.4) was created to pre-process the raw input features so the output could have the values/attributes that will contribute on classifying the damage level. The first process consists of the extraction of the inundation depth values from the raster inundation grid and joins them with the buildings shapefile. The second process reclassifies the buildings shapefile attributes so the final classification can be standardized.

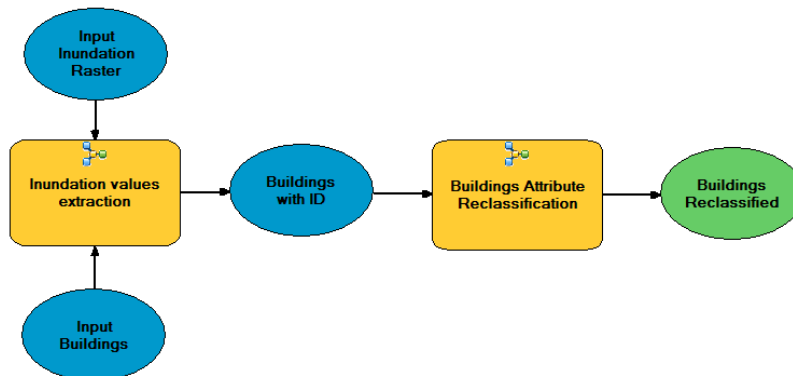


Figure 3.1.4. Diagram of the “Data Preparation” submodel.

-Inundation value extraction: in order to include the inundation depth values into the buildings shapefile, the inundation raster are converted to points. Each point has the raster cell value as attribute. The “spacial join” tool joins the inundation points within a distance of 10m from each building polygon; which allows generating a new feature that has all the inundation

values from the points that satisfy the condition. The “Summary Statistics” calculates the maximum for the grid value field. Finally, join field depending on the line “OBJECTID” from the input buildings and the “TARGET_ID” from “MAX_ID” table a new field is added to the Buildings shapefile with the max inundation depth. Figure 3.1.5 depicts the diagram used for inundation values extraction.

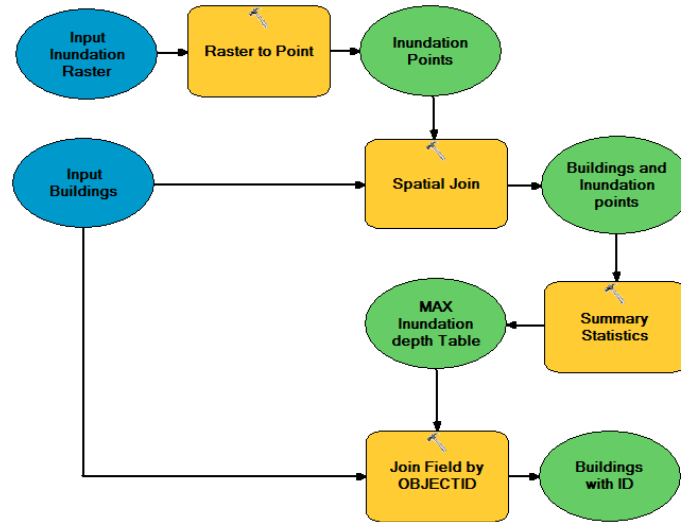


Figure 3.1.5. Diagram for inundation value extraction

- **Buildings Attributes Reclassification:** This process is intended to aggregate the building type parameters on the same field (column of the attribute table). In order to homogenize the source data from the field survey the “Buildings Attributes Reclassification” process is developed and the corresponding diagram is highlighted in Figure 4.1.6.

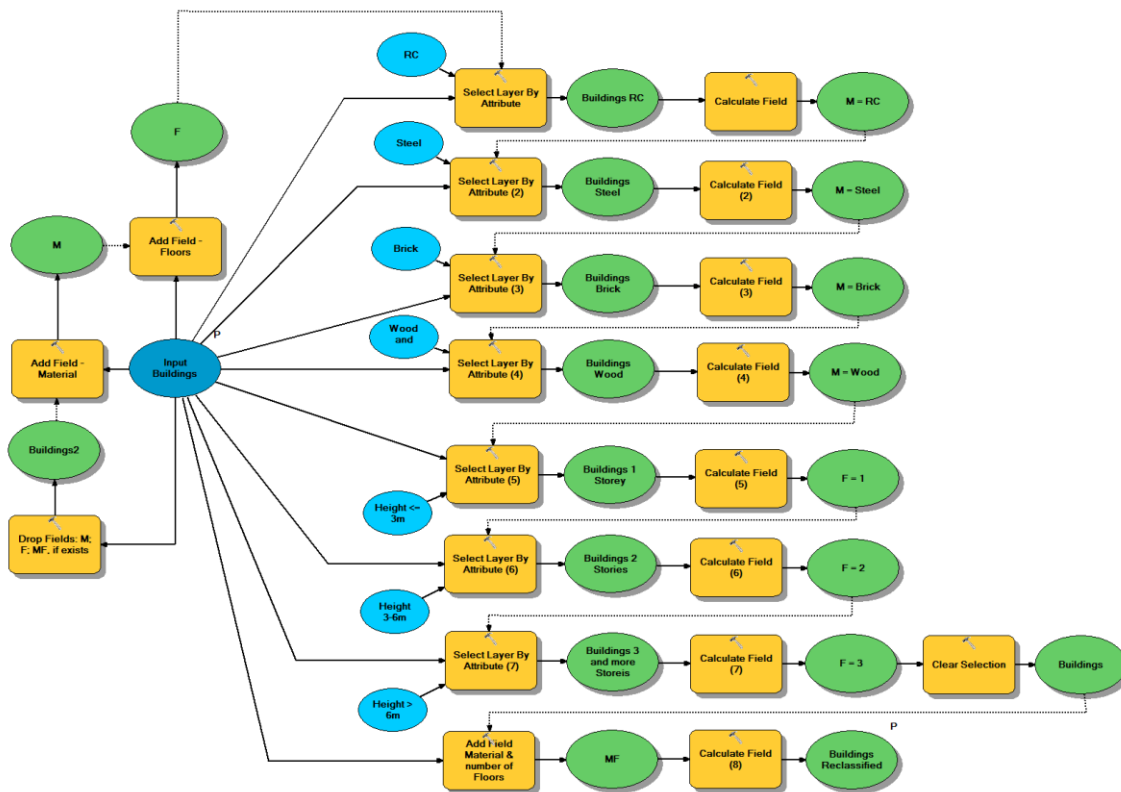


Figure 3.1.6. Diagram for Buildings Attributes Reclassification.

o Damage Level Classification submodel

The “Damage Level Classification” submodel is arranged by four third-tier models corresponding to each construction material type (Figure 3.1.7). Within the third-tier models (Figure 3.1.8, masonry or brick structures example) the damage level field (DL) is added.

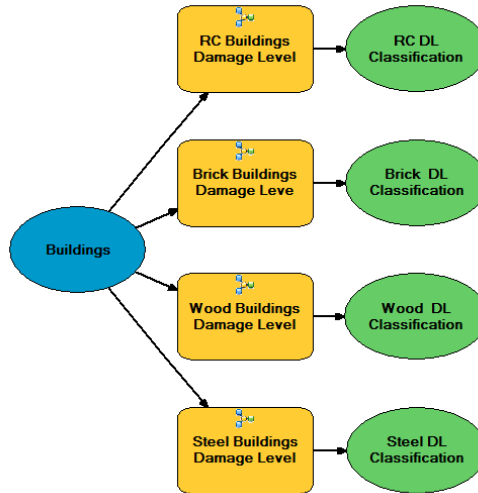


Figure 3.1.7. Diagram of Damage Level Classification model.

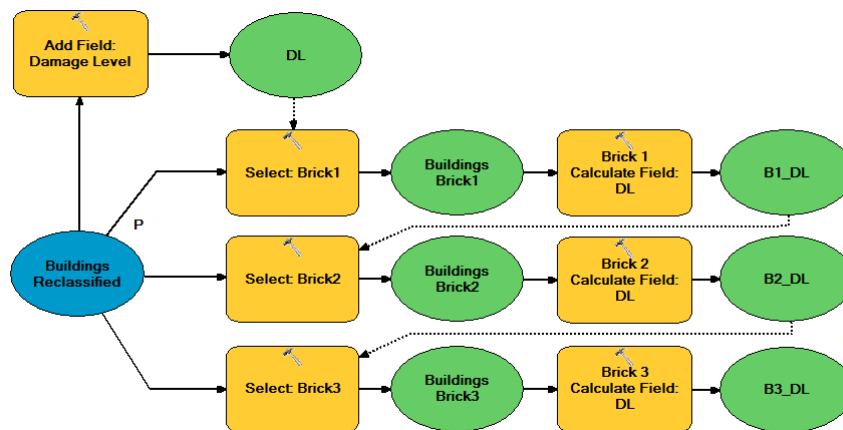


Figure 3.1.8. Diagram for Brick Buildings Damage Level Classification.

3.1.2.2 Results

The tsunami vulnerability results for Sines test-site are presented in terms of building tsunami vulnerability maps with probabilities of occurrence of 20%, 50%, and 80% respectively.

Tsunami Vulnerability with 20% probability of occurrence. Figures 3.1.9 and 3.1.10 show the building tsunami vulnerability for Sines test-site. The tsunami vulnerability is expressed by the means of building damage level that is expected to occur with a probability of 20%.

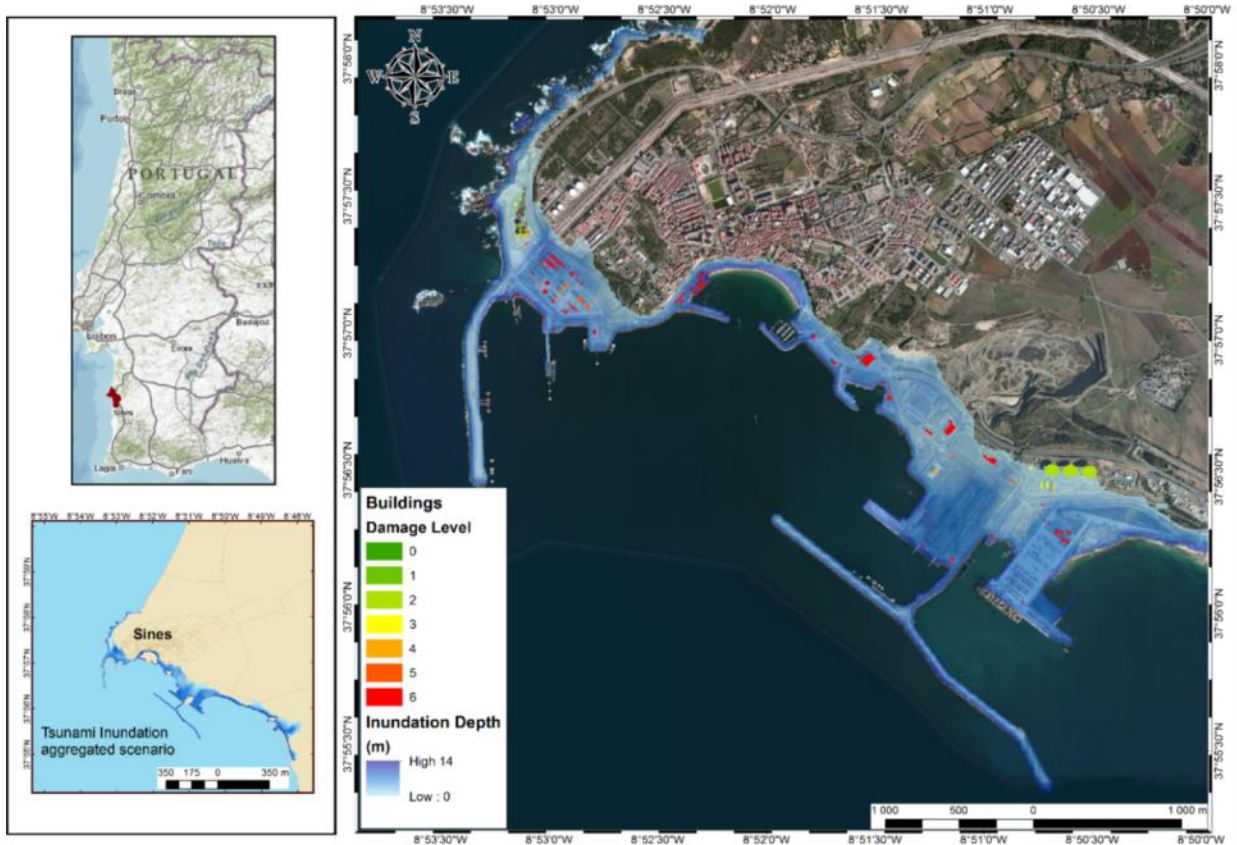


Figure 3.1.9. Building tsunami vulnerability maps for Sines test-site with 20% probability of occurrence



Figure 3.1.10. 3D view of the vulnerability map

Tsunami Vulnerability with 50% probability of occurrence. Figures 3.1.11 and 3.1.12 depict the building tsunami vulnerability for Sines test-site. The tsunami vulnerability is expressed by the means of building damage level that is expected to occur with a probability of 50%.

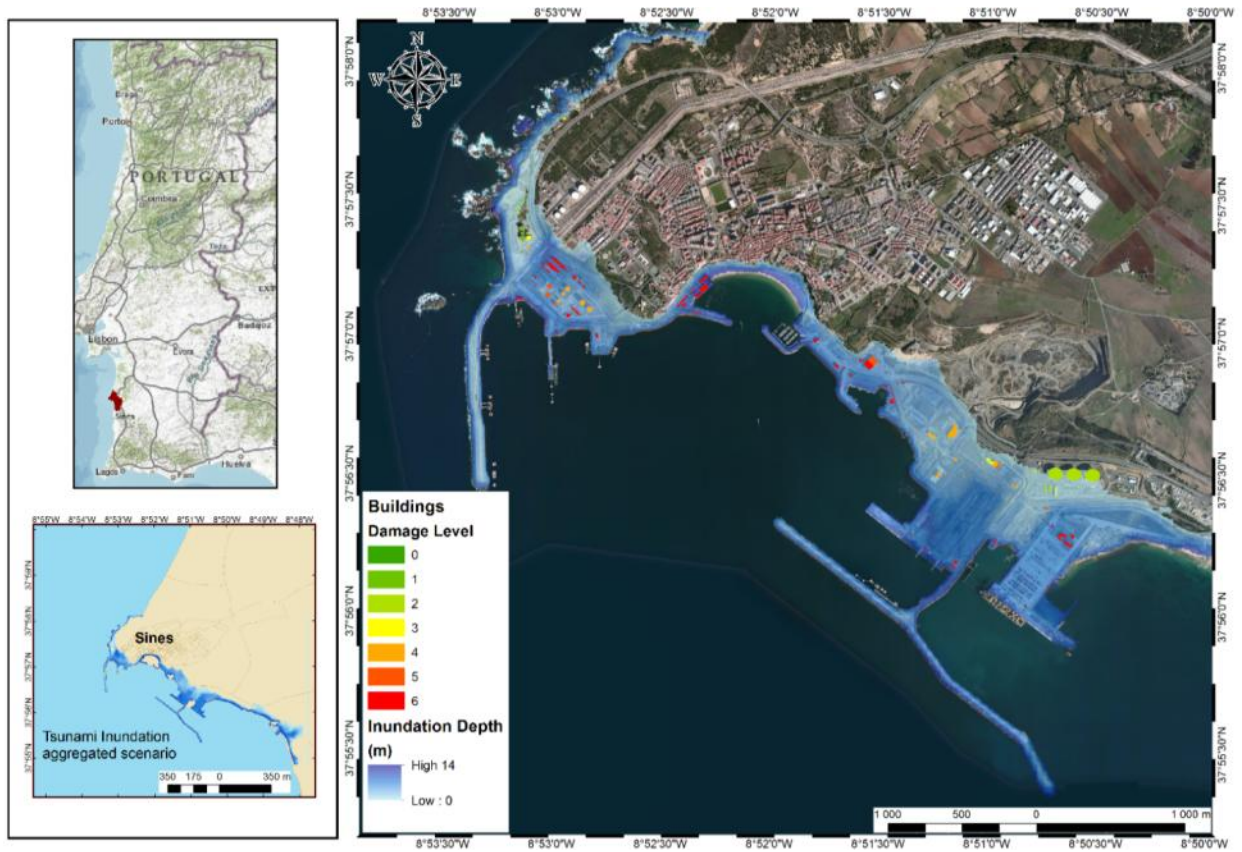


Figure 3.1.11. Building tsunami vulnerability maps for Sines test-site with 50% probability of occurrence



Figure 3.1.12. 3D view of the vulnerability map

Tsunami Vulnerability with 80% probability of occurrence. Figures 3.1.13 and 3.1.14 depict the building tsunami vulnerability for Sines test-site. The tsunami vulnerability is expressed by the means of building damage level that is expected to occur with a probability of 80%.

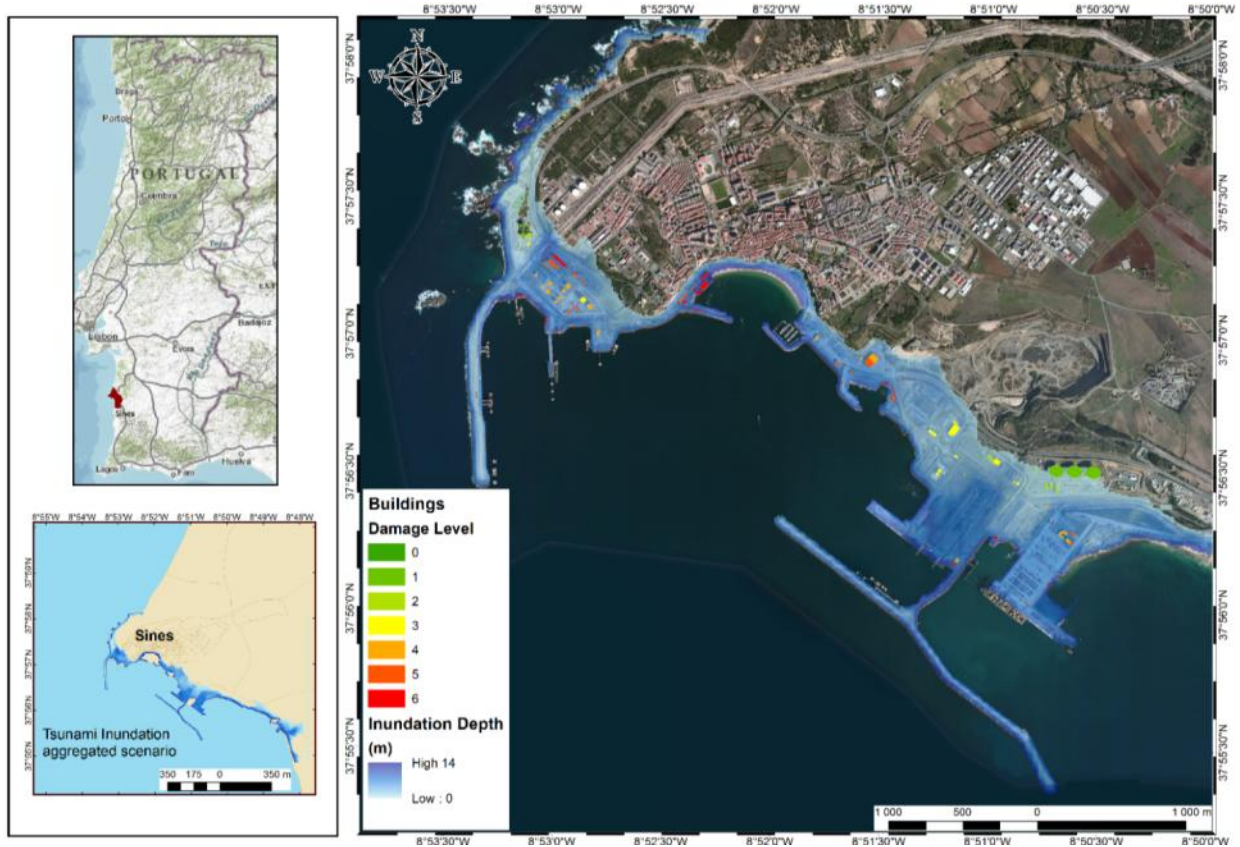


Figure 3.1.13. Building tsunami vulnerability maps for Sines test-site with 80% probability of occurrence



Figure 3.1.14. 3D view of the vulnerability map

The building tsunami vulnerability results clearly show that the coastal structures located close to the shore are highly vulnerable to tsunami impact with estimated damage levels ranging from D2 to D5. This vulnerability decreases with the onshore distance from the shoreline where the tsunami flow depth is not significant. Also the estimated tsunami building damage level varies significantly with the probability of occurrence. The comparison between results in Figures 3.1.9-3.1.14 show that increasing the probability of occurrence from 20 to 80%, leads to decrease the estimated damage level for some coastal structures.

In addition to the construction material, the structure elevation plays an important role in controlling the tsunami vulnerability. In Figure 3.1.15 we plot, for the same structure, the damage probability for the different considered levels, with and without considering the number of floors. Results (blue and green curves) clearly show that the number of floor reduces significantly the vulnerability of coastal buildings to tsunami, in particular their probability to suffer major damages (level D4, D5, D6).

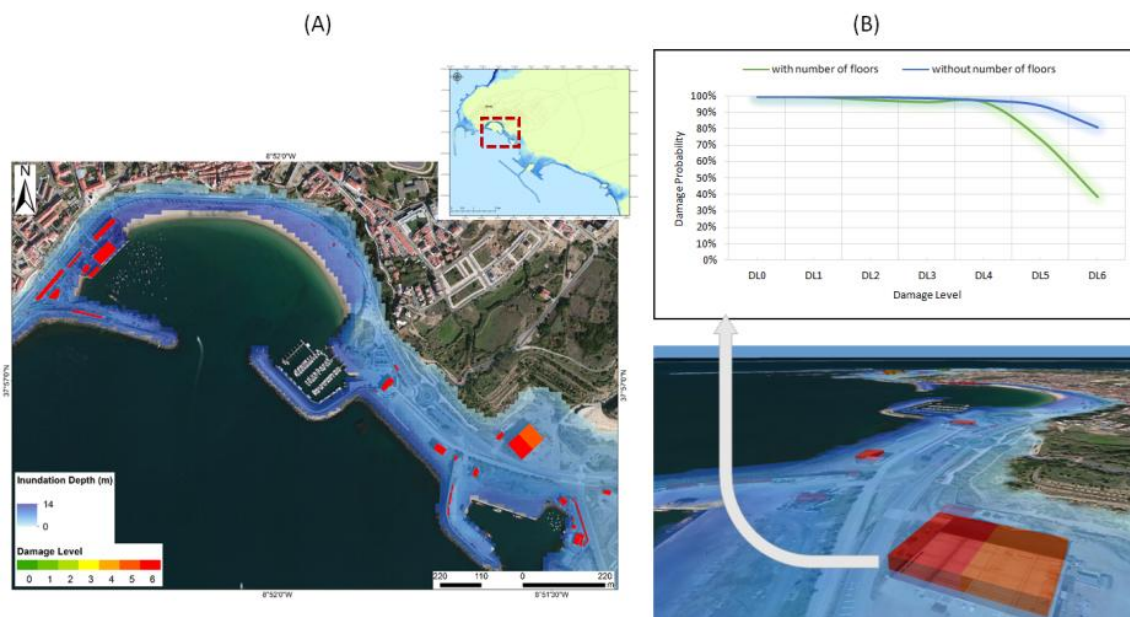


Figure 3.1.15. (A) zoom on the building tsunami vulnerability map of Sines, (B) Effect of considering the building number of floors on tsunami vulnerability

3.1.3 References

Câmara Municipal de Sines (2007): Município de Sines. [online] Available at: <http://www.sines.pt/PT/Negocios/potencialidades/turismo/Paginas/default.aspx> [accessed 18th September 2014].

Instituto Nacional de Estatística (2011): Census 2011. [online] Available at: http://censos.ine.pt/xportal/xmain?xpid=CENSOS&xpgid=censos2011_apresentacao [accessed 18th September 2014].

Instituto Nacional de Estatística (2012): Estatísticas territoriais. [online] Available at: http://www.ine.pt/xportal/xmain?xpid=INE&xpgid=ine_unid_territorial&menuBOUI=13707095&contexto=ut&selTab=tab3 [accessed 18th September 2014].

Koshimura S., Oie T., Yanagisawa H., Imamura F., 2009. Developing fragility functions for tsunami damage estimation using numerical model and post-tsunami data from Banda Aceh, Indonesia. *Coastal Engineering Journal*, 51(03), 243-273.

Porto de Sines, 2014a. Administração dos portos de Sines e do Algarve S.A. [online] Available at: <http://www.portodesines.pt/pls/portal/go> [accessed 18th September 2014].

Suppasri A., Mas E., Charvet I., Gunasekera R., Imai, K., Fukutani, Y., Imamura, F., 2013. Building damage characteristics based on surveyed data and fragility curves of the 2011 Great East Japan tsunami. *Natural Hazards*, 66(2), 319-341.

3.2 Tanger

3.2.1 Description of the site

Tanger is a port city in northern Morocco, which is in the extreme North West tip of Africa to the west entrance of the Strait of Gibraltar. The population of this city is estimated at 974,000 inhabitants (census 2014). Tanger is characterized by the presence of a bay in the city center that stretches over 10 km, harbor and sandy beach. The infrastructure and the resorts of this coastal town, experience a significant economic and tourism development. The coastal area of this city is characterized by:

- i) a port that manages and integrates the flow of goods and passengers;
- ii) a marina with a fishing port;
- iii) a sandy beach that experiences high tourist pressure and activities during peak seasons;
- iv) hotels and tourist resorts that proliferate through domestic and foreign investment.



Figure 3.2.1. Geographical map and airphoto of the Tanger harbor

Tanger Port full restructuring

The city of Tanger and in particular its harbor infrastructure are currently undergoing a metamorphosis to become one of the cities with a more dynamic port in the Euro-Mediterranean region. The Tanger harbors are undergoing infrastructure conversions and extensions to become a ports-system with the aim of responding to an urgent request to accommodate large cruise ships, and providing more possibilities of pleasure. Furthermore, a large transformation is planned for the existing fishing and the local and international travel services.



Figure 3.2.2. The Tanger harbor: Before / After

3.2.2 SCHEMA

3.2.2.1 Introduction

During the SCHEMA project (2007-2010) new tsunami damage functions were developed in order to assess the potential of tsunami damage to different buildings located in the European-Mediterranean coasts. These damage curves give the expected damage level for the different classes of buildings depending on the flow depth hazard parameter. This methodology consists of producing a tsunami hazard map based on high resolution modeling of the worst-case credible scenario and a map with vulnerability classes resulting from a buildings inventory. These maps are implemented in an ArcGIS tool (DamASCHE tool) which helps in assessing the level of damage on buildings using a damage matrix. In the frame of SCHEMA project, this approach was tested and validated by several partners on five pilot sites located in the NE Atlantic; Morocco (Atillah et al. 2011) and Portugal, the Mediterranean (France and Italy) and Black Seas (Bulgaria).

Buildings typology

In order to develop new damage functions, it was necessary to adopt a standardized building typology description in order to group the constructions located in the coasts exposed to tsunami hazard into different classes. The building typology used was initially derived from several authors (Leone et al., 2006, 2011; Peiris, 2006; Garcin et al., 2007) after the tsunami of the December 26th, 2004. It was later extended and completed in order to include the types of constructions existing in the five test sites of the SCHEMA Project. Thus, four main classes of buildings (divided in sub-classes) have been distinguished on the basis of their structural characteristics of resistance (Table 3.2.1). They are (i) light constructions,(ii) masonry constructions and not reinforced concrete constructions,(iii) reinforced concrete constructions, and (vi) other constructions.

Damage functions and damage matrix

The damage functions proposed for the identified building types were elaborated from a database compiled in the southwest area of Banda Aceh (Sumatra, Indonesia) after the 2004 Indian Ocean tsunami. These functions were developed from real observations of the mean damage level related to the maximum flow depth observed in damaged areas. They concerned only the building classes A, B, C, D and E1 that were identified in the studied area by field surveys and by photo-interpretation (Fig.3.2.3). As we can notice in this figure there are no empirical laws for average damages to the building types E2, F and G due to the lack of similar buildings in the database of Banda Aceh. A detailed description of the method can be found in the work of Valencia et al. (2011).

Table 3.2.1. Standardized building typology based on structural characteristics of resistance of the constructions (SCHEMA project)

Class	Building types	Height & storeys
I. Light	A1 Beach or sea front light construction of wood, timber, clay	0 to 1 level, Rarely 2
	A2 Very light constructions without any design. Very rudimentary huts, built using wood or clay, timber, slabs of zinc	1 level only
II. Masonry, and not reinforced concrete	B1 Brick not reinforced, cement, mortar wall, fieldstone, masonry	1 to 2 levels
	B2 Light and very concentrated constructions: wooden, timber and clay materials	1 to 2 levels
	C1 Individual buildings, villas: Brick with reinforced column & masonry filling	1 to 2 levels
	C2 Masonry constructions made of lava stones blocks, usually squared-off, alternating with clay bricks	1 to 2 levels
	D Large villas or collective building, residential or commercial buildings: Concrete not reinforced	1 to 3 levels
III. Reinforced concrete	E1 Residential or collective structures or offices, car parks, schools: reinforced concrete, steel frame	0 to 3 levels
	E2 Residential or collective structures or offices, car parks, schools, towers: reinforced concrete, steel frame	> 3 levels
IV. Other	F Harbour and industrial buildings, hangars: reinforced concrete, steel frames	Undifferentiated
	G Other, administrative, historical, religion buildings	Undifferentiated

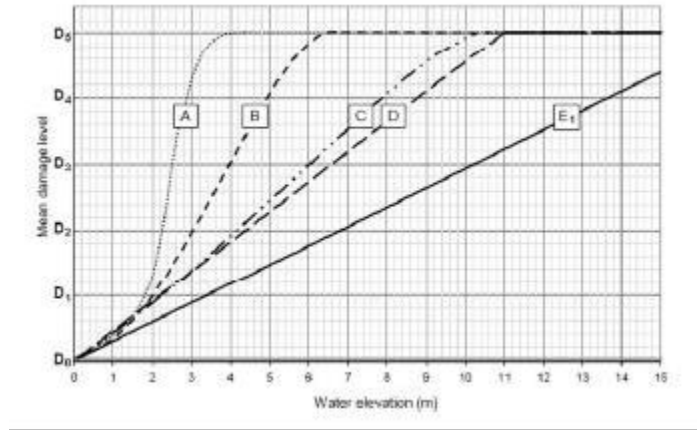


Figure 3.2.3. Damage functions for buildings classes A, B, C, D, and E1 as a function of water elevation in meters (After Gardi et al. 2009)

The damage function gives the relation between a continuous variable (flow depth) with a discrete variable (mean damage level). Each damage level can be associated with an interval of flow depth values. Consequently, damage functions can also be given under the form of a matrix called damage matrix as shown in Table 3.2.2. For each building class, a potential damage is associated with an interval of water depth.

The damage level is classified through a 6-degree scale with increasing severity: D0: 4 damage, D1: -light damage, D2: important damage, D3: heavy damage, D4: partial collapse and D5: total collapse.

Table 3.2.2. Damage matrix adopted in SCHEMA project

Damage level		Class A	Class B	Class C	Class D	Class E
No damage	D0	0 m	0 m	0 m	0 m	0 m
Light damage	D1	0 – 1.8 m	0 – 2 m	0 – 2.5 m	0 – 2 m	0 – 3 m
Important damage	D2	1.8 – 2.2 m	2 – 3 m	2.5 – 4 m	2 – 4.5 m	3 – 6 m
Heavy damage	D3	2.2 – 2.6 m	3 – 4 m	4 – 6 m	4.5 – 6.5 m	6 – 9.5 m
Partial collapse	D4	2.6 – 3.8 m	4 – 5 m	6 – 8 m	6.5 – 9 m	9.5 – 12.5 m
Total collapse	D5	> 3.8 m	> 5 m	> 8 m	> 9 m	> 12.5 m

Building damage map

In order to produce maps of the expected damage for different building vulnerability classes, the continuous vulnerability functions are translated into damage matrices. A specific GIS application named “DamASCHE tool” was developed on the ArcGIS (ESRI) platform during the SCHEMA project. This tool allocates to each point of the buildings layer the value of the hazard which is read from the inundation depth map. Then using the damage matrix file, damage levels are calculated for each building included in the inundated zone. The result is presented as a shapefile layer of buildings with their attended level of damage ranging from no damage D0 to total collapse D5.

Application of the SCHEMA approach to Tangier test site

Tsunami hazard assessment

To assess tsunami impact on the coastal zone of Tangier, we used the single scenario-based approach (Tinti & Armigliato 2003), based on the most credible earthquake scenarios (MCESSs). Tsunami historical studies in Morocco have shown that the southwest Iberia margin is the major source of damaging tsunamigenic earthquakes that affected the Atlantic coast of Morocco (Kaabouben et al, 2009, Zitellini et al. 2009). The most important active structures detected in this zone are the Marques de Pombal fault, the Horseshoe fault, the Gorrige Bank fault and the Cadiz Wedge fault. These structures are supposed to be eventually the source of the 1st November 1755 great earthquake and tsunami and were largely studied by many authors. The Omira et al. (2009) study presents the radiation patterns of the tsunamis associated with these typical faults. This study clearly shows that the Cadiz Wedge earthquake scenario is the more effective in radiating tsunami energy towards the strait of Gibraltar coastal areas where Tangier site is located. For that, in this study, we select the Cadiz Wedge source, as the scenario able to cause the higher tsunami impact along the coastal area at the Tangier site. The characteristics of fault parameters used are described by Gutscher et al. (2006) and grouped in table 3.2.3. They correspond to an earthquake magnitude of Mw 8.8.

Tsunami numerical modeling from this source to the target area, including inundation, is performed using a validated shallow water model; the COMCOT-lx code (Liu et al. 1998; Omira et al. 2009; Baptista et al. 2011). The code solves both linear and nonlinear shallow water equations (SWEs) using a finite differences numerical scheme in a system of nested grids from the source towards the coastal area. A nested grid system with increasing resolution, can be implemented in the model to carry out the need for tsunami simulations at different scales. Larger grids are used in the open sea for tsunami generation and propagation, while finer grids are adopted for inundation of the coastal region of interest.

Table 3.2.3. Fault parameters of the source tsunamigenic scenario. L: fault length in kilometers; W: fault width in kilometers; D: depth from the sea bottom to the top of the fault in kilometers and Mw: the moment magnitude.

Source Model	L (Km)	W (Km)	D (Km)	Epicentre coordinates		Slip(m)	Strike(°)	Dip(°)	Rake(°)	Mw
				Longitude	Latitude					
CWF (Cadiz Wedge Fault)	180	210	5	-8.059	35.407	20	349.0	5	90	8.8

In this present work, we use four grids with various resolutions (640m,160m 40m and 10m). The finer grid (10m) is used for the Tangier port and its surrounding areas. The Digital Terrain Model (DTM) was generated from a compilation of multisource altimetry and bathymetric data. Topographic data (contours and spot elevations) was provided by ANCFCC at 1/25.000. Bathymetric data were acquired at 1/20.000 by the Medocean society from marine map N°1701 of Tangier which was updated by SHOM in 2003. Bathymetry was completed by a 1-m resolution data provided by the Med-Ocean company after a dredging operation. Data of different scales were merged on a unique database and transformed to UTM30 coordinates using datum WGS84.

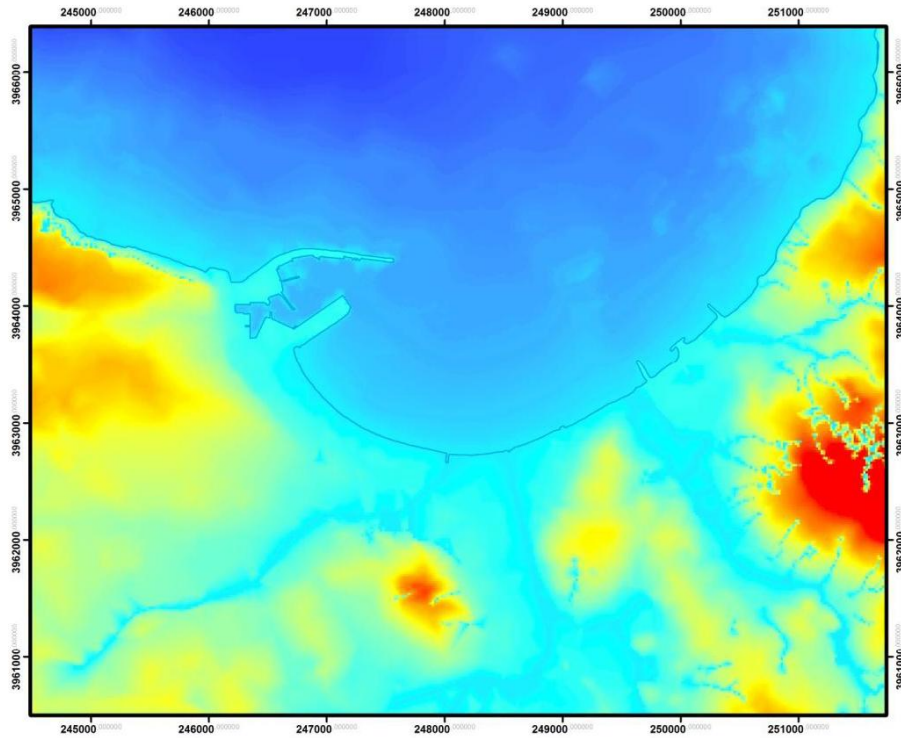


Figure 3.2.4. High-resolution DTM (Digital Terrain Model) of 10 m used in inundation modelling.

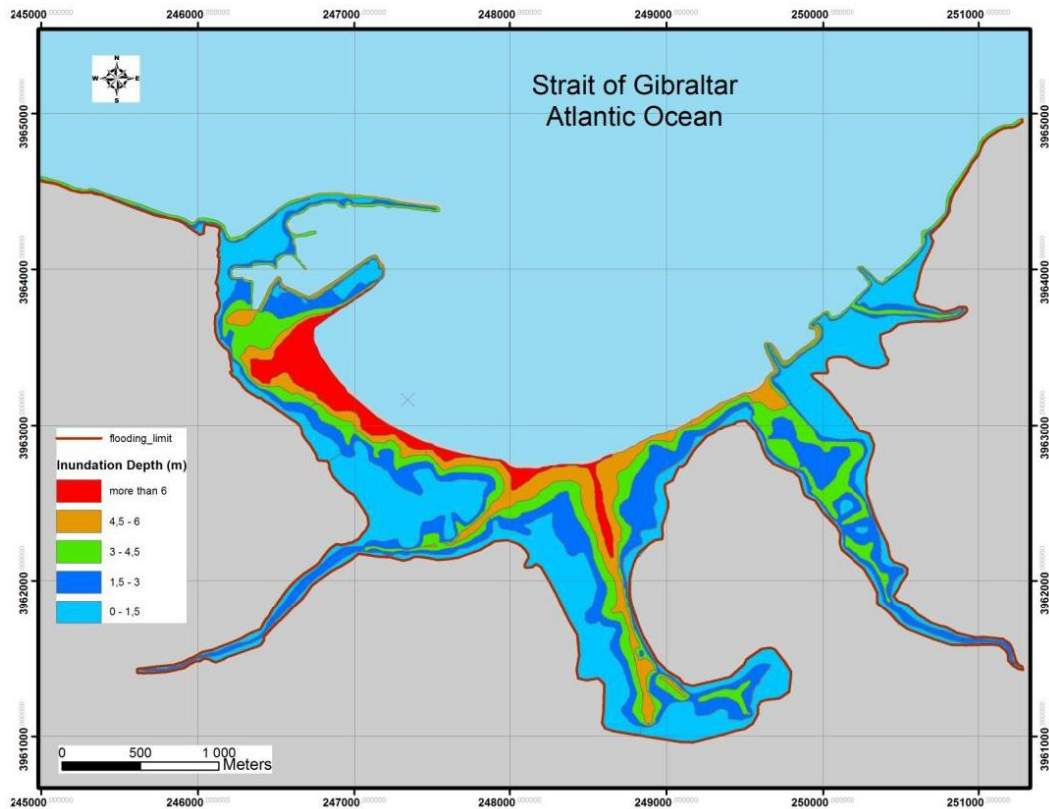


Figure 3.2.5. Inundation map considering the Cadiz Wedge scenario as the most credible earthquake tsunami source

The results of inundation modeling are illustrated in figure 3.2.5. The map displays the predicted maximum flow depths and the horizontal distance inundation following the occurrence of the Cadiz Wedge earthquake scenario assumed to trigger the worst tsunami impact at the coastal areas of

Tangier. Along the coastline, tsunami flow depths range from 1 m to more than 6 m with significant flooding along the sandy beach. The Tangier-City harbor is completely flooded with an inundation depth around 3 m. This low value is due to the presence of sea defence structures (concrete tetrapods and sea walls). The maximum flow depths decrease progressively from the shoreline towards the inundation limit where only a few centimeters of flood are computed. Along the flat topography areas of the rivers, the maximum flow depths are relatively small, while maximum horizontal inundation distances are computed in these areas (1.8 to 2.7 Km). In the west side of the coastal zone, tsunami waves do not advance overland more than a distance of 30 m from the shoreline, this limited inundation distance is due to the presence of high topography (more than 20m) that prevent the penetration of tsunami waves. The maximum flow depth in these zones reaches about 4 m near-shore.

Building vulnerability assessment

In order to make an inventory of the buildings positioned in the inundated zone along the coastal areas of Tangier, a field survey was accomplished to the study area. Seven types of buildings were distinguished according to their structural characteristics.

- Type1: 0 level masonry constructions with thin reinforced concrete (RC) frames and roofs made up by sheets of crumpled metal. They represent harbor and industrial buildings, most of them are hangars used for storing merchandises.

- Type 2: 0 to 1 level constructions with RC columns and infill masonry walls. At their side located in front of the sea they are characterized by glasses sustained by thin wood or metal frames. These constructions are located along the beach in front of the bay. They represent restaurants, cafes, clubs and discos.

- Type 3: 0 rarely 1 level constructions with RC columns and infill masonry walls. They constitute religious buildings (Mosques).

- Type 4: old buildings that were restored and partially rebuilt with concrete reinforcement mixing with the original traditional materials. They have 2 to 4 levels.

- Type 5: individual buildings with 1 or 2 levels. Constructed with RC frames and masonry infill walls. The beams and columns are sub-standard of small sections lightly reinforced with plain bars. Most of them are villas or individual dwellings.

- Type 6: engineered RC buildings. Most of these constructions are built according to the Moroccan seismic building code (RPS 2000: Règlement de construction ParaSismique). These buildings represent collective residential units. They are rarely used for administrative or commercial aims. They have 3 to 5 levels.

- Type 7: multi-storey new buildings (more than 5 levels). These constructions are well designed with strong RC columns and beams. These buildings are used throughout for habitation, their ground floors mostly have commercial use.

In order to be compatible with the classification adopted in the SCHEMA project, the identified building types were grouped into different classes or subclasses as described in Table 3.2.1. This classification is based on structural characteristics or intrinsic factors of the building, like construction materials, number of floors (height of building), conditions of the ground soil and design of the buildings. The distinguished buildings types were assigned to different building classes, from Class A to class G, according to their resistance properties (Fig.3.2.6).

In order to establish the vulnerability map, we used Arc GIS tool. Buildings were digitized using aerial photos with 40cm resolution in polygon features. Individual buildings or houses were identified according to their colors, shapes, sizes or shadows. Sometimes, it was difficult to identify individual buildings, especially when they were imbricated and small in sizes. In such a case, we digitized a block of homogeneous buildings that we considered as a single building. According to the SCHEMA requirement methodology, the polygon features are converted into a shapefile of points located at the center of each polygon.



Figure 3.2.6. Examples of constructions indicating different building vulnerability classes at the city of Tangier.

The map in Fig 3.2.7 shows the spatial distribution of building vulnerability classes in the potentially flooded areas of Tangier. This map shows that most of the buildings belong to the E2 class (262 entities, Fig .3.2.8) which correspond to well-constructed building, newly constructed and located along the coastal area. This class is considered as the most resistant. The second class (180 entities) is represented by buildings of class C. Most of them constitute individual villas or buildings corresponding to restaurants and cafés located in front of the bay. Buildings of Class E1 and F are moderately represented. They correspond to residual or collective buildings made with reinforced concrete and to industrial buildings, respectively. A large number of these latter are located in the vicinity of the harbor. The vulnerable buildings of class B (51 entities) are relatively unfrequent. They consist of old houses which have been restored, while their structures have been reinforced. Finally, 3 religious buildings (mosques) belong to Class G.

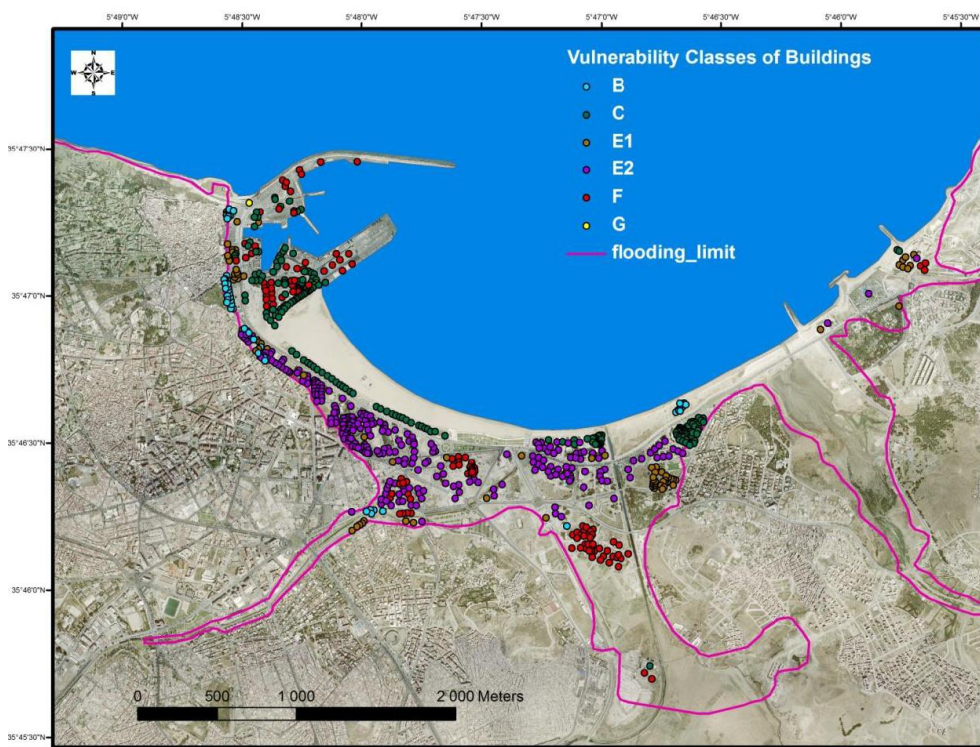


Figure 3.2.7. Spatial distribution of buildings vulnerability at the coastal zone of Tangier

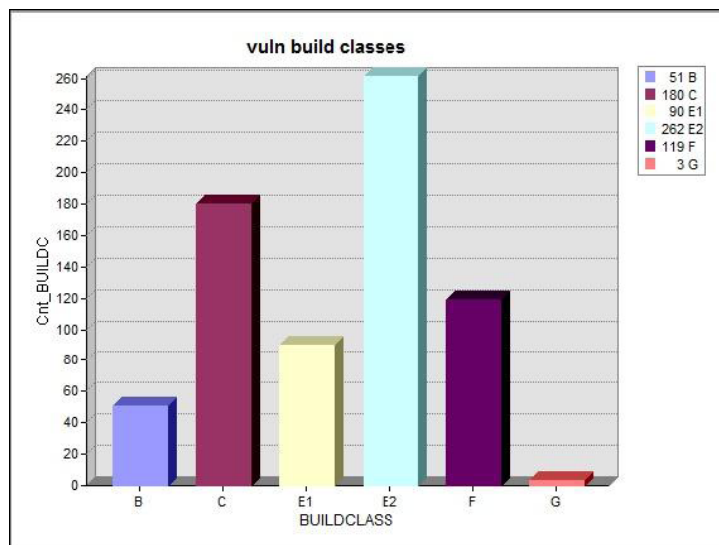


Figure 3.2.8. Number of buildings according to different classes of vulnerability.

The damage map of the buildings located in the flooded zone was established by intersecting the building vulnerability map and the inundation map using Arc GIS DamASCHE tool (Fig.3.2.9). Applying the damage matrix, a damage level was attributed to each building from D0 (no damage) to D5 (total collapse) according to the damage scale (table 3.2.2). The results indicate that 133 buildings will suffer minor damage D1, most of them correspond to Class E1. These buildings are well designed and constructed with RC structures. So they resist well to hydrodynamic forces. Then, 43 units will undergo important damage D2, most of them belong to class C and are located in the Tangier-Ville harbor or in its vicinity. Buildings located in front of the bay (78 units) will experience heavy damage (D3 and D4). Structural damages will affect the buildings stability with partial collapse of floors and excessive scouring because of the high values of water depth in these zones. Finally, complete collapse is expected for 15 buildings within the high flooded zone. They are located either along the beach and correspond to class B buildings (more vulnerable) or line up in the first range in front the sea, although they belong to class C.

The damage map shows also that many buildings (355 units) have no damage level assigned. This is due to the lack of a damage function for the building classes E2, F and G identified in the study area.

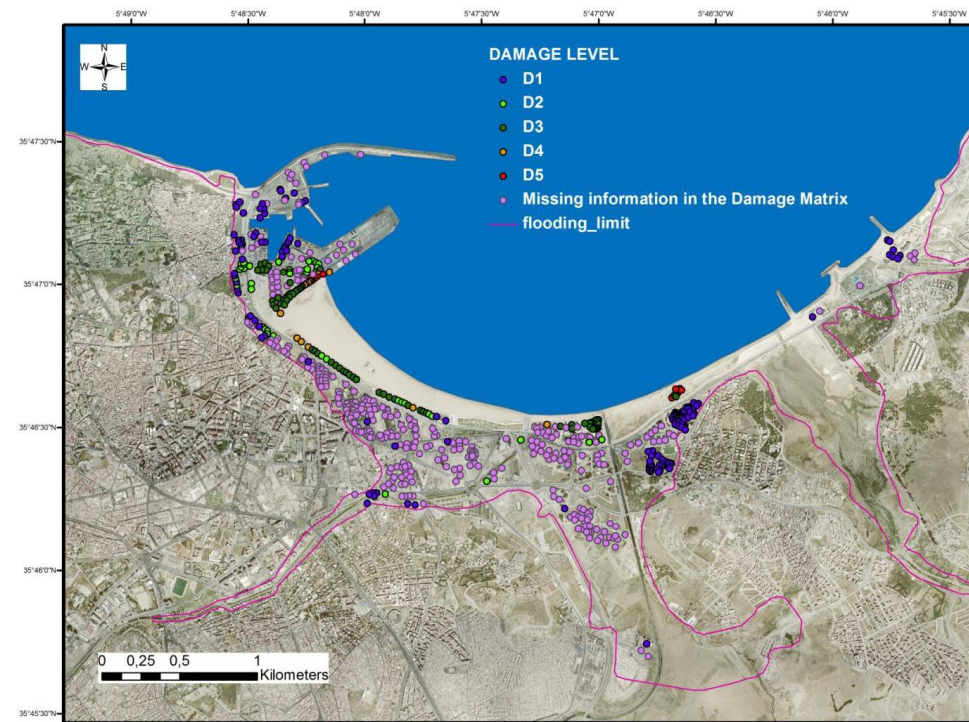


Figure 3.2.9. Map displaying the level of damage to buildings caused by the most credible earthquake tsunami impact along the bay of Tangier

3.2.3 Comparison of the results

In this work, we assess tsunami impact and vulnerability in the test site of Tangier. The result of the building vulnerability based on the SCHEMA approach is presented in a damage map which indicates the expected damage level for each building located in the flooded area. This map shows that buildings with high level of damage (D3 and D4) are located in the first line along the coastal zone in front of the bay and in the city harbor. This is due to the high values of inundation depth computed in these zones. Buildings constructed with RC structures (Class E1) present a low damage level (D1) and have a high degree of resistance. Recently, another study for investigating tsunami impact and vulnerability has been carried in Tangier harbor and surroundings areas (Bencheckroun et al., 2013) using an approach based on multi criteria GIS analysis combined with the tsunami hazard map. The results of this study were relatively similar to the ones obtained in our study. Most vulnerable structures are located in the city harbor and along the sandy beach due to significant values of inundation depths. The differences between the two damage maps concern E2 and F building classes for which no damage level was attributed in the SCHEMA approach because of the absence of suitable damage functions for these structures, while Bencheckroun et al. (2013) showed that for the E2 class, which are multi-level RC buildings, belong to medium and low vulnerability level and for class F, which are harbor and industrial buildings, they belong to a high vulnerability level.

For the Tangier test site, the main limitation of the SCHEMA approach is the large number of buildings in the impacted area which correspond to missing information in the damage matrix and thus, no damage level could be allocated to these structures.

3.2.4 References

- Atillah A., El Hadani D., Moudni H., Lesne O., Renou C., Mangin A., Rouffi, 2011. Tsunami vulnerability and damage assessment in the coastal area of Rabat and Sale, Morocco. *Nat. Hazards Earth System Sci.*, 11, 3397–3414.
- Baptista MA, Miranda J.M., Omira R., Antunes C. 2011. Potential inundation of Lisbon downtown by a 1755-like tsunami. *Nat. Hazards Earth Syst. Sci.*, 11, 3319-3326.
- Benchekrout S., Omira R., Baptista M. A., El Mouraouah A., Iben Brahim A., Toto E. A., 2013. Tsunami impact and vulnerability in the harbor area of Tangier, Morocco, *Geomatics, Natural Hazards and Risk*, DOI: 10.1080/19475705.2013.858373.
- DamASCHE: Damage Assessment SCHEMA tool for ArcGIS. User Manual SCHEMA Scenarios for Hazard-induced Emergencies Management Specific Targeted Research Project Space Priority. Project n° 030963.
- Garcin M., Prame B., Attanayake N., De Silva U., Desprats J. F., Fernando S., Fontaine M., Idier D., Lenotre N., Pedreros R., Siriwardana, 2007. C. H. E. R.: A Geographic Information System for Coastal Hazards. Application to a pilot site in Sri Lanka (Final Report), BRGM Open file BRGM/RP-55553-FR, 124 pp.
- Gardi A., Valencia N., and Sheer S., 2009. WP3.3 – GIS conceptual model and processing for production of elements required for test sites scenarios, Deliverable 3.1 part II, SCHEMA project.
- Gutscher M-A, Baptista M. A, Miranda J. M., 2006. The Gibraltar Arc seismogenic zone (part 2): constraints on a shallow east dipping fault plane source for the 1755 Lisbon earthquake provided by tsunami modelling and seismic intensity. *Tectonophysics*, 426, 153–166.
- <http://bluedoorhotel.com/2012/04/05/tangier-is-getting-a-new-port-and-marina/>
- Kaabouben F., Baptista M. A., Iben Brahim A., El Mouraouah A., Toto A., 2009. On the Moroccan tsunami catalogue. *Nat. Hazards Earth System Sci.*, 9, 1227–1236.
- Leone F., Denain J.C., Vinet F., Bachri S. 2006: Analyse spatiale des dommages au bâti de Banda Aceh (Sumatra, Indonésie): contribution à la connaissance du phénomène et à l'élaboration de scénarios de risque tsunami, in: Scientific internal report of TSUNARISQUE programme (2005–2006), Délégation Interministérielle pour l'aide Post-Tsunami (DIPT), consortium francoindonésien, 306 pp., 2006.
- Leone F., Lavigne F., Paris R., Denain Jc., Vinet F., 2011. A spatial analysis of the December 26th, 2004 tsunami-induced damages: lessons learned for a better risk assessment integrating buildings vulnerability. *Appl Geogr.*, 31, 363–375.
- Liu PL-F, Woo S-B and Cho, Y-S., 1998. Computer programs for tsunami propagation and inundation. Technical report. Ithaca, NY: Cornell University.
- Omira R., Baptista M. A., Matias L., Miranda J. M., Catita C., Carrilho F., Toto E., 2009. Design of a Sea-level Tsunami Detection Network for the Gulf of Cadiz. *Nat. Hazards Earth System Sci.*, 9, 1327–1338.
- Peiris N., 2006, Vulnerability functions for tsunami loss estimation. First European conference on Earthquake Engineering and Seismology (a joint event of the 13th ECEE and 30th General Assembly of the ESC), Geneva, Switzerland, Paper number 1121.
- Scenarios for tsunami Hazard-induced Emergencies Management (SCHEMA) project, www.schemaproject.org.
- Tinti S., Armigliato A. 2003. The use of scenarios to evaluate the tsunami impact in southern Italy. *Marine Geology*, 199, 221-243.

Valencia N., Gardi A., Gauraz A., Leone F., Guillande R., 2011. New tsunami damage functions developed in the framework of SCHEMA project: application to European-Mediterranean coasts, *Nat. Hazards Earth System Sci.*, 11, 2835–2846.

Zitellini N., Gracia E., Matias L., Terrinha P., Abreu M. A., Dealteris G., Henriot J. P., Danobeitia J. J., Masson D. G., Mulder T., Ramella R., Somoza L., Diez S., 2009. The quest for the Africa–Eurasia plate boundary west of the Strait of Gibraltar. *Earth Planet Sci. Lett.*, 280(1–4), 13–50.

3.3 *Colonia Sant Jordi*

3.3.1 Description of the site

Colònia Sant Jordi test site covers an area of about 266 km² located some 55 km southeast of Palma de Mallorca. The site, located between 39°14'N and 39°21'N, and between 2°59'E and 3°11'E, represents the southwestern tip of Mallorca Island, in the Autonomous Community of Illes Balears (Balearic Islands), Spain (Fig. 3.3.1). It partially includes the municipalities of Ses Salines and Santanyí. Ses Salines municipality has an area of 39.12 km² and a total population of 5050 inhabitants (Instituto Nacional de Estadística, 2014), of which 2900 (2011) live in the coastal town of Colònia San Jordi (Fig. 3.3.1). Santanyí municipality has an area of 124.86 km² and a total population of 11636 inhabitants (Instituto Nacional de Estadística, 2014), of which the coastal developments of Cala Figuera, Cala Santanyí (Fig. 3.3.1) and Cala Llombards account for 614, 487 and 304 (2006), respectively. Cape Ses Salines is located in the southernmost tip of the area.

Nevertheless, with its approximately 30 km of coastline, this test site has a strong seasonal variability in population, with a considerable increment during summer months due to its touristic development. Its crowded beaches and several sea side facilities, such as leisure harbours and tourism infrastructure, notably increase the population exposure in this site. For example, a total of 99482 overnight stays by 12741 tourists took place in July 2008 only in Ses Salines municipality (Instituto Nacional de Estadística, 2008). Popular beaches included in our study area are: Es Trenc, Es Port, Es Dolç, Es Carbó and Ses Roquetes in the municipality of Ses Salines, and Cala en Tugores, Es Caragol, Cala Llombards and Cala Santanyí in the municipality of Cala Santanyí. Those beaches nearby the main towns usually offer some services, including nearshore bars and restaurants. Fishing and leisure ports are located in Cala Figuera (111 berths) and Colònia Sant Jordi (315) (Ports de les Illes Balears, 2014), although in summer time unofficial berthing takes places in many of the pocket beaches. Colònia Sant Jordi port serves as a base for touristic activities to Cabrera islands National Park to the south. Further inland, the populations of Ses Salines and Santanyí are the main administrative centers of the area.

Morphologically, this region includes two main domains east and west of Cape Ses Salines. To the west, the site is occupied with lowlands (<10 m), with a coastal strip made of relatively long sandy beaches or low rocky cliffs less than 1-3 m high. Beyond the coastal strip far from the towns, the area is mainly unpopulated with dune-like deposits, low vegetation and scrubland, farmland and occasional small farms, and also relatively large ponds (Estany de Ses Gambes) laying at sea level. To the east of Cape Ses Salines, the area displays higher topographies (40-60 m), with a coastal strip made of 20-30 m high rocky cliffs interrupted occasionally by low-lying ria-like bays. Cala Santanyí (Fig. 3.3.1) is one of these embayments, highly sensible to sea-level oscillations.

The submerged area around Colònia Sant Jordi test site is occupied by a narrow continental shelf (8-13 km) ending in an abrupt continental slope. The Balearic Islands were affected by the tsunami triggered by the Zemmouri-Boumerdes earthquake on May 21st2003. More than 200 boats sank or grounded, and the tsunami damaged coastal and harbour infrastructures. Some seaside shops and restaurants were flooded, as well as local roads. Luckily no human lives were lost, probably due to low exposure caused by time and date of the event. This tsunami evidenced that this area is directly exposed to tsunami waves generated by earthquakes in the North African margin, in particular the Algerian margin, as well as by other sources such as landslides in the surrounding continental margins. Three other tsunamis originating from the North African margin have impacted the Balearic Islands in historical times (1756, 1856, 1980), with inundations reported in Cala Santanyí in 1756, when sea water entered ~5 km inland. Imbricated boulder fields (~20 t per single boulder) occur along the coastline from Colònia Sant Jordi to Cape Ses Salines, lying on the lower slopes as well as in the supratidal zone, on top of 1-3 m high cliffs. These have been identified as possible tsunami deposits, which have been radiocarbon dated at 500 BP and 1400 BP (Scheffers and Kelletat, 2004).

Due to this location in the path of tsunamis originating from the North African margin and from other distant sources, the study of this area is of great interest, also taking into account the comparatively large unaware floating population in summer months. Currently there is no land use or evacuation planning underway in Colònia Sant Jordi test site.

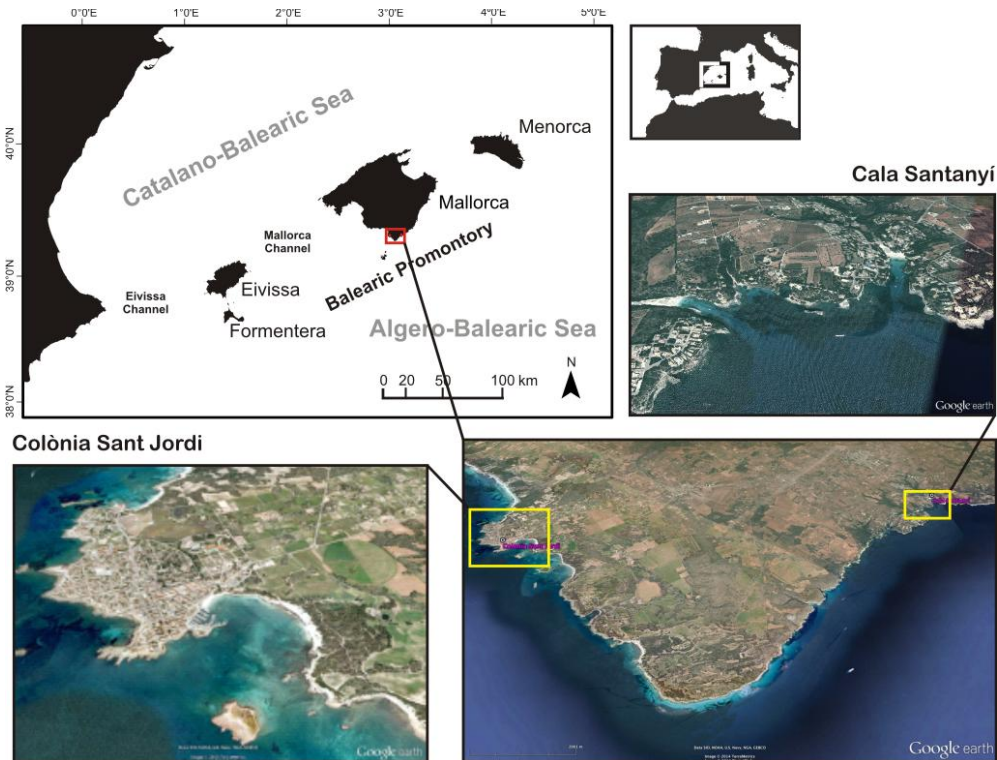


Figure 3.3.1. Colònia Sant Jordi test site: Location in the northwestern Mediterranean and satellite view (Google Earth image) of the site and its two main populations (Colònia Sant Jordi and Cala Santanyi).

Data sets available for applying tsunami exposure and vulnerability methods include:

- HR multibeam bathymetry and topographic data (Fig. 3.3.2).
- Location of urban areas, building and road network, obtained from cadastre (Fig. 3.3.3).
- Storey height of each building, obtained from cadastre (Fig. 3.3.4).
- Number of basement levels of each building, obtained from cadastre (Fig. 3.3.5).
- Minimum distance to coastline of each plot of land (Fig. 3.3.6).
- Minimum topographic height of each plot of land (Fig. 3.3.7).
- Location of special buildings or sensitive locations: schools, health centers and pharmacies, gas stations, town hall, beaches and port (Fig. 3.3.8).

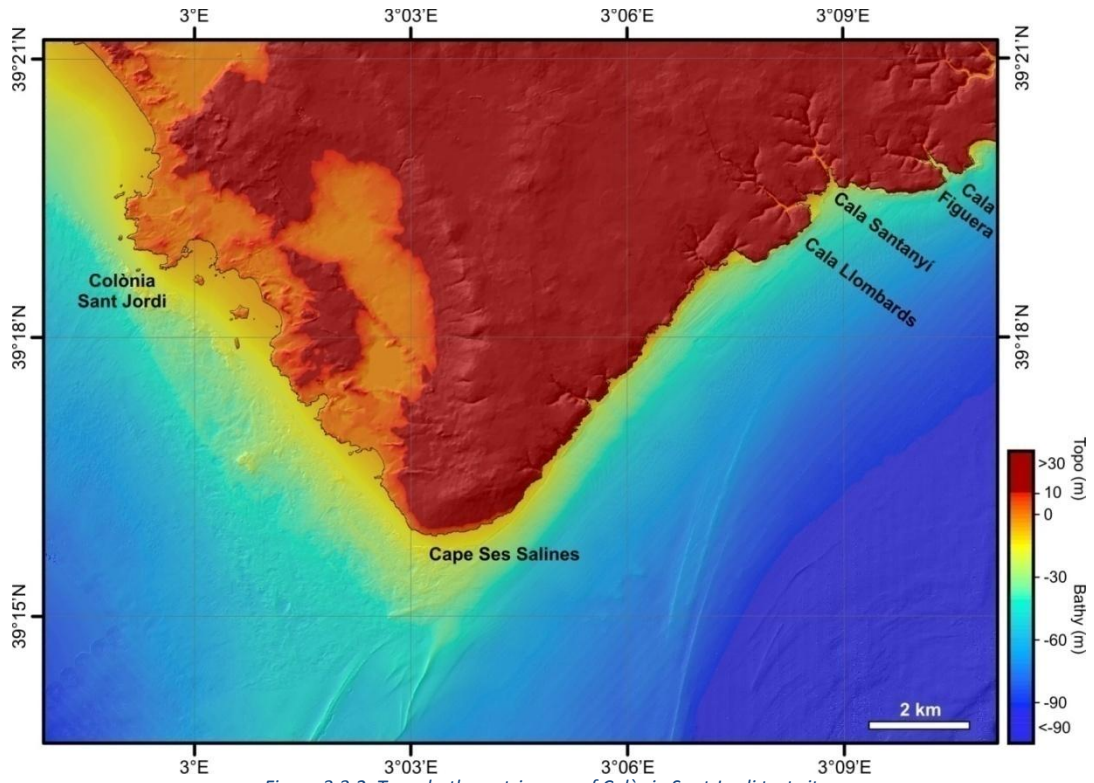


Figure 3.3.2. Topo-bathymetric map of Colònia Sant Jordi test site.

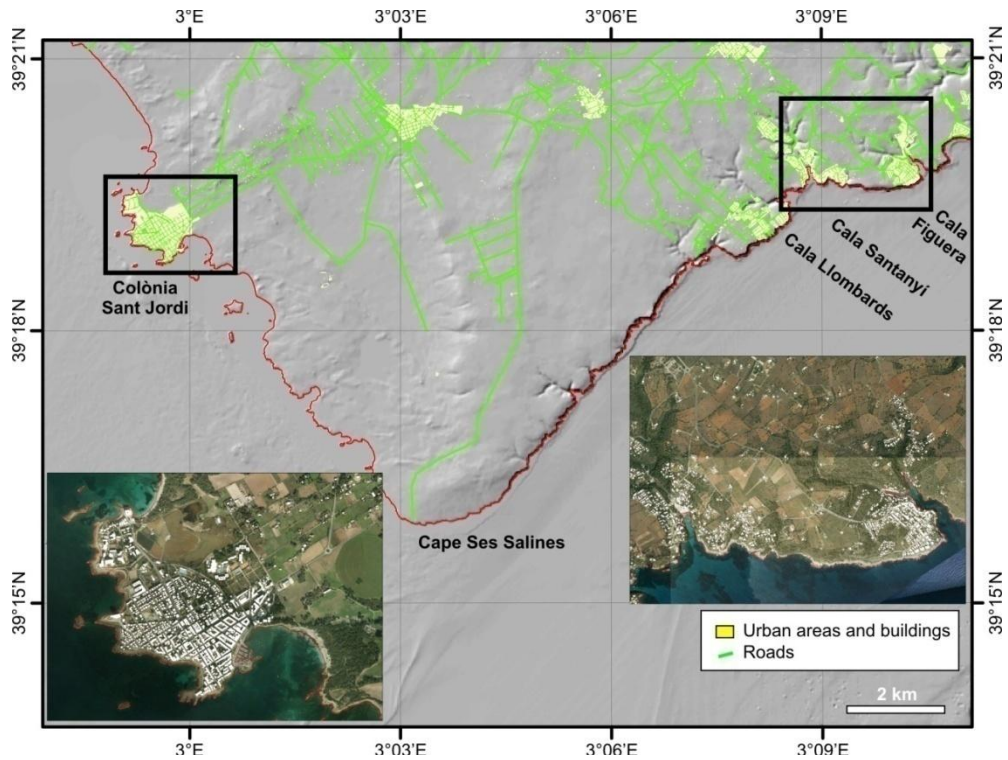


Figure 3.3.3. Location of urban areas, buildings and roads in Colònia Sant Jordi test site. Zooms to Colònia Sant Jordi and Cala Santanyi towns are provided, only indicating the location of buildings.

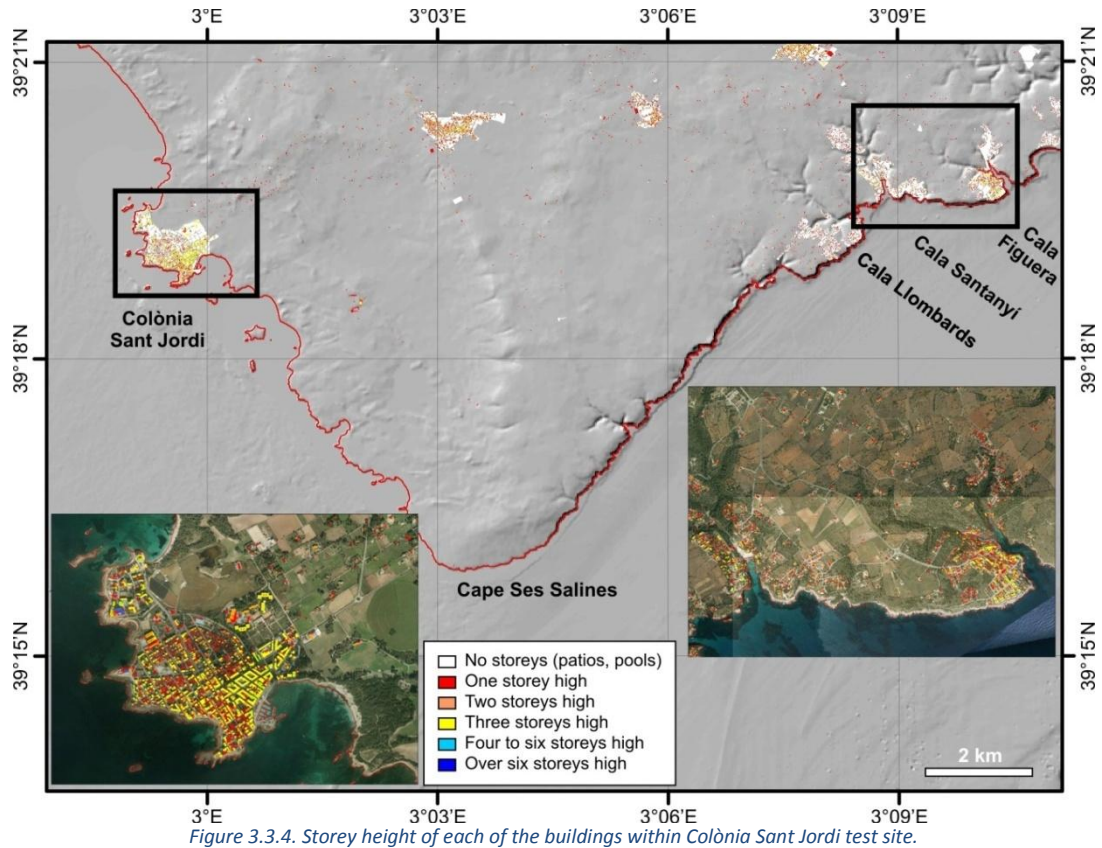


Figure 3.3.4. Storey height of each of the buildings within Colònia Sant Jordi test site.

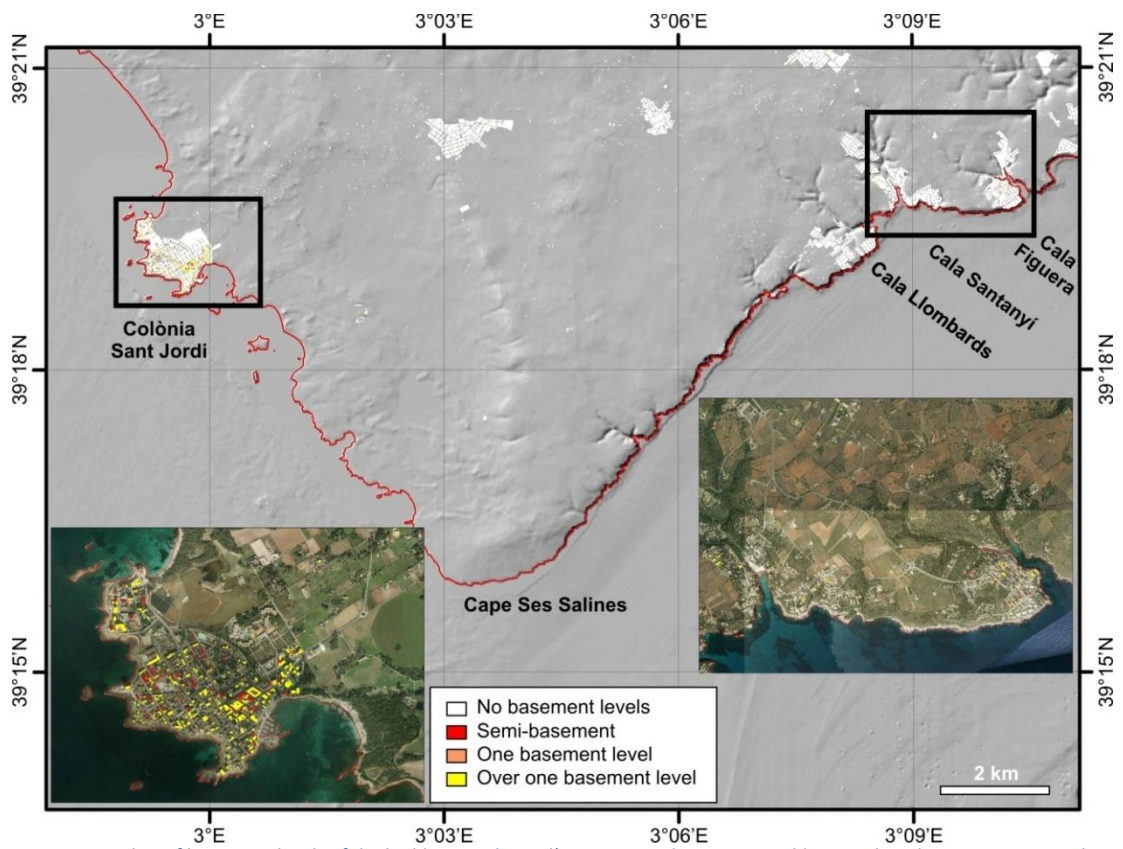


Figure 3.3.5. Number of basement levels of the buildings within Colònia Sant Jordi test site. Buildings with no basement are not depicted.

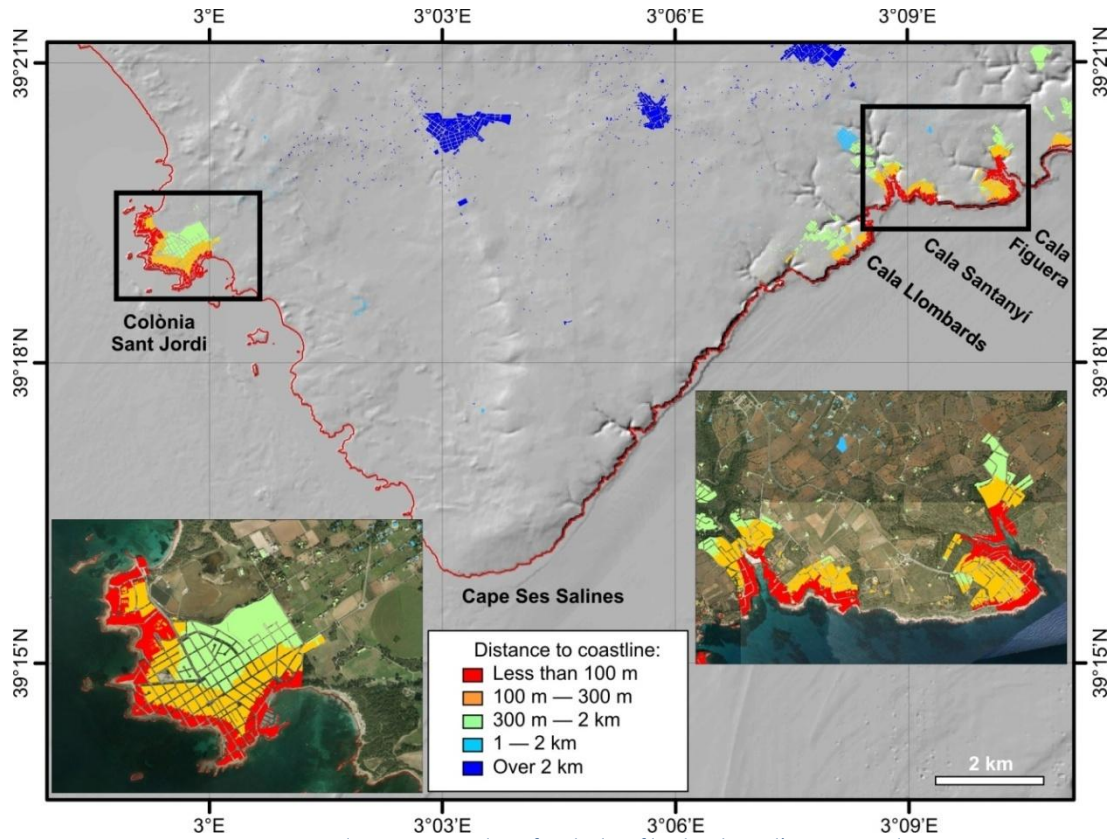


Figure 3.3.6. Minimum distance to coastline of each plot of land within Colònia Sant Jordi test site.

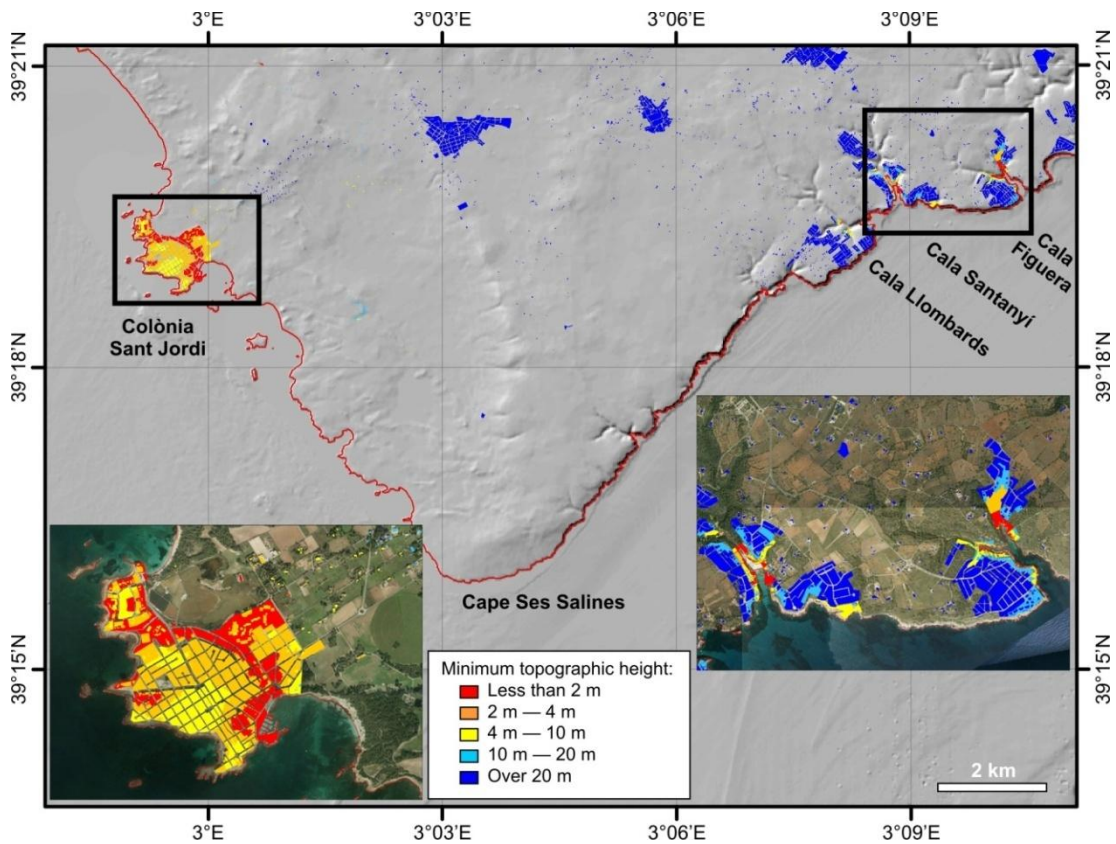


Figure 3.3.7. Minimum topographic height of each plot of land within Colònia Sant Jordi test site.

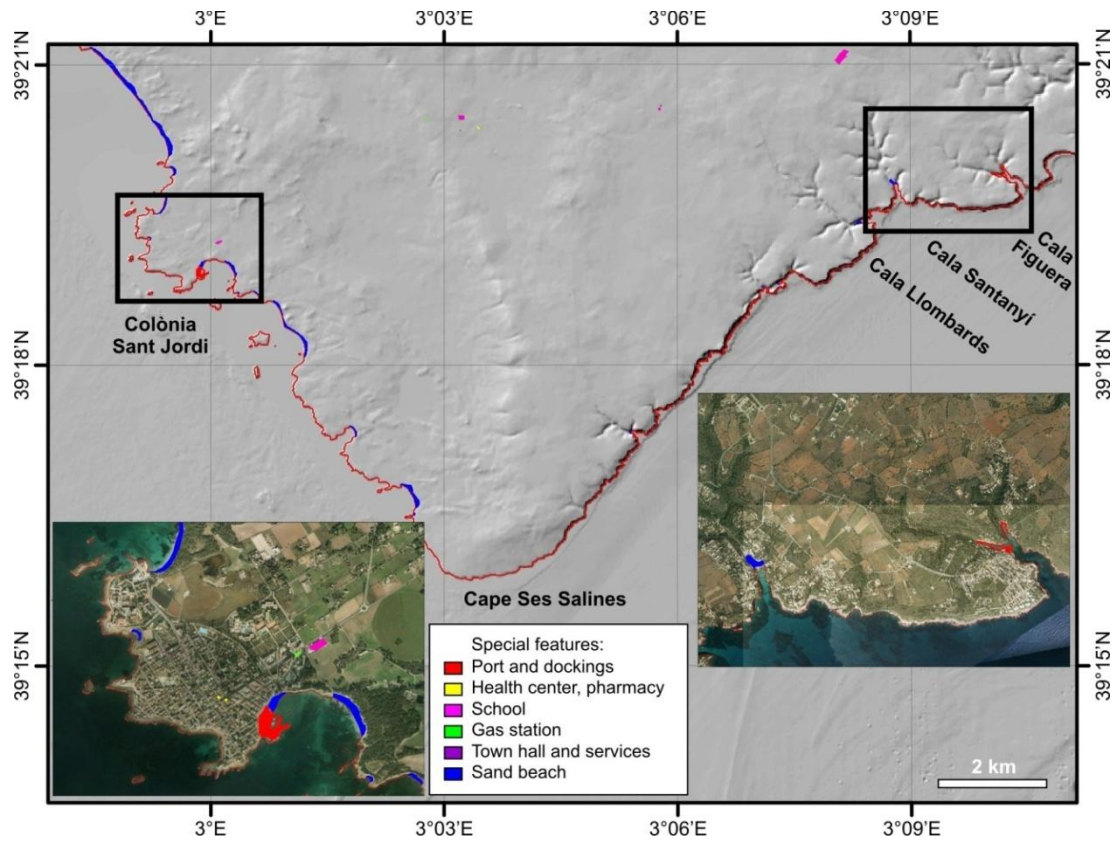


Figure 3.3.8. Location of special buildings in Colònia Sant Jordi test site.

3.3.2 PTVA-3

The PTVA-3 model (Papathoma Tsunami Vulnerability Assessment-Version 3) has been applied to Colònia Sant Jordi Test Site in order to assess the vulnerability of the structures located within the test site. Taking into account that not all data needed as an input to calculate the Relative Vulnerability Index (RVI) was available for the structures in the Test Site, we first explain how the model has been slightly modified in order to make the available data to be fitted in on the basis of the schema of Dall’Osso et al. (2009).

Relative Vulnerability Index has been calculated as $(RVI)=(2/3) \cdot (SV)+(1/3) \cdot (WV)$, where SV is the structural vulnerability, and WV is the vulnerability to water intrusion, scaled from 1 to 5. Structural vulnerability has been calculated as $(SV)=(Bv) \cdot (Ex) \cdot (Prot)$, where Bv are the building attributes, Ex is the depth of flood water where the building is located, and Prot is the degree of protection, all scaled from 1 to 5 as explained by Dall’Osso et al. (2009). The building attributes have been calculated as

$$(Bv)=(1/423) \cdot (100 \cdot s+80 \cdot m+63 \cdot g+60 \cdot f+51 \cdot mo+46 \cdot so+23 \cdot pc)$$

where s relates to the number of storeys, m relates to the construction material, g relates to the ground floor hydrodynamics, f relates to the foundation strength, so relates to the shape and orientation, mo relates to the movable objects, and pc relates to the preservation condition, all scaled from -1 to +1. The depth of flood water is calculated by $(Ex)=(TH)-(z)$, where TH is the expected tsunami maximum height and z is the minimum topographic height at which the building is located. The degree of protection is calculated by $(Prot)=(1/301) \cdot (100 \cdot br+73 \cdot nb+73 \cdot sw+55 \cdot w)$, where br relates to the building row, nb relates to the natural barriers, sw relates to the seawall height and shape, and w relates to the brick wall around the building, all scaled from -1 to +1. Finally, the vulnerability to water intrusion is calculated by $(WV)=(IL)/(LN)$, where IL is the number of inundated levels and LN is the number of levels (number of storeys plus basement levels). The number of inundated levels was determined by $(IL)=\text{ceil}((Ex)/2.5)$, being 2.5 m considered as the mean height of each level, and considering always $(IL) \leq (LN)$.

For Colònia Sant Jordi Test Site, building location and number of storeys (s) has been obtained for each building from the cadastre. Building material (m), ground floor hydrodynamics (g), slope and orientation (so) and preservation condition (pc) were unavailable, and have been fixed to 0 for all constructions. Foundations strength (f) has been related to the number of basement floors (Table 3.3.1), which was the only available related data. Regarding movable objects (mo), it has been determined that those buildings located in front of the port have higher probabilities of being impacted by movable objects (such as ships and small boats). Building row (br) has been related to distance to the coastline (Table 3.3.2). No natural barriers (nb) or seawalls (sw) exist in the Test Site, so all buildings were set to the lowest protection level regarding these two attributes. Since all plots have to be delimited, it has been considered that all buildings have a brick wall around building, so w was set to the highest protection level for all buildings.

Scaled building vulnerability and level of protection, which are not dependant of TH, are presented in Figs. 3.3.9 and 3.3.10. The only variable is TH, the expected tsunami maximum height, which was set to 1 m, 4 m, 8 m and 10 m (cf. Deliverable 8.8). For such values, scaled exposure and scaled vulnerability to water intrusion were calculated, and are presented, as an example for a TH of 4 m, in Figs. 3.3.11 and 3.3.12, respectively. RVI has then been calculated for all buildings in the Test Site for a TH of 1 m (Fig. 3.3.13), 4 m (Fig. 3.3.14), 8 m (Fig. 3.3.15) and 10 m (Fig. 3.3.16).

Table 3.3.1. Attributes influencing the structural vulnerability of a building (Bv).

Parameter	-1	-0.5	0	0.5	1
s (number of storeys)	Five or more	Four	Three	Two	One
m (material)	-	-	All buildings	-	-
g (ground floor hydrodynamics)	-	-	All buildings	-	-
f (foundations strenght)	One basement floor		Semi-basement		No basement
so (shape and orientation)	-	-	All buildings	-	-
mo (movable objects)	-	-	Other	Near port	-
pc (preservation condition)	-	-	All buildings	-	-

Table 3.3.2. Attributes influencing the level of protection of a building (Prot).

Parameter	0	0.25	0.5	0.75	1
br (building row)	>600 m from coast	250-600 m from coast	125-250 m from coast	75-125 from coast	<75 m from coast
nb (natural barriers)	-	-	-	-	All buildings
sw (seawall height and shape)	-	-	-	-	All buildings
w (brick wall around building)	All buildings	-	-	-	-

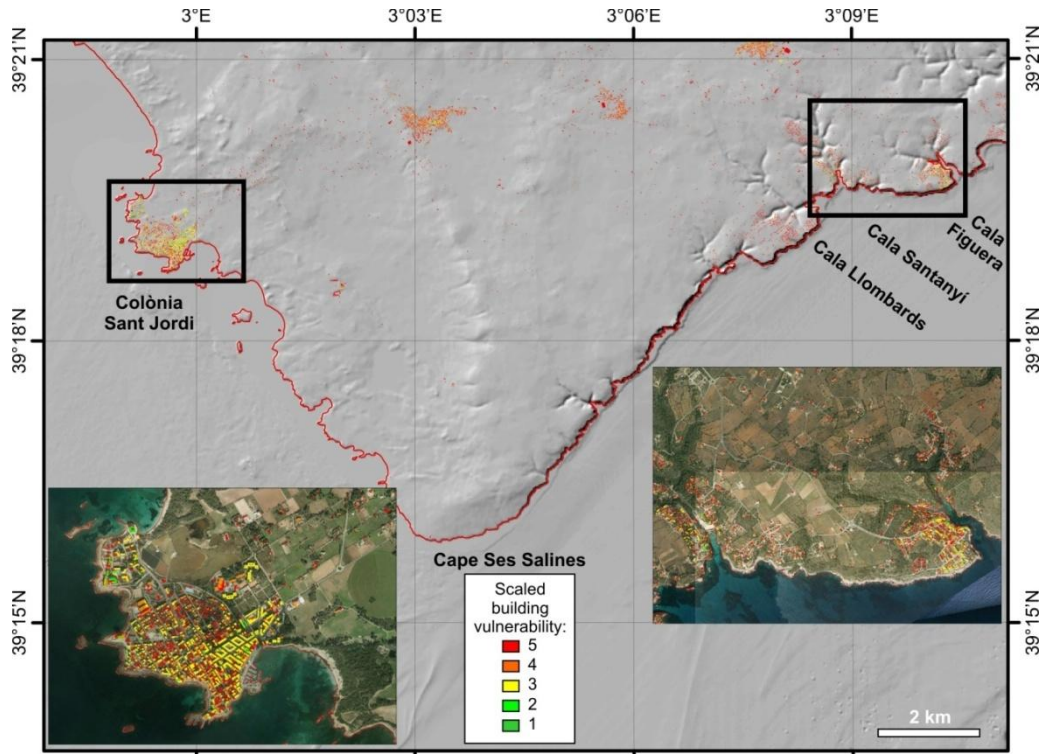


Figure 3.3.9. Scaled building vulnerability for Colònia Sant Jordi test site. Higher values indicate an increase of the average building vulnerability.

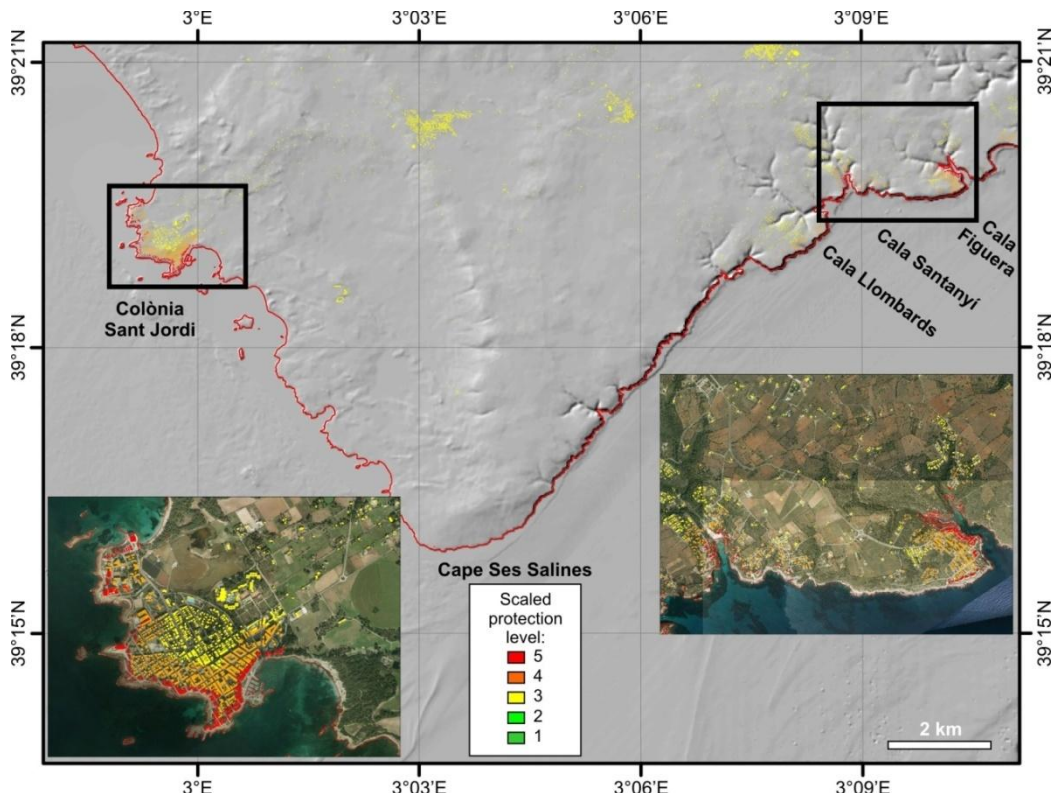


Figure 3.3.10. Scaled protection level of each building within Colònia Sant Jordi test site. Higher values indicate a lesser level of protection.

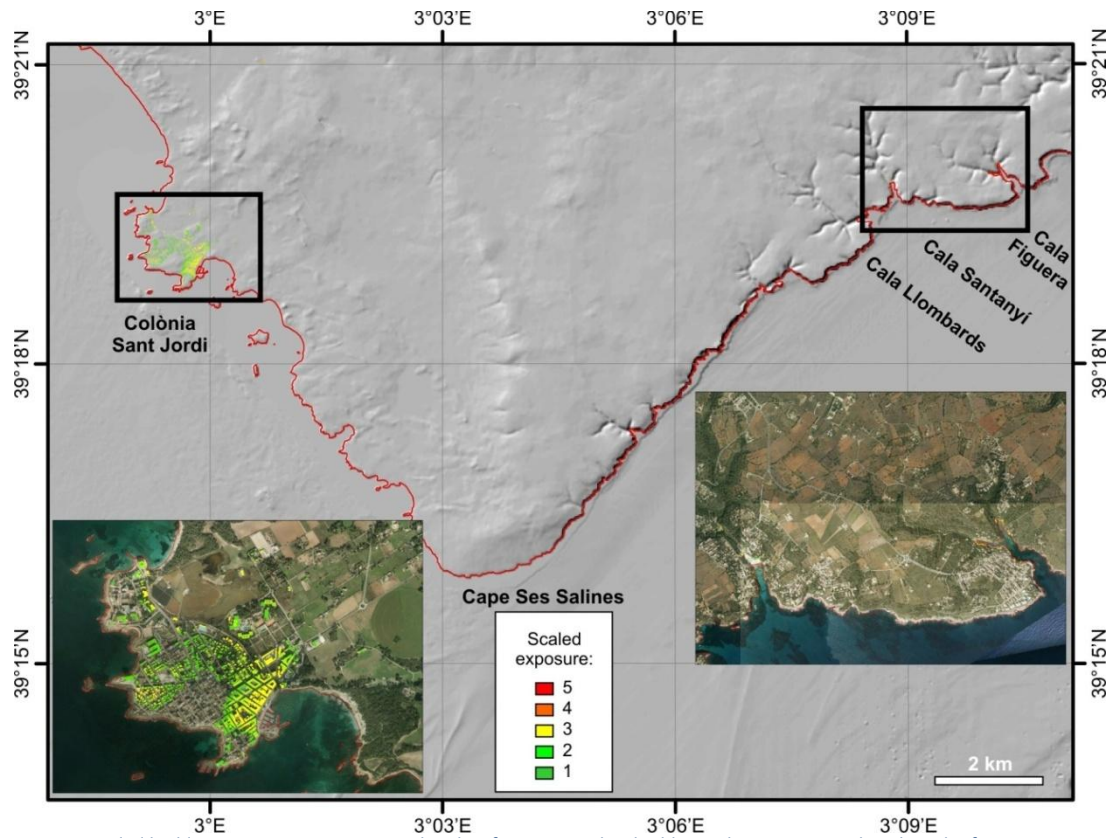


Figure 3.3.11. Scaled building exposure to a tsunami height of 4 m. Note that buildings above a topographic height of 4 m are not exposed.

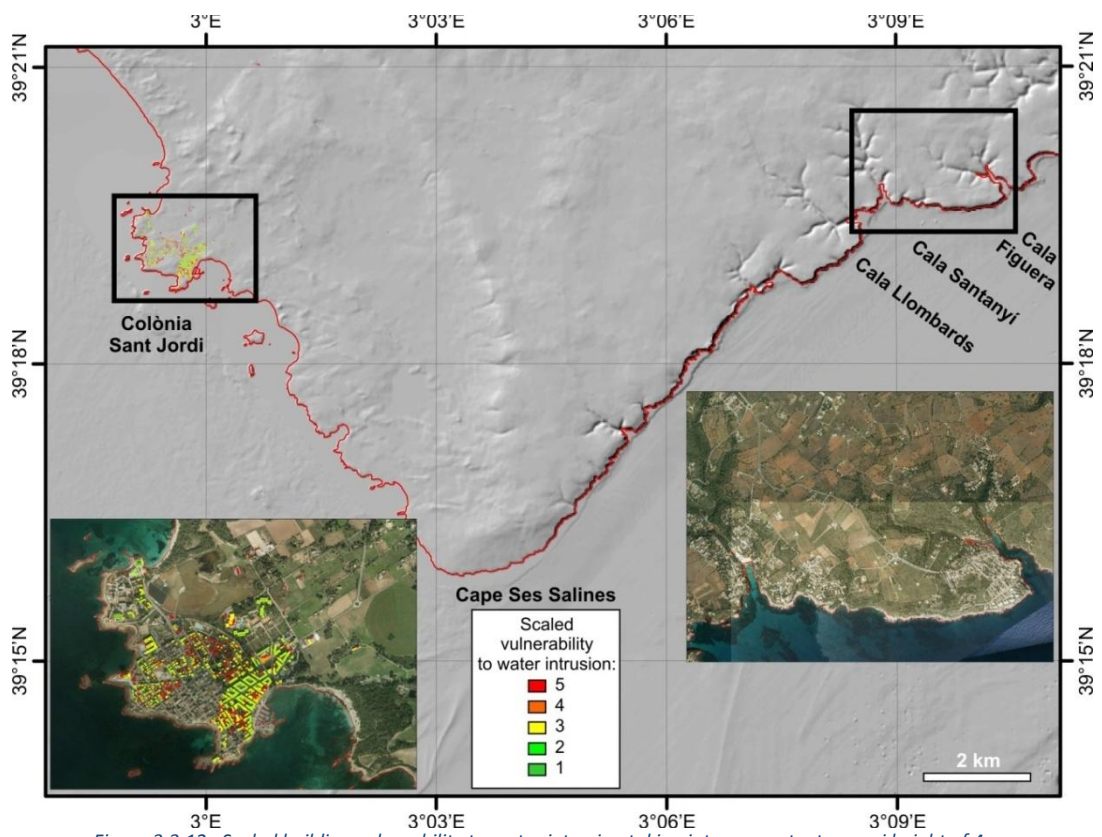


Figure 3.3.12. Scaled building vulnerability to water intrusion taking into account a tsunami height of 4 m.

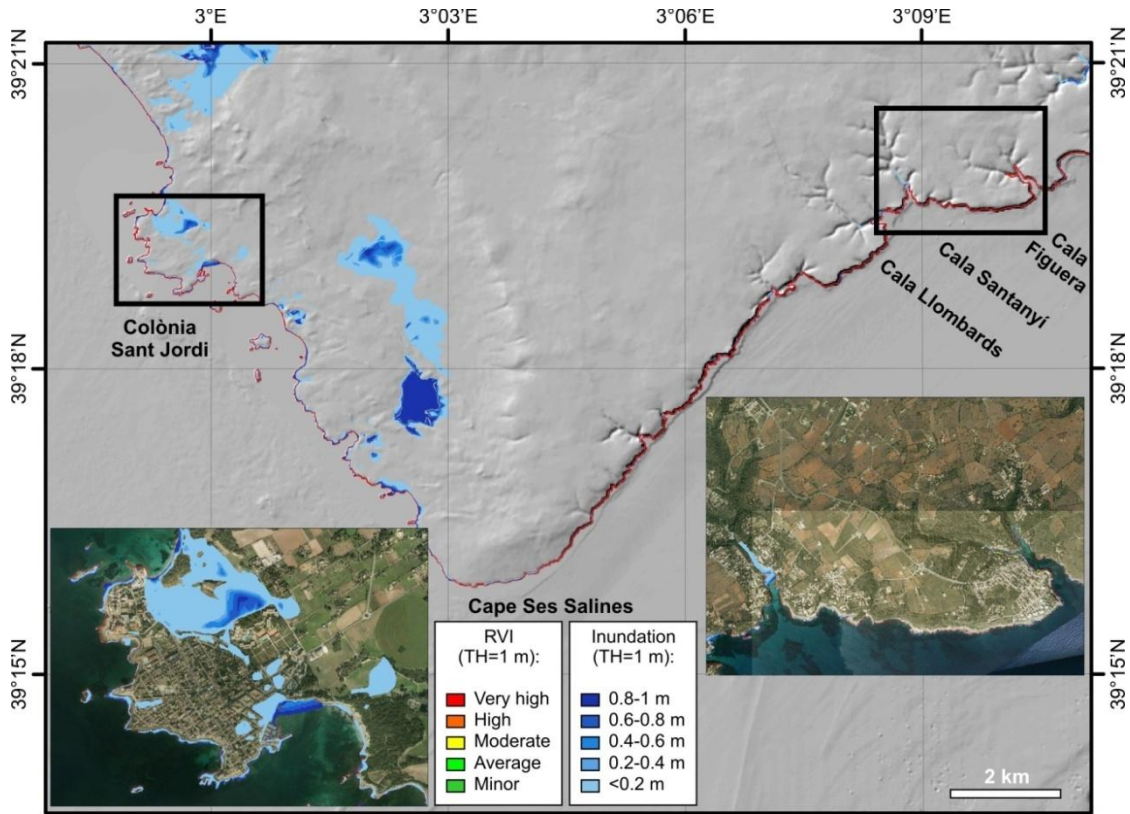


Figure 3.3.13. Scaled building vulnerability to water intrusion taking into account a tsunami height of 1m.

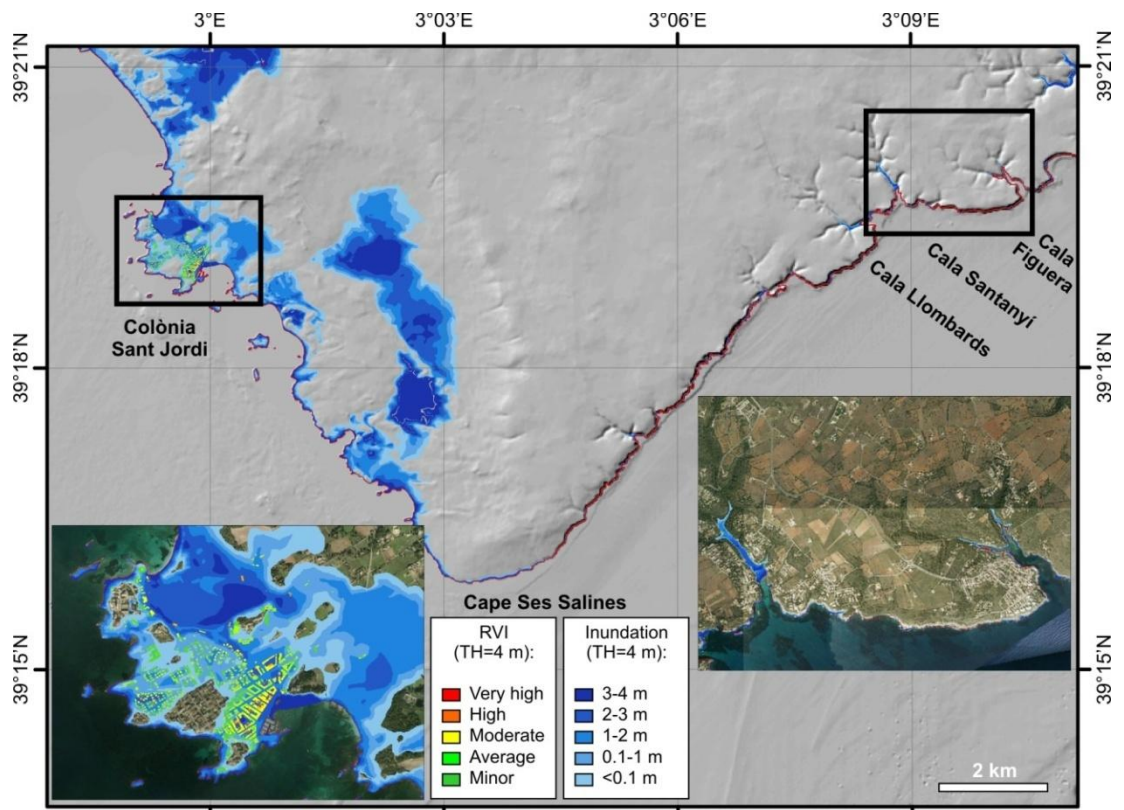


Figure 3.3.14. Scaled building vulnerability to water intrusion taking into account a tsunami height of 4m.

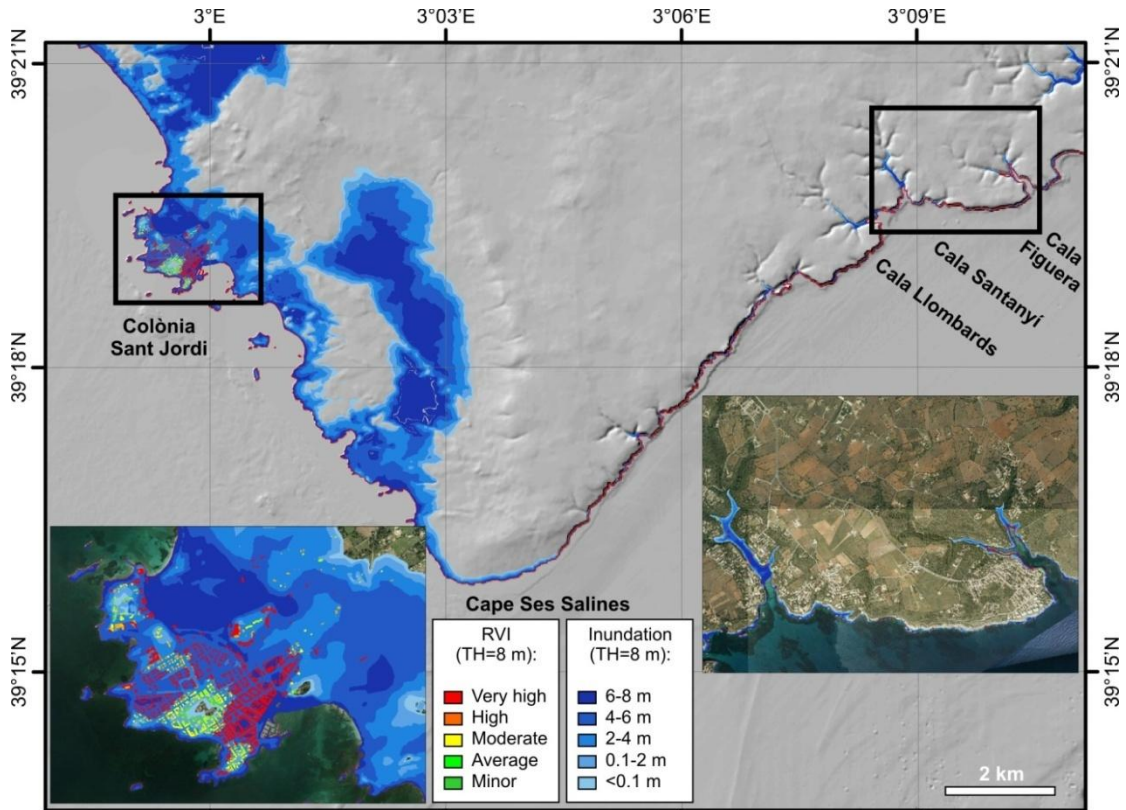


Figure 3.3.15. Scaled building vulnerability to water intrusion taking into account a tsunami height of 8m.

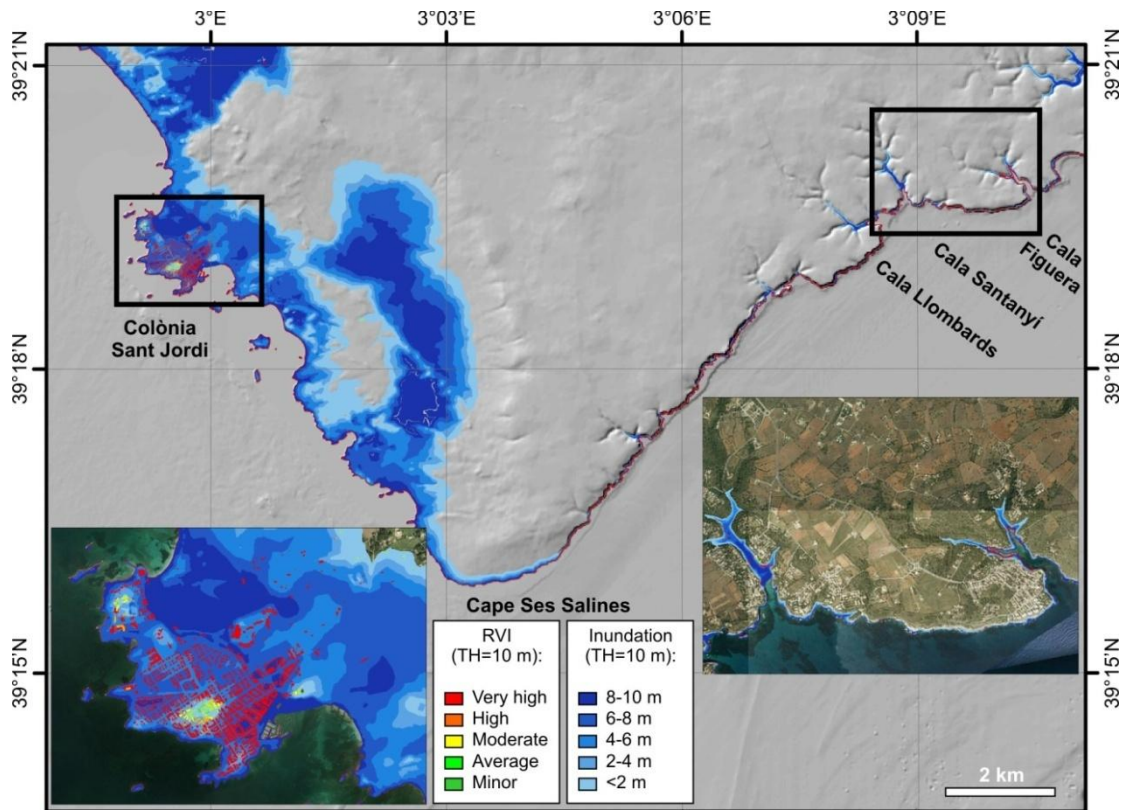


Figure 3.3.16. Scaled building vulnerability to water intrusion taking into account a tsunami height of 10m.

The results of the application of PTVA-3 model to Colònia Sant Jordi Test Site indicate that very few structures are vulnerable in the area for a tsunami height below 1 m, with the exception of the port of the town of Colònia Sant Jordi and few buildings within the first meters of the coastline in Cala Santanyí and Cala Figuera. Increased tsunami heights increase the vulnerability of the first-line buildings in front of Colònia Sant Jordi port, which were the main tourist activities take place in the town (restaurants and pubs). Higher tsunami waves would have dramatic effects to the town. Due to the topographic configuration, Cala Santanyí and Cala Figuera buildings would be better protected from tsunami impact, but it has to be taken into consideration that such topographic configuration could create resonance effects that in turn would aggravate tsunami height. In addition, this modelization does not take into consideration beach vulnerability.

3.3.3 SCHEMA

The SCHEMA (Scenarios for tsunami Hazard-induced Emergencies Management) model has been applied to a limited area of Colònia Sant Jordi town within Colònia Sant Jordi Test Site in order to compare the results of the vulnerability assessment of the structures with PTHA-3 model. Structures have been classified following an adapted version of the building typology classification proposed by Tinti et al. (2011), based on satellite imagery and building characteristics. Accordingly, six types of buildings were defined: class A represents very light constructions in the beach or sea front, made of wood, timber, or relatively light materials (for example, restaurants under glass pergolas in the sea front); class C1 are individual small villas mostly made of brick with reinforced column and masonry filling; class D are either individual large villas or 1-3 levels high attached old residential buildings made of brick or not reinforced concrete; class E1 are 1-3 levels high attached modern residential or commercial buildings with reinforced concrete; class E2 are more than 3 levels high residential or commercial buildings; class F are harbour buildings, although in this case these could also be classified as C1.



Figure 3.3.17. Building typology in a limited area within Colònia Sant Jordi test site.

Damage matrix adopted is based on Tinti et al. (2011) and presented in Table 3.3.3. Damage values for type E2 buildings have been established tentatively based on E1, but it has to be taken into account that no empirical laws of average damage have been calculated for this class in previous studies.

Table 3.3.3. Damage matrix adapted for Colònia Sant Jordi test site. Values of the flow depth are given in meters.

Damage level	A	C1, F	D	E1	E2
D0 (no damage)	0	0	0	0	0
D1 (light damage)	0-1.8	0-2.5	0-2	0-3	0-3
D2 (important damage)	1.8-2.2	2.5-4	2-4.5	3-6	3-8
D3 (heavy damage)	2.2-2.6	4-6	4.5-6.5	6-9.5	8-12
D4 (partial collapse)	2.6-3.8	6-8	6.5-9	9.5-12.5	12-16
D5 (total collapse)	>3.8	>8	>9	>12.5	>16

Since flow depth for a tsunami wave height TH=1 m is extremely limited, damage scenarios for Colònia Sant Jordi have been calculated for tsunami wave heights of TH=2 m (Fig. 3.3.18), TH=4 m (Fig. 3.3.19), TH=8 m (Fig. 3.3.20) and TH= 10 m (Fig. 3.3.21).

It has to be noted that results highly rely on the exactitude of the topographic grid used to compute the scenarios. Note, for example, the class “A” building located on the beach across the bay east of Colònia Sant Jordi. Although that building, a small wooden hut used as a small bar on the beach is located at less than 1 m above sea level, only light damage is calculated for a tsunami of 4 m wave height, probably due to an incorrect topographic value.

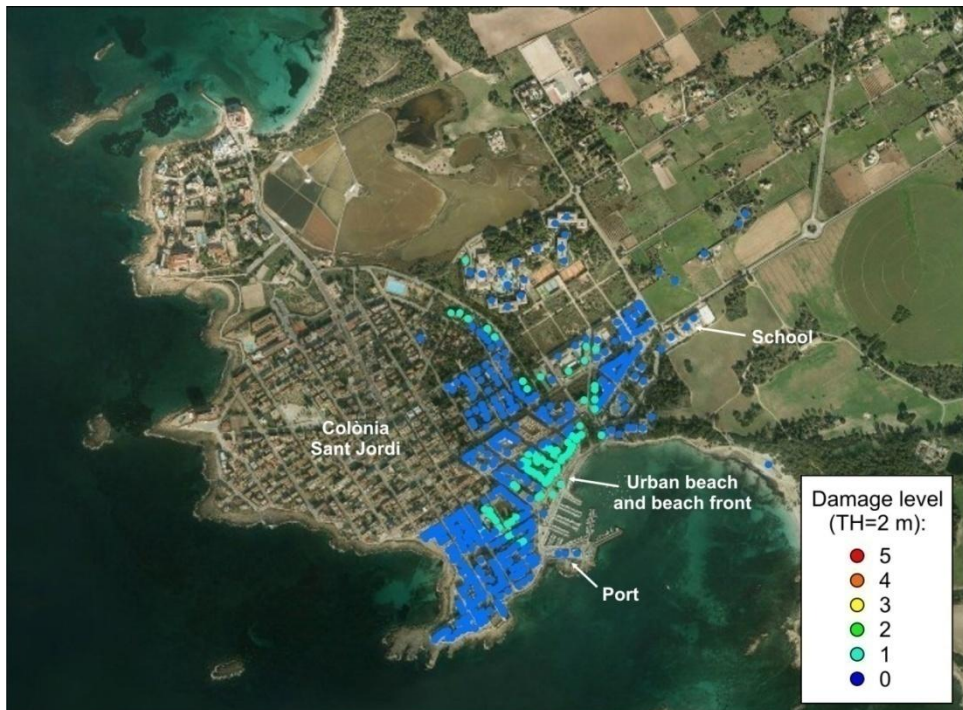


Figure 3.3.18. Damage level calculated for a limited area within Colònia Sant Jordi test site and a tsunami height of 2 m.



Figure 3.3.19. Damage level calculated for a limited area within Colònia Sant Jordi test site and a tsunami height of 4 m.



Figure 3.3.20. Damage level calculated for a limited area within Colònia Sant Jordi test site and a tsunami height of 8 m.



Figure 3.3.21. Damage level calculated for a limited area within Colònia Sant Jordi test site and a tsunami height of 10 m.

3.3.4 Comparison of the results

Both SCHEMA and PTHA-3 models indicate that moderate tsunami heights ($TH > 2$ m) could produce light to important damage to buildings located in the first and second lines in the port and urban beach front area of Colònia Sant Jordi. This area would also be prone to impact by moving objects originating from the port itself (loose barges and ships). Only catastrophic tsunamis would generate widespread damage in Colònia Sant Jordi, with the area occupied with small isolated villas in the area to the northeast of the town having a high vulnerability and a potential damage level implying partial or total collapses. SCHEMA model is able to clearly differentiate the higher potential damage level of these small villas with respect to the buildings in the first line in the port, which, although are more exposed, in general terms are higher and of a better construction class.

The limitations of the data set regarding the calculation of the results of PTHA-3 model should be taken into account, since a number of building characteristics were unknown and have been extrapolated from other data or considered homogeneous throughout the test site. In addition, flow depth relies on a topographic base that should be improved in order to apply these models at higher resolution.

3.3.5 References

Dall'Osso F., Gonella M, Gabbianelli G., Withycombe G., Dominey-Howes D., 2009. A revised (PTVA) model for assessing the vulnerability of buildings to tsunami damage, Nat. Hazards Earth System Sci., 9, 1557-1565.

Instituto Nacional de Estadística, 2008. Hostelería y turismo. Encuesta de ocupación hotelera. <http://www.ine.es/jaxi/menu.do?type=pcaxis&path=%2Ft11%2Fe162eoh&file=inebase&L=0>

Instituto Nacional de Estadística, 2014. Padrón. Población por municipios. Población a 1 de enero de 2014. <http://www.ine.es/jaxi/menu.do?type=pcaxis&path=%2Ft20%2Fe260&file=inebase&L=0>

Ports de les Illes Balears, 2014. Nuestros puertos. <http://www.portsib.es/es/paginas/inicio/puertos-y-amarres/>

Scheffers A., Kelletat D., 2004. Bimodal tsunami deposits - a neglected feature in paleo-tsunami research. Schernewski, G., Dolch, T., (eds.), Geographie der Meere. und Küsten. Coastline Reports, 1: 67-75.

Tinti, S., Tonini, R., Bressan, L., Armigliato, A., Gardi, A., Guillande, R., Valencia, N., Scheer, S., 2011. Handbook of tsunami hazard and damage scenarios. JRC Scientific and Technical Reports, European Commission, Luxemburg, 41 pp.

3.4 *Siracusa-Augusta*

3.4.1 Description of the site

In ASTARTE, under the name of “Siracusa” we indicate two distinct coastal areas in eastern Sicily: the town of Siracusa itself (to the south) and the area including the town of Augusta and the homonymous Gulf (to the north). The two sites have already been presented in some detail in Deliverable D8.8 entitled “Tsunami Hazard Assessment Methods: Application in the NEAM region and in the ASTARTE test sites”. In that document, the reader can find information on the towns’ histories, on the historical and paleotsunami evidences of past tsunami impacts, on the present relevance of the two sites in terms of population, cultural heritage, economy and industrial/commercial activities.

In this document, we focus on the aspects that are relevant to vulnerability assessment and to the approaches we are going to implement: they are mainly the buildings’ distribution and classification. We also anticipate that we will be focusing mainly on residential areas, but with some attention also devoted to commercial and industrial areas.

Finally, we stress that the damage estimation in both test sites is performed by means of the "bathtub" technique, in which the inundation level is imposed as a uniform flooding level, where the water column is calculated as the difference between the flooding and the topographic level of the buildings’ basement. Two different bathtub levels have been used for Siracusa and Augusta, as will be discussed later on.

3.4.1.1 *Siracusa*

The classification of buildings was carried out by identifying the buildings through numerical map sat 1: 2000 scale provided by the “Servizi Informatici Territoriali e Cartografia, Nodo Regionale S.I.T.R.” of the “Regione Siciliana, Assessorato Territorio e Ambiente, Dipartimento Urbanistica, Area 2 Interdipartimentale” (<http://www.sitr.regione.sicilia.it/geoportale/it/Metadata/Details/51>). Due to the limited availability of these maps for Siracusa, the classification could be performed only in the area north of the gulf (see Figure 3.4.1). This does not represent a substantial issue, since Figure 3.4.1 allows to appreciate that the most relevant part of the residential and commercial areas is found in this domain. More in detail, the classified area includes the peninsula of Ortigia, which coincides with the historical part of Siracusa, the north residential area, which was built in more recent times and that is comprised between the “Porto Piccolo” and “Porto Grande” basins (indicated as “Small harbour” and “Big harbour” in Figure 3.4.1, see also D8.8, Figure 5.5.2), and the western zone, which is a commercial and industrial area, with a relevant presence of industrial warehouses. The three zones, into which we have divided the area, are characterized by different types of buildings, as will be discussed in the next sections.

The 1:2000 maps constitute a data base that provides information about various elements, in particular it is possible to locate the different buildings and to estimate the topographic level of the buildings’ ground floor. This is important because, as we mentioned in the introductory paragraphs, we apply a "bathtub" technique, involving a uniform flooding level. The maximum flood level used in Siracusa is 5 m. As a result, the total number of classified buildings is 2446: they are all located under the topographic level of 5 m.

Satellite images (Google Earth), photographic images (Google Street View, hereafter referred to as GSV) and a field survey helped for the classification of the buildings.



Figure 3.4.1. Google Earth view of the Siracusa areas involved in the vulnerability assessment.

3.4.1.2 Augusta

Similarly to the case of Siracusa, the classification of buildings for Augusta was made possible by the availability of numerical maps at 1: 2000 scale provided by the “Servizi Informatici Territoriali e Cartografia, Nodo Regionale S.I.T.R.” of the “Regione Siciliana, Assessorato Territorio e Ambiente, Dipartimento Urbanistica, Area 2 Interdipartimentale” (<http://www.sitr.regione.sicilia.it/geoportale/it/Metadata/Details/51>). As was anticipated in Deliverable D8.8, when referring to the site of Augusta we mean a quite extended area comprising not only the Augusta town itself, whose position is displayed in Figure 3.4.2. but also the large bay (called Augusta bay) which is nowadays protected by a set of three long breakwaters. Since one of the main results proposed in D8.8 is that the breakwaters are able to largely reduce the hazard for the inner Augusta bay, for the vulnerability assessment presented in this document we privilege the “external zones” which are not protected by any offshore structure and that are consequently most exposed to tsunami hazard. In particular, we divided the area into three main parts (see figure 3.4.2): the peninsula on which the historical Augusta downtown is located (“Augusta’s island in Figure 3.4.2), the residential area found on the mainland just north of the historical downtown, and the inhabited district placed east of Augusta and close to “Punta Izzo”. This last one consists in a short coastal stretch facing the inner bay called “Porto Xifonio”: it comprises some beach facilities and small marinas that used to be public, but have recently passed under the jurisdiction of the Italian navy.

The Augusta peninsula exhibits a topography pattern with elevations larger than 10 m in a very wide portion of the peninsula itself: the topography slopes down only in correspondence with the entire western coast and with the south-eastern coast. The southern and south-eastern sectors are widely below 5 m. The residential area to the north lies between two salt pits and exhibits mostly low topography, which reaches 5 m only in its south-western part. Finally, the area found on the eastern coast of Porto Xifonio and close to Punta Izzo presents only a narrow stretch below 10 m: the topography slope up very quickly moving away from the sea in this area.

Again similarly to Siracusa, we adopted for Augusta a “bathtub” approach, with a selected uniform level of 10 m. This choice was dictated by two main reasons. The first is related to the information on topography, discussed above. The second deals with the reconstruction of the historical 11 January 1693 tsunamigenic earthquake ($M_w = 7.4$), capable of producing a maximum run-up in the order of 8 m in Augusta: although no widely agreed upon solution exists for the parent source of this event, we favour the idea that it was generated by a fault rupturing just offshore the Augusta area (e.g. Tinti et al., 2001; Argnani et al., 2012).

The vulnerability classification in the three selected areas of Augusta, which involved 2307 buildings, was carried out based on the 1:2000 maps and with the complementary aid of satellite images and, when available, photographic material.



Figure 3.4.2. Google Earth view of the Augusta areas involved in the vulnerability assessment.

3.4.2 PTVA-3

The method called PTVA-3, where PTVA stands for “Papathoma Tsunami Vulnerability Assessment”, is the third version of a methodology first proposed by Papathoma and Dominey-Howes in 2003 and applied to different portions of the Greek coasts by Papathoma et al. (2003). PTVA-3 was proposed by Dall’Osso et al. (2009) and applied shortly after to the island of Stromboli (Dall’Osso et al., 2010). In PTVA-3 the vulnerability of a building (BV) is computed by taking into account 7 structural characteristics or attributes (Table 3.4.1) according to the following formula, where the numerical constants are proper weights:

$$BV(-1,+1)=1/423(100\cdot s+80\cdot m+63\cdot g+60\cdot f+51\cdot mo+46\cdot so+23\cdot pc)$$

BV attains values in the range [-1, +1], but for the PTVA-3 purposes it is rescaled to a [+1, +5] interval, where 1 refers to the most resistant buildings and 5 to the least resistant.

Table 3.4.1. Attributes influencing the structural vulnerability of a building “BV”. Positive values indicate an increase of the average building vulnerability given by the attribute

Attribute	Attribute values						
	-1	-0.5	0	+0.25	+0.5	+0.75	+1
s (n° of stories)	>5	4	3		2		1
m (material)	reinforced concrete		double brick		single brick		timber
g (ground floor hydrodynamics)	100% open plane	75% open plane	50% open plane		25% open plane		not open plane
f (foundation strength)	deep pile		average depth				shallow
so (shape and orientation)	high		average				poor
mo (movable objects)			minimum	moderate	average	high	extreme
pc (preservation condition)	excellent	good	average		poor		very poor

The analysis of the damage, expressed through the “Relative Vulnerability Index” (RVI), requires the calculation of three more variables related to the water column (Ex and WV) and to the level of protection (Prot). The parameter Ex depends directly from the water column, while WV is expressed as the ratio between the number of flooded stories and the total number of stories. The parameter Prot expresses the level of protection against the tsunami according to the type of obstacles that can mitigate the effects of the tsunami itself: houses, stone walls, seawalls, trees or other natural protections.

Note that “natively” the different parameters may attain values in different intervals: anyway, in the PTVA-3 procedure they are all rescaled to a [+1, +5] interval. RVI is computed as:

$$RVI=2/3 \cdot SV+1/3 \cdot WV$$

where

$$SV = (BV) \times (Ex) \times (Prot) \text{ and } WV = (n^\circ \text{ inundated floors}) / (n^\circ \text{ floors})$$

Similarly to what already commented for the other parameters, SV can vary by definition between 1 and 125, but is then rescaled to the interval [+1, +5]: it is this scaled value that enters the definition of RVI. The same applies to WV. As a result, RVI ranges from 1 to 5 but does not necessarily attain an integer value. As a consequence, this interval has been further divided into 5 equal sub-intervals of 0.8 extension, corresponding to the relative level of the expected damage of the building: minor, moderate, average, high and very high.

3.4.2.1 Application of PTVA-3 to Siracusa

Figure 3.4.3 illustrates the results concerning the BV parameter for the site of Siracusa, while Figure 3.4.4 provides the geographical distribution of the BV classification.

The first aspect that one may notice is that no buildings fall into class 1, meaning that no building is included in the most resistant class. The second aspect is that 91% of the buildings fall into the least resistant classes relative to values 4 and 5, 75% being in class 4.

However, we must stress that the definition of at least two of the attributes contained in Table 3.4.1 that enter the definition of BV suffers from some degree of subjectiveness. These attributes are the “foundation strength” (f) and the “shape and orientation” (so). Regarding the first, we made some assumptions, originating from discussion with local Civil Protection experts. In particular, we assumed that:

- industrial warehouses and the largest part of the buildings in the Ortigia area fall into the “shallow” value for “f”,
- buildings with more than three stories belong to the “deep pile” category.

Clearly, these assumptions are quite difficult to be checked building per building. Moreover, regarding the “so” attribute, a “poor” value has been assigned to the largest part of the buildings. In the absence of a strict criterion to discriminate among the various possibilities, we preferred to stand on the high side, keeping a “worstsituation” approach.

A certain degree of uncertainty characterises also the “mo” parameter (movable objects). These are typically cars parked along the streets or in parkings. Their number has been assessed on the basis of GSV images inspection, but we are conscious that this information can be highly time-dependent.

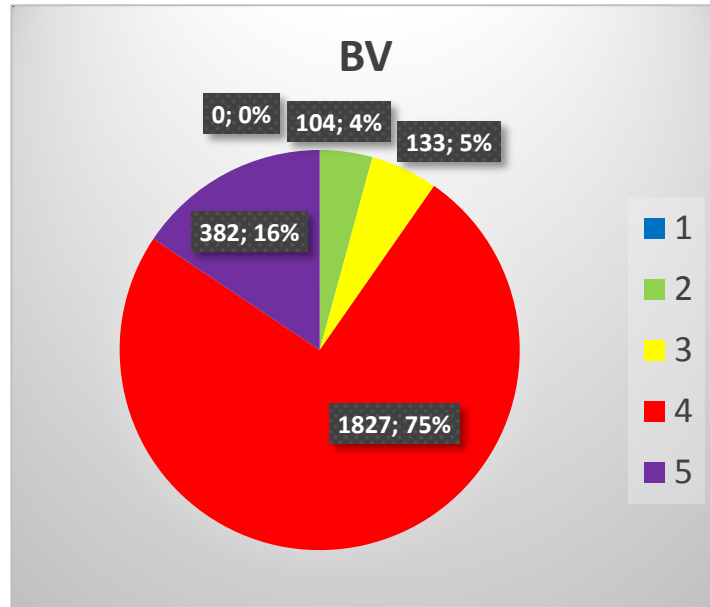


Figure 3.4.3. Results of vulnerability classification. The number of buildings and the percentage is specified for each class.

The geographical distribution of the BV values portrayed in Figure 3.4.4 shows that buildings in classes 4 and 5 are found mainly in the commercial and industrial area and in the shantytown that is found in the north-western part of the bay. Regarding the industrial area, the largest part of storehouses and hangars typically are classified as one-story buildings; we assume they are made of a material that from the vulnerability point of view can be assimilated to a double brick; finally, we define the ground floor to be at least a 50% open plan and with shallow foundation. Hence they result to be highly vulnerable to tsunami waves.

For the shanty town the situation is even worse, being the buildings lighter and made in a material that can be assimilated to timber. The status of preservation can also be considered poor. In Ortigia that largest number of the buildings are in class 4, but we also note that only a small part of the buildings on the island lie below the 5 m level. A large density of historical buildings can be found here: they typically lack a concrete reinforcement, have no more than two stories and are often in a poor preservation status. The residential area to the north of Ortigia exhibits a relatively high variability of BV, determined by the variability of building types and ages.

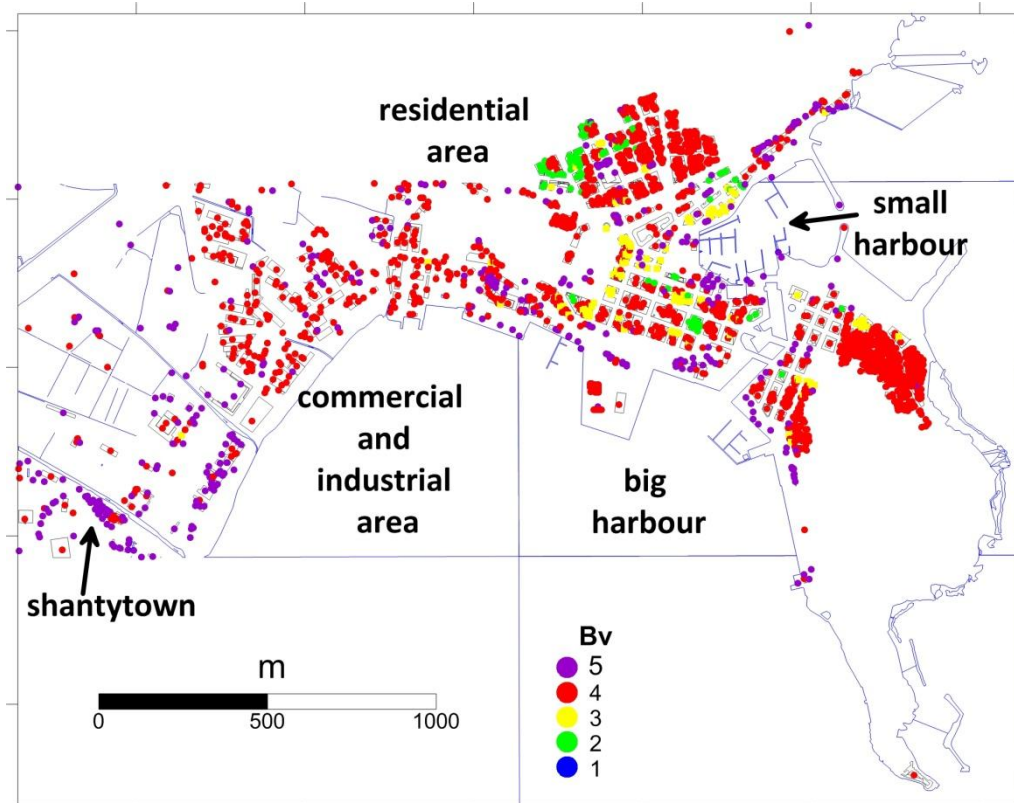


Figure 3.4.4. Map of building vulnerability (BV) calculated by means of the PTVA-3 model for Siracusa.

Figures 3.4.5 and 3.4.6 show the results in terms of building damage levels.

The PTVA-3 provides a damage level where about 60% of the damage is classified from MODERATE to HIGH. About 32% of the buildings have a minimum level of damage (MINOR) and only 9% (219) have a level of damage equal to VERY HIGH. If we compare this information with the BV classification we can appreciate the role of the tsunami water column in the definition of the damage level. For example, the Ortigia island is characterized by highly vulnerable buildings, but the expected water column in the chosen case of a 5-m bathtub is quite modest. As a result, the foreseen damage level for this part of the Siracusa area is “minor” to “moderate”. For the same reason, the commercial and the industrial area are expected to be the most severely damaged, because here the high vulnerability combines with large values for the water column, being this area topographically flat. We also stress the importance of protections in the definition of damage. Investigating the same two examples, the Ortigia coastlines are rather high, and the harbor structures play an additional protecting role. On the opposite side, the industrial area and the shantytown lack any real protection structure, the only potentially protecting factors being the vegetation, which is anyway not homogeneously distributed. Finally, for the residential area the same variability observed for BV applies. As expected, the largest damage is foreseen for buildings located close to the shore.

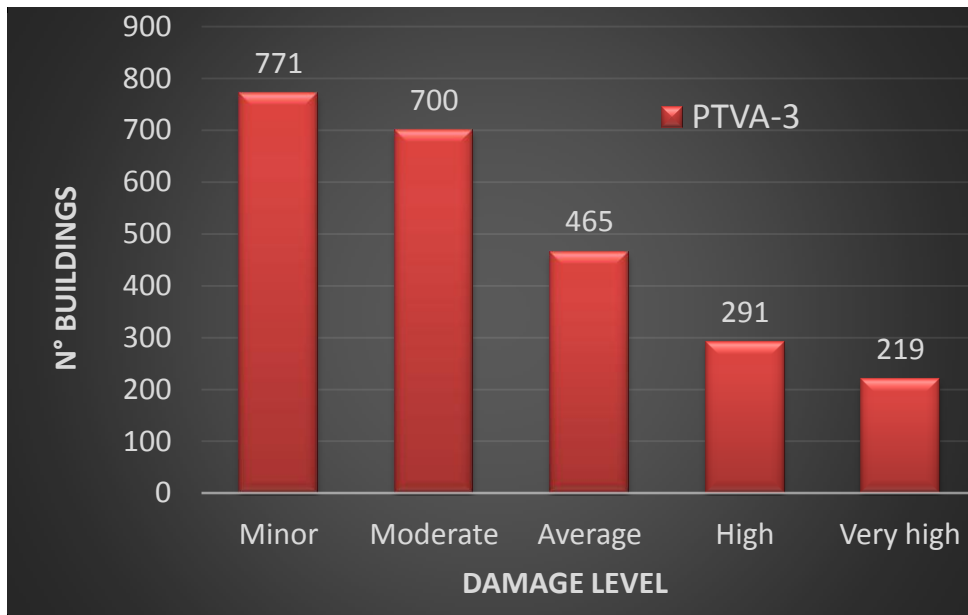


Figure 3.4.5. Damage level for Siracusa obtained through the PTVA-3 approach.

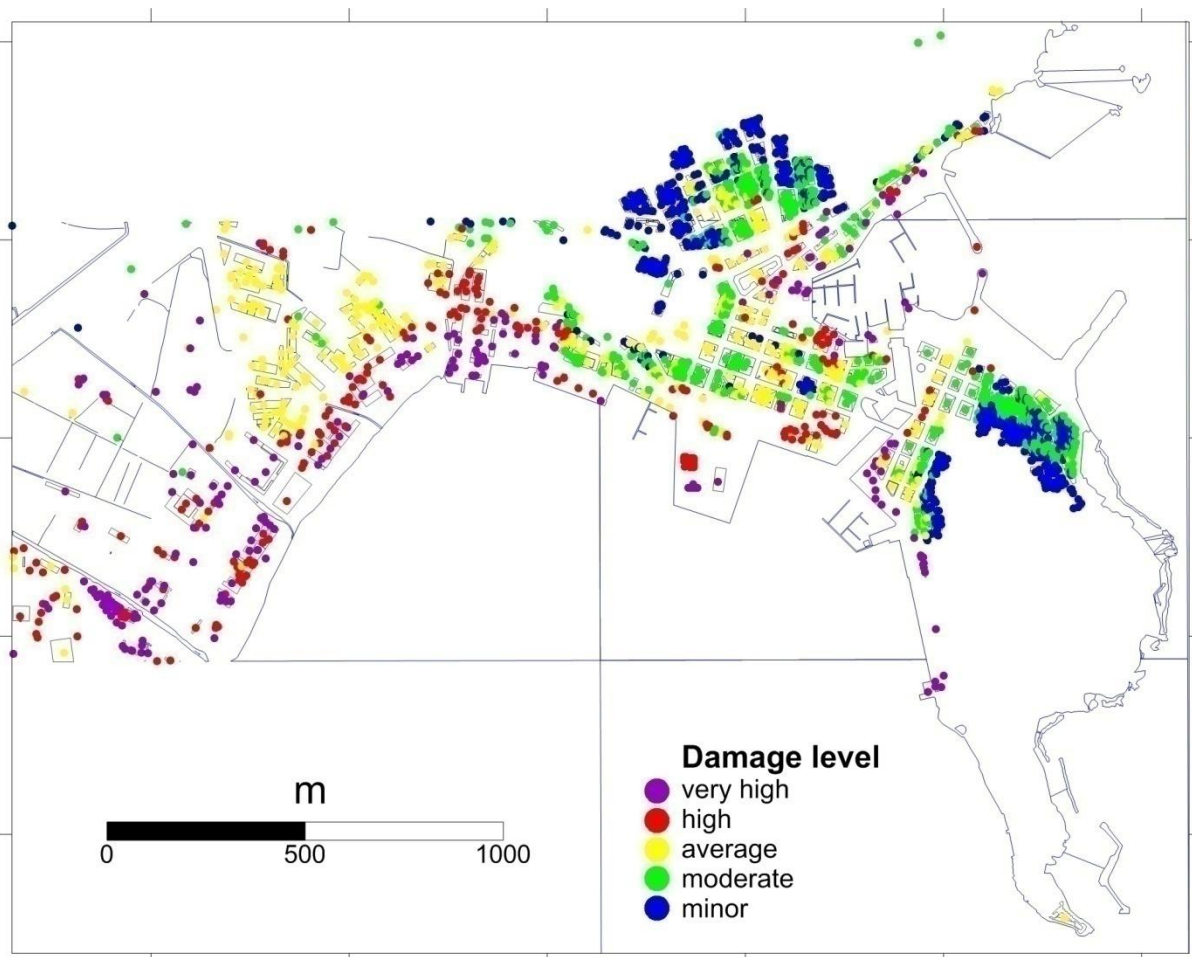


Figure 3.4.6. Geographical distribution of the damage level for Siracusa obtained through the PTVA-3 approach.

3.4.2.2 Application of PTVA-3 to Augusta

Figure 3.4.7 shows the percentage distribution of the Building Vulnerability (BV) function. As for Siracusa, no building falls in class 1. With respect to Siracusa, the distribution among the other four classes appears to be more homogeneous: only 8% of the buildings attain the highest value for BV (5), while classes 2, 3 and 4 have comparable population density, with a slight predominance (38%) of buildings in class 4.

The geographical distribution of the classified edifices is shown in Figure 3.4.8. The central part of the Augusta peninsula has no classified buildings because of the topography being higher than 10 m, as already mentioned in the introductory section. The most vulnerable structures (classes 4 and 5) are found along the western and eastern coasts of the Augusta peninsula, to the west of the residential area and on the upper limit of the salt pit placed to the east of it, and along the Punta Izzo area. This is due to the fact that the western coast of the Augusta peninsula hosts several harbours, mainly belonging to the Italian Navy: mostly warehouses and light, 1-2 floor structures. The same applies to the Punta Izzo area and to the area to the west of the residential zone where industrial settlements are found, mainly involved in ship repairing. Regarding the east coast, here old buildings lacking concrete reinforcement and often exhibiting poor preservation conditions are concentrated. The southern part of the historical downtown and the residential area show a quite variable distribution of buildings, with a general presence of recent, resistant many-floor buildings mixed with more vulnerable edifices.

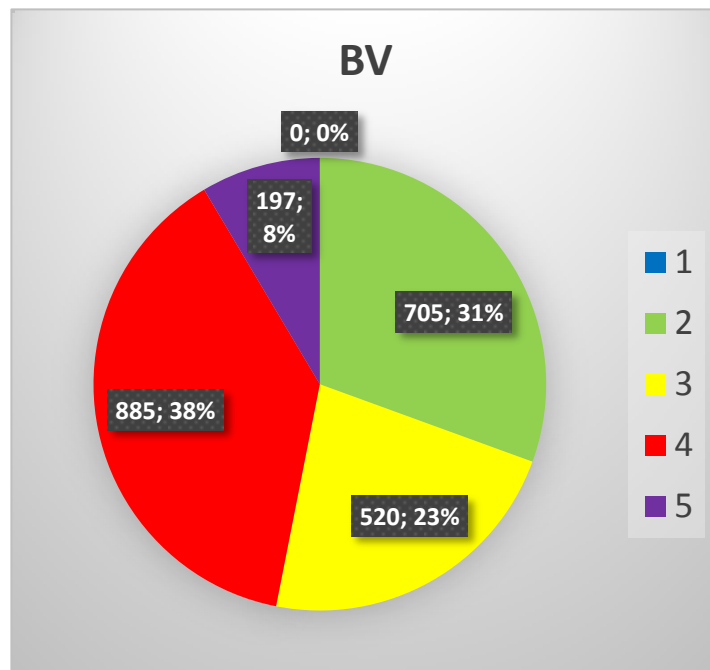


Figure 3.4.7. Results of vulnerability classification. The number of buildings and the percentage are specified for each class.

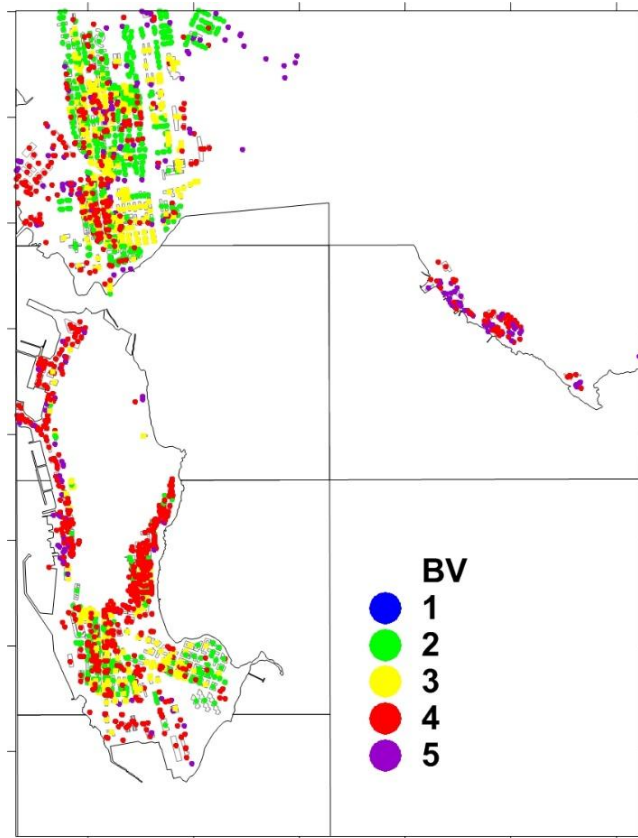


Figure 3.4.8. Map of building vulnerability (BV) provided by PTVA-3 model for Augusta.

The damage level computed for Augusta is shown in Figures 3.4.9 and 3.4.10. The 18% of the buildings have low to moderate damage; by looking at the geographical distribution in Figure 4.5.10, we argue that this percentage refers to buildings found on the south-eastern part of the Augusta historical downtown, that result to be protected by the topographic factor. The 31% of the edifices suffer “average” damage. Figure 4.4.10 shows that these edifices are placed mainly in the northern residential area and in the southern part of the peninsula. As a result, 51% of the buildings suffer high to very high damage. This is expected to happen in the low-lying areas where least resistant structures are found (harbours and marinas, industrial areas).

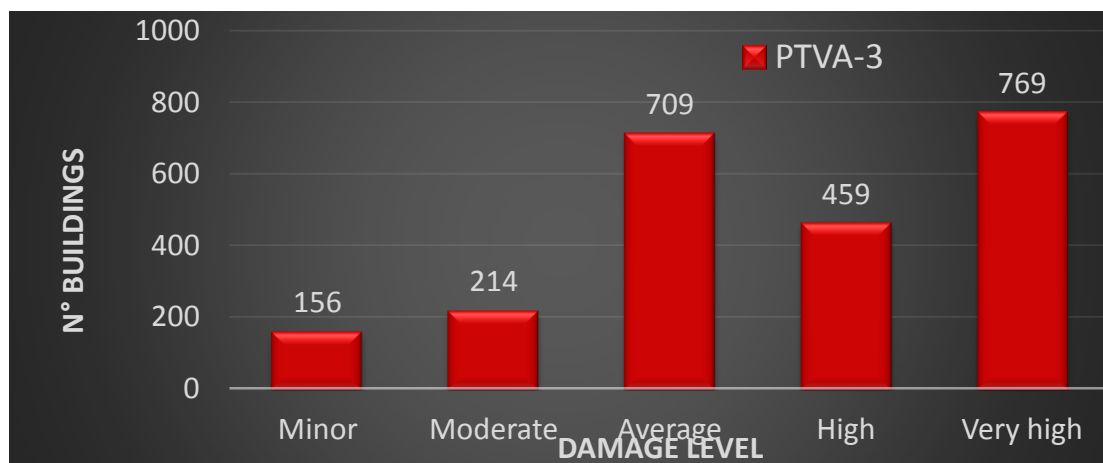


Figure 3.4.9. Damage level for Augusta obtained through the PTVA-3 approach.

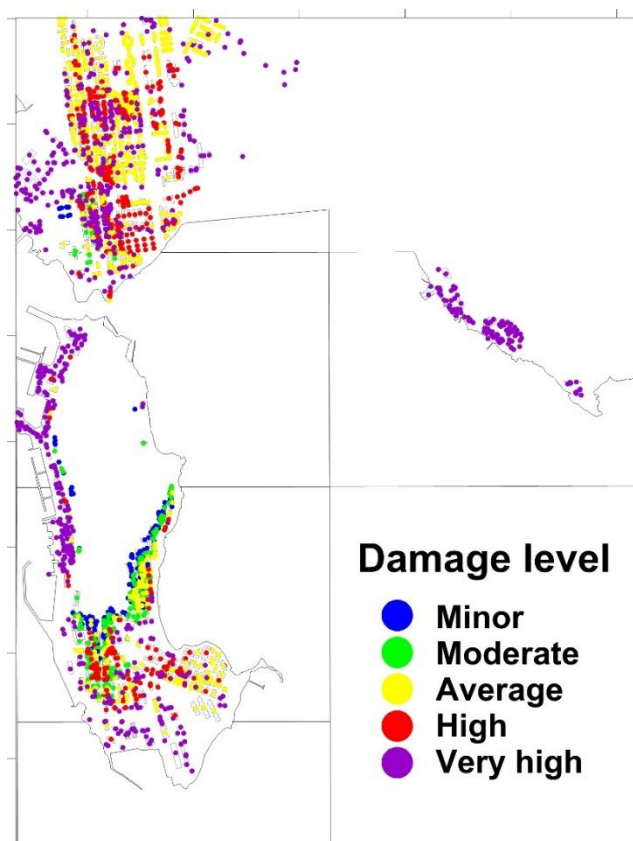


Figure 3.4.10. Geographical distribution of the damage level for Augusta obtained through the PTVA-3 approach.

3.4.3 SCHEMA

In the FP7 European project SCHEMA a methodology to evaluate buildings' vulnerability to tsunamis and potential damage was developed and applied. It is based on fragility and damage curves built by using the database of the buildings damaged by the 2004 tsunami in Banda Aceh (Valencia et al., 2011). On the basis of their structural characteristics (Table 3.4.2), buildings are assigned to vulnerability classes, from which one can determine the level of damage that a given water column is able to cause (Table 3.4.3). The original SCHEMA damage matrix was modified here following the fragility curves presented in Reese et al. (2007). The method is of easy application and can fully exploit satellite imagery for buildings classification.

Table 3.4.2. Building classes depending on the resistance characteristics of the constructions.

Class		Building types	Floor
I. Light constructions	A	Beach or sea-front light constructions / Shanty town/ Old town. Wooden, timber, clay materials, slabs of zinc	0 – 1
	B	Bricks not reinforced, Cement mortar wall, Fieldstone, Masonry	1 – 2
II. Masonry constructions & not reinforced concrete	C	Individual buildings, villas Bricks with reinforced column & masonry filling	1 – 2
	D	Large villas or collective buildings, residential or commercial buildings. Concrete not reinforced	1 – 3
III. Reinforced concrete constructions	E	Residential or collective structures or offices, car parks, schools. Reinforced concrete, steel frames	0 - >3

Table 3.4.3. Damage matrix obtained by discretizing the damage functions. Yellow boxes indicate the modified level of the new damage matrix with respect to the damage matrix presented by Valencia et al. (2011).

Damage level		Class A	Class B	Class C	Class D	Class E
Light damage	D1	0-0.5m	0-1 m	0-2 m	0-2.8 m	0-3m
Important damage	D2	0.5- 1m	1-2m	2-4m	2.8-4.5m	3-6m

Heavy damage	D3	1-2m	2-4m	4-6m	4.5-6.5m	6-9.5m
Partial collapse	D4	2-3m	4-5m	6-8m	6.5-9m	9.5-12.5m
Total collapse	D5	> 3m	> 5m	> 8m	> 9m	> 12.5m

3.4.3.1 Application of the SCHEMA method to Siracusa

In the SCHEMA approach the first step to implement is the inventory of the building and their partition in the classes from A to E following the scheme of Table 3.4.2. This building classification can be performed individually, that is building by building, but we have assumed that the very detailed categorization made within the 1:2000 mapping program could be exploited by suitably mapping the 28 categories of the program layer B (the one related to buildings) to 5 classes of the SCHEMA model, and by further testing the hypothesis by direct verification (through GSV and/or field survey).

The results of the classification carried out for Siracusa are presented in Figure 3.4.11. About 73% of the buildings fall into class C, that is “Individual buildings, villas – bricks with reinforced column & masonry filling”. Historical edifices very likely lack any concrete reinforcement and can exhibit at most reinforced columns; warehouses usually have mixed compositions, but the external walls are often made of weak materials. The 12% of buildings falling into class A is composed by tents and cabins, often positioned close to warehouses. Only 8% of the buildings belong to the most resistant classes, D and E: these are the most recent edifices and those with the largest number of floors (typically larger than three). The geographical distribution of the classified buildings is shown in Figure 3.4.12: the distribution closely depends on the criteria just mentioned for the classification. In the commercial/industrial area the largest part of buildings is in A and mostly C. The shantytown was also classified in A. In Ortigia most of the edifices are in class C, while the most resistant ones are found in the residential zone.

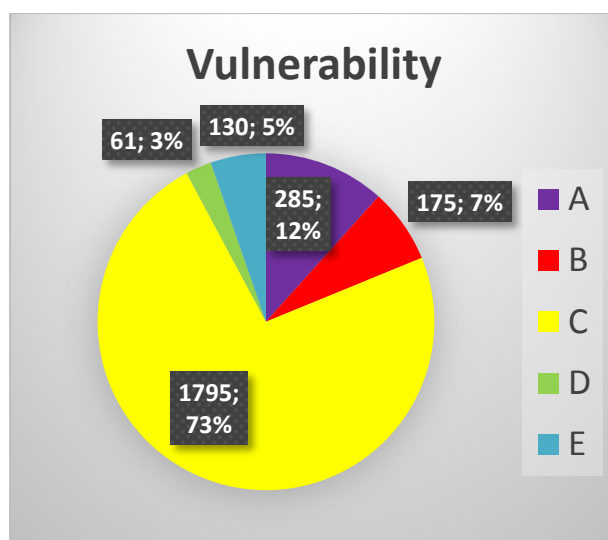


Figure 3.4.11. SCHEMA vulnerability classes for Siracusa.

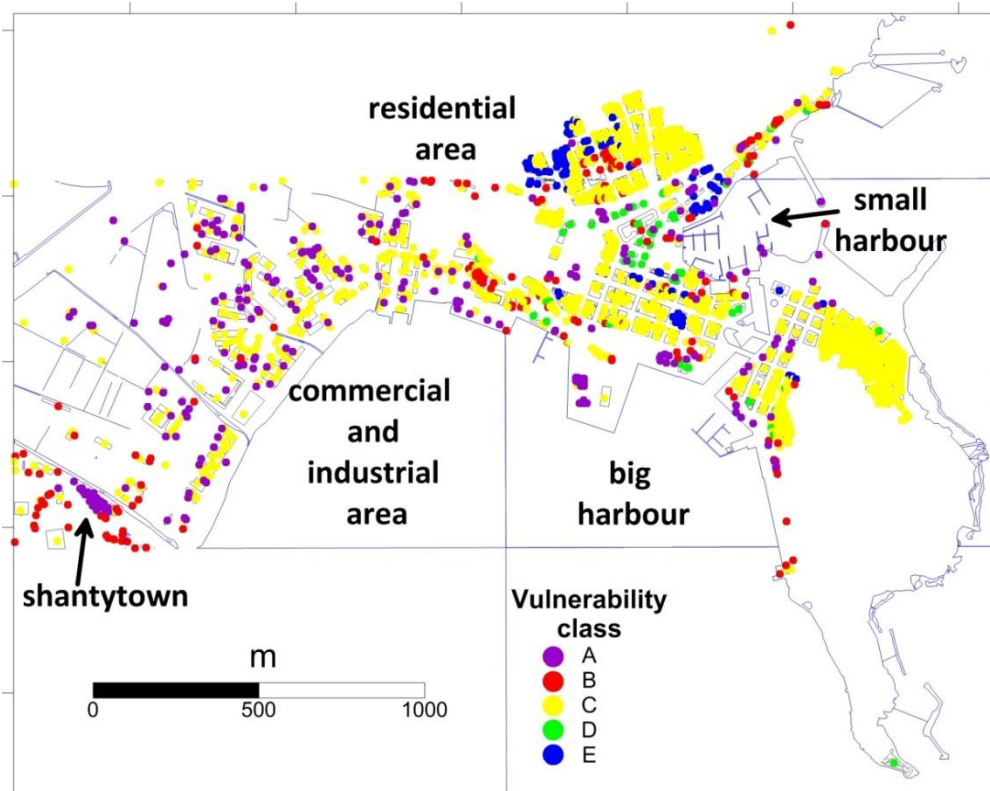


Figure 3.4.12. Geographical distribution of the SCHEMA vulnerability classes for Siracusa.

Figures 3.4.13 and 3.4.14 represent the results related to the damage level assessment. From Figure 3.4.13 we deduce that 83% of the edifices are foreseen to suffer only light to important damage in the hypothesis of a uniform 5 m level of inundation. Only 10% would exhibit a relevant structural damage leading to partial or even total collapse.

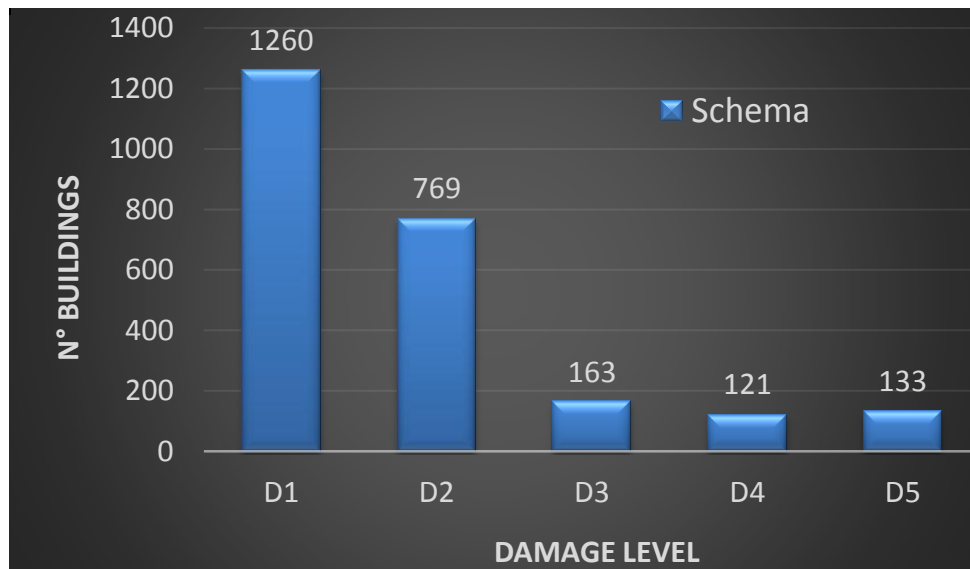


Figure 3.4.13. Damage level for Siracusa estimated through the SCHEMA approach.

Figure 3.4.14 shows the geographical distribution of the expected damage. The areas where the most severe damage concentrates are the harbour areas, the commercial/industrial areas and the shanty town. This can be justified by the fact that these areas are characterised by low topography; moreover the D5 level is diffused throughout the entire studied area and it can be related to the presence of

edifices in class A. Finally, both Ortigia and the residential area are dominated by the blue colour in Figure 3.4.14, indicating the predominance of light damage.

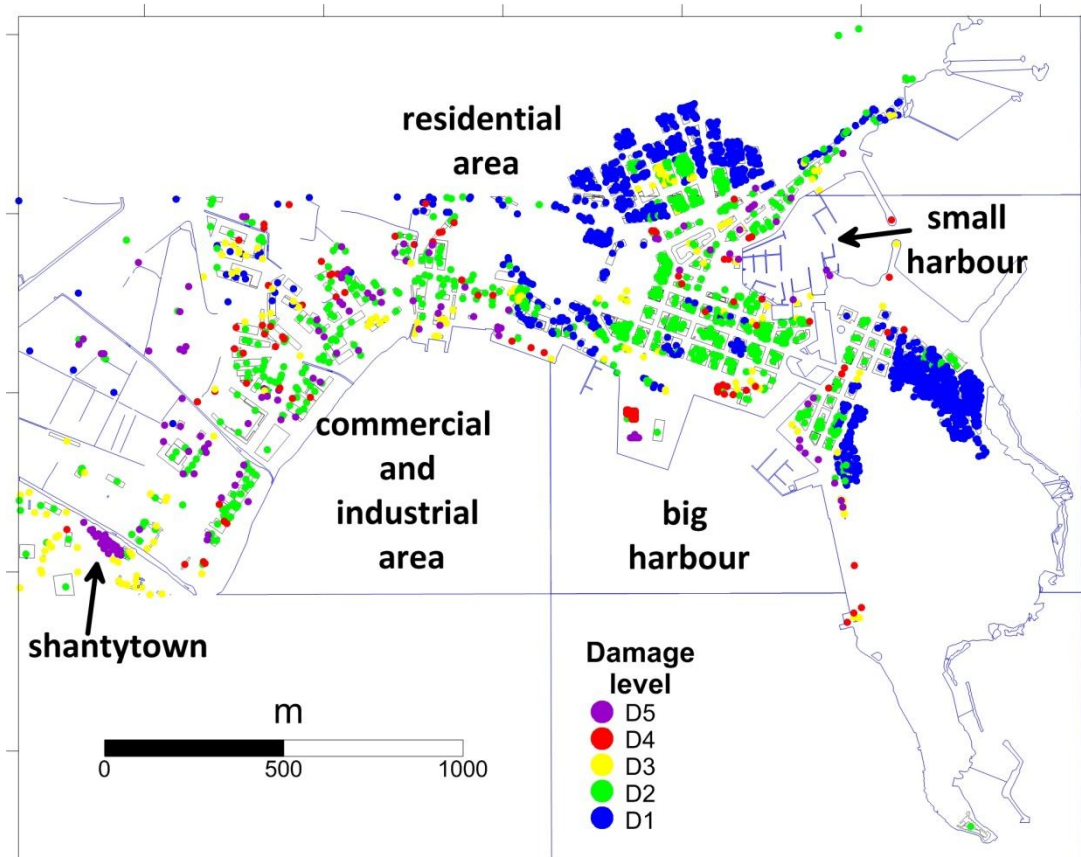


Figure 3.4.14. Geographical distribution of the SCHEMA damage level for Siracusa

3.4.3.2 Application of SCHEMA to Augusta

Figure 3.4.15 indicated that in Augusta 11% of the buildings are classified as A or B, which are the most vulnerable. They are mostly concentrated in the Punta Izzo area (Figure 3.4.16), but evenly distributed in all other zones. Class C dominates the pie-chart with 42% of population: these include warehouses and deposits, harbour structures, as well as old buildings without any concrete. It is then straightforward to find the yellow colour dominating the western and eastern coasts of the Augusta historical centre, of the western part of the northern district including the industrial area. The least vulnerable structures (47%) are mainly in the residential area and in the southern portion of the peninsula.

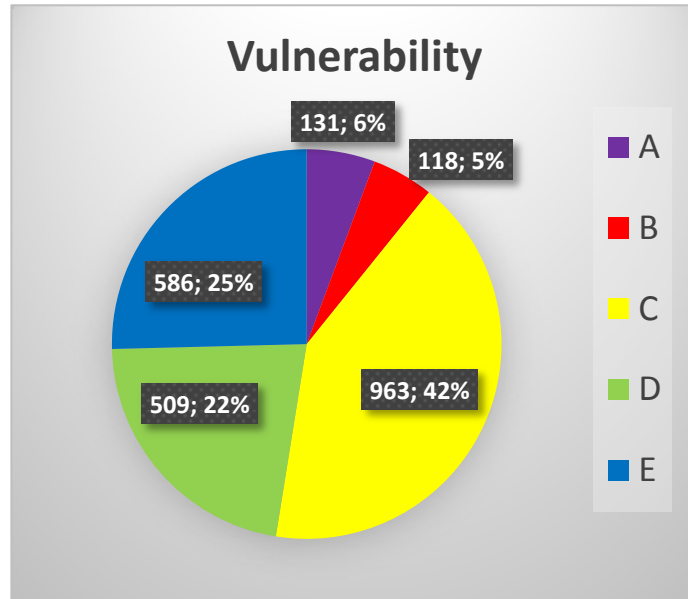


Figure 3.4.15. SCHEMA vulnerability classes for Augusta.

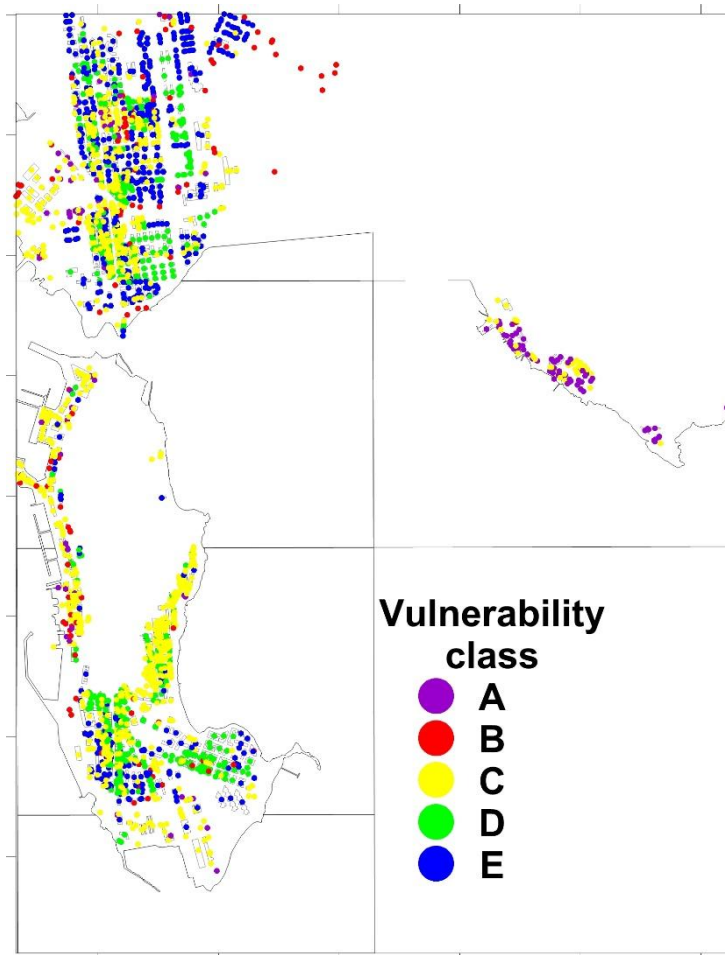


Figure 3.4.16. Geographical distribution of the SCHEMA vulnerability classes for Augusta.

The damage level computed for Augusta with the SCHEMA approach (Figure 3.4.17) shows a more gentle distribution among the different classes with respect to the Siracusa case, but at the same time it tends to privilege the highest damage levels. The main reason is related to the bathtub level chosen (10 m in Augusta vs. 5 m for Siracusa), which implies that also buildings in vulnerability classes C and D can reach the highest damage levels (see Table 3.4.3). Only 15% of the edifices experience light damage: they are concentrated in the inner part of the historical town (eastern side, see Figure

3.4.18). On the contrary, all the buildings found along the coast and in the low-lying areas suffer partial or total collapse: these sum up to 39% of the total. Noticeably, among these are the edifices of the Italian Navy harbours and marinas. It is anyway worth stressing that the use of the bathtub approach somehow neglects the importance protection effect played by the offshore breakwaters closing the Augusta bay. This implies that, especially as regards the western coast of the peninsula and the western part of the northern area, the predicted damage level might be too high.

Finally, we observe that damage levels D2 and D3 are dominant in the residential area and, to a lesser extent, the southern part of the peninsula: here buildings are mainly classified with low vulnerability but the water column can be significantly high.

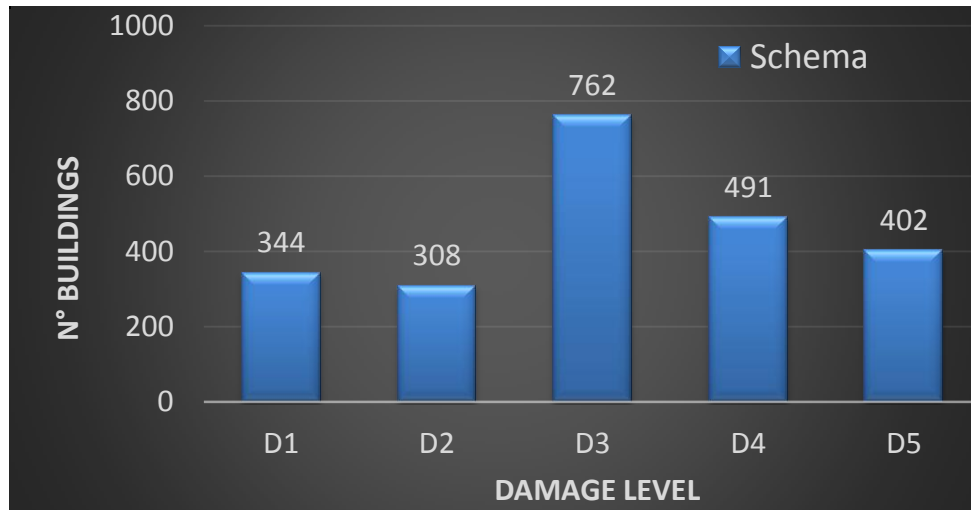


Figure 3.4.17. SCHEMA damage level for Augusta.

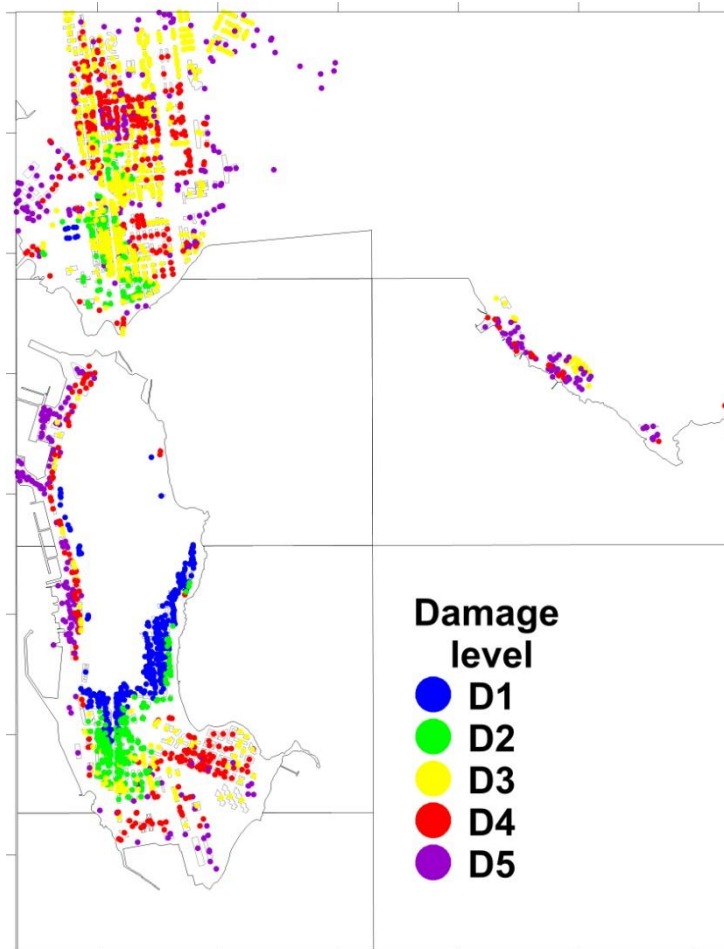


Figure 3.4.18 Geographical distribution of the SCHEMA damage level for Augusta

3.4.4 Comparison of the results

As we are not taking into consideration time-dependent vulnerability, the only comparison we can carry out is between the results obtained from the application of the PTVA-3 and SCHEMA approaches separately to Siracusa and Augusta. In the following two sections the results of the comparison for the two sites is discussed.

3.4.4.1 Comparison for Siracusa

We recall that the buildings classified in Siracusa are 2446. In the double-entry frequency Table 3.4.4 we compare the 5 vulnerability classes of the SCHEMA method (A to E) with the 5 classes of PTVA-3 (5 to 1).

Table 3.4.4. Buildings in Siracusa classified according to the vulnerability approaches of the PTVA-3 and SCHEMA methods

Class of vulnerability	A	B	C	D	E	Total
BV						
5	176	128	78	0	0	382
4	109	47	1637	34	0	1827
3	0	0	79	24	30	133
2	0	0	1	3	100	104

1	0	0	0	0	0	0
Total	285	175	1795	61	130	2446

As we already pointed out, none of the buildings results to have BV=1, which means that as a matter of fact, the PTVA-3 classes are only 4 rather than 5. The diagonal elements should be the most populated in case of 1:1 correspondence between the SCHEMA and the PTVA-3 classes. But they are not. Table 3.5.4 suggests a different correspondence: Class A-B (SCHEMA) corresponds to class 5(PTVA-3); class C corresponds to class 4; class D corresponds to classes 4 and 3 and eventually class E corresponds to class 2.

Table 3.4.5 and Figure 3.4.19 highlight that in 45% of cases the method PTVA-3 results in a damage level larger than SCHEMA and in only 3% it gives a smaller damage (66 buildings). In other words, SCHEMA tends to underestimate the damage level with respect to PTVA-3. We observe that we are implicitly assuming that the two damage scales are comparable, though the two scales might differ since RVI is a relative damage scale, while the SCHEMA scale is an absolute one.

Table 3.4.5. Frequency distribution of damage levels of PTVA-3vs. SCHEMA for Siracusa. The color palette shows the differences calculated as SCHEMA-RVI (purple=+2, red=+1, yellow=0, green=-1, cyan=-2, blue=-3)

Damage level	D1	D2	D3	D4	D5	Total
RVI						
Minor	767	4	0	0	0	771
Moderate	433	263	4	0	0	700
Average	60	314	53	29	9	465
High	0	143	45	83	20	291
Very high	0		61	9	104	219
Total	1260	769	163	121	133	2446

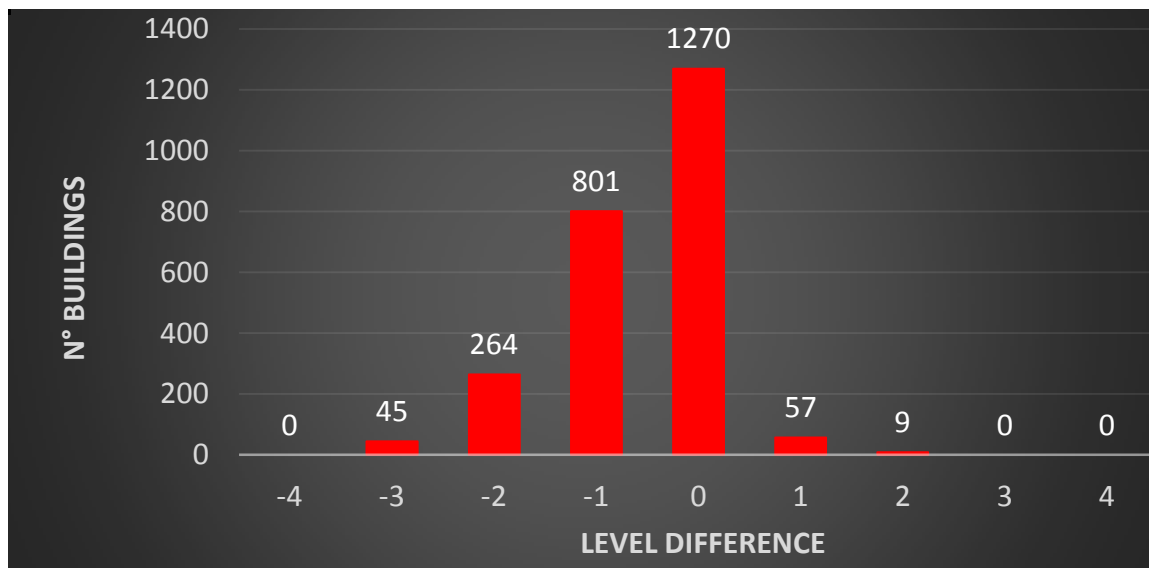


Figure 3.4.19. Histograms of the difference between damage levels, computed as SCHEMA - PTVA-3 for Siracusa.

Figure 3.4.20 shows the geographical distribution of the differences in damage levels between the two methods. First, we observe that PTVA-3 and SCHEMA provide almost the same results in Ortigia and the residential area. Where differences can be appreciated, they consist in a light predominance of the results obtained through SCHEMA. Secondly, the largest negative differences (SCHEMA estimates larger than the PTVA-3 ones) are found in the harbour areas and along the entire coastal segment of the inner gulf. Nonetheless, at the same time the area where SCHEMA provides lower damage levels

with respect to PTVA-3 is found in the north-western portion of the inner gulf, behind the commercial/residential buildings closer to the coastline. Here, the two groups of edifices are separated by a 2.5 – 3 m high wall delimiting the area of a dismissed factory. In PTVA-3 this wall is taken into account as a protecting factor, while in SCHEMA it is not. Anyway, the damage predicted by SCHEMA is much lower than the one predicted by PTVA-3, which in a sense represents a somewhat unexpected result. As a final remark, we observe that the damage levels foreseen for the shantytown coincide in the two approaches.

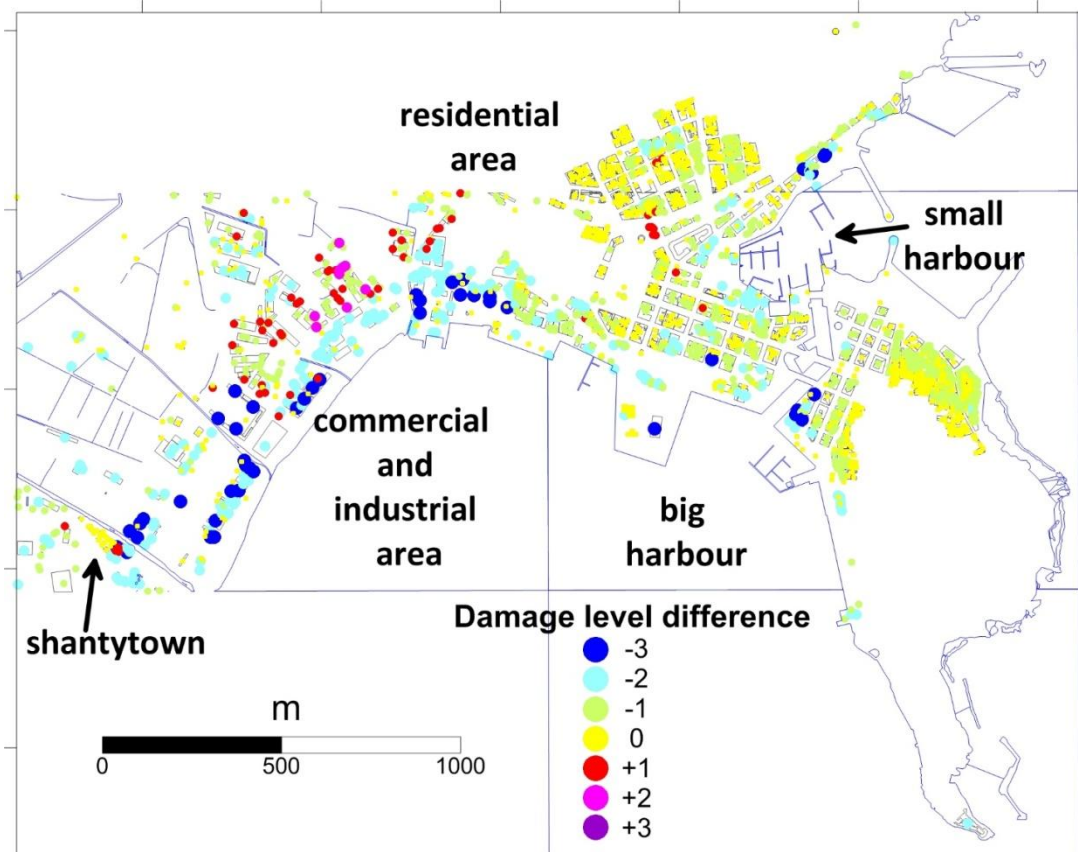


Figure 3.4.20. Geographical distribution of the difference between damage levels, computed as SCHEMA - PTVA-3.

3.4.4.2 Comparison for Augusta

Table 3.4.6 shows the results of the comparison of the vulnerability classification carried out for Augusta by means of the PTVA-3 (Figure 3.4.7) and of the SCHEMA (Figure 3.4.15) approaches. As we discussed in the case of Siracusa, a correspondence between the SCHEMA classes and the PTVA-3 BV values can be introduced, basically consisting in the identification of BV class 5 with the combination of SCHEMA classes A and B, of BV class 4 with SCHEMA class C, of BV class 3 with SCHEMA class D and of BV class 2 with SCHEMA class E.

We note that in the case of Augusta this classification is more grounded than in the case of Siracusa, especially as regards SCHEMA class D, which indeed has a peak in correspondence with PTVA-3 class 3. This was not the case for Siracusa, mainly due to the small overall number of edifices falling into SCHEMA class D.

Table 3.4.6. Buildings in Augusta classified according to the vulnerability approaches of the PTVA-3 and SCHEMA methods

Class of vulnerability	A	B	C	D	E	Total
BV						
5	96	88	13	0	0	197
4	35	30	788	31	1	885
3	0	0	159	299	62	520
2	0	0	3	179	523	705
1	0	0	0	0	0	0
Total	131	118	963	509	586	2307

Table 3.4.7 and Figure 3.4.21 highlight that in 41% of cases the method PTVA-3 results in a damage level larger than SCHEMA and in only 4% it gives a smaller damage (100 buildings). Again, as already observed in the case of Siracusa, SCHEMA tends to underestimate the damage level with respect to PTVA-3. Keeping in mind that we adopted two different bathtub levels in the two areas (10 m for Augusta and 5 m for Siracusa), this implies that this underestimation by SCHEMA remains valid throughout the entire damage range.

Table 3.4.7. Frequency distribution of damage levels of PTVA-3vs. SCHEMA for Augusta. The color palette shows the differences calculated as SCHEMA-RVI (purple=+2, red=+1, yellow=0, green=-1, cyan=-2, blue=-3)

Damage level	D1	D2	D3	D4	D5	Total
RVI						
Minor	155	1	0	0	0	156
Moderate	126	81	7	0	0	214
Average	63	127	443	76	0	709
High	0	81	166	196	16	459
Very high	0		146	219	386	769
Total	344	308	762	491	402	2307

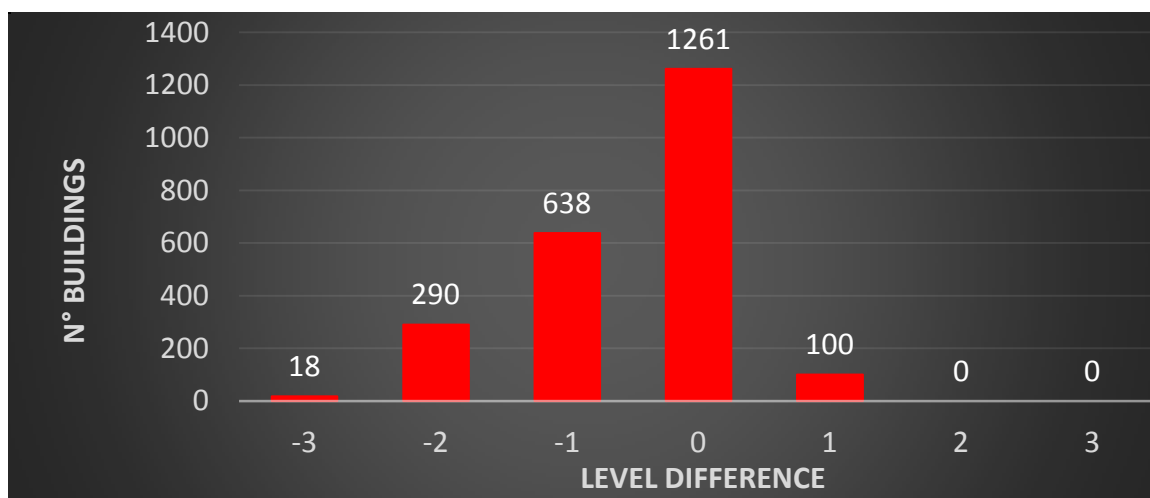


Figure 3.4.21. Histograms of the difference between damage levels, computed as SCHEMA - PTVA-3 for Augusta.

As a last comment, inspection of Figure 3.4.22 tells us that SCHEMA provides slightly larger damage values in two areas, namely a localised portion of the southern-eastern district of the peninsula and some spots aligned in NW-SE direction of the residential area. On the opposite, the largest underestimation by SCHEMA is observed in the south-western part of the residential area and along an elongated strip in the eastern and inner part of the peninsula.

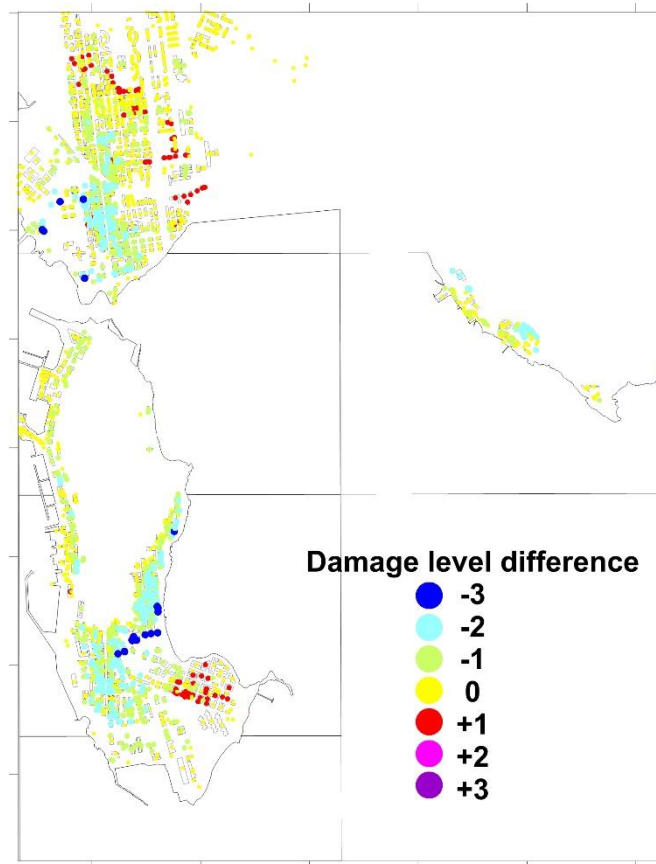


Figure 3.4.22. Geographical distribution of the difference between damage levels, computed as SCHEMA - PTVA-3 for Augusta.

3.4.5 References

Argnani A., Armigliato A., Pagnoni G., Zaniboni F., Tinti S., Bonazzi C., 2012. Active tectonics along the submarine slope of south-eastern Sicily and the source of the 1693 earthquake and tsunami. *Nat. Hazards Earth System Sci.*, 12, 1311-1319.

Dall'Osso F., Gonella M, Gabbianelli G., Withycombe G., Dominey-Howes D., 2009. A revised (PTVA) model for assessing the vulnerability of buildings to tsunami damage, *Nat. Hazards Earth System Sci.*, 9, 1557-1565.

Dall'Osso F., Maramai A., Graziani L., Brizuela B., Cavalletti A., Gonella M., Tinti S., 2010. Applying and validating the PTVA-3 Model at the Aeolian Islands, Italy: assessment of the vulnerability of buildings to tsunamis.

Papathoma M., Dominey-Howes D., 2003. Tsunami vulnerability assessment and its implications for coastal hazard analysis and disaster management planning, Gulf of Corinth, Greece, *Nat. Hazards Earth System Sci.*, 3, 733-747.

Papathoma M., Dominey-Howes D., Zong Y., Smith D., 2003. Assessing tsunami vulnerability, an example from Herakleio, Crete, *Nat. Hazards Earth System Sci.*, 3, 377-389.

Reese S., Cousins W.J., Power W.L., Palmer N.G., Tejakusuma I.G., Nugrahadi S., 2007. Tsunami vulnerability of buildings and people in South Java? Field observations after the July 2006 Java tsunami, *Nat. Hazards Earth System Sci.*, 7, 573–589.

Tinti S., Armigliato A., Bortolucci E., 2001. Contribution of tsunami data analysis to constrain the seismic source: the case of the 1693 eastern Sicily earthquake. *J. Seismol.*, 5, 41-61.

Valencia N., Gardi A., Gauraz A., Leone F., Guillaude R., 2011. New tsunami damage functions developed in the framework of SCHEMA project: application to European-Mediterranean coasts. *Nat. Hazards Earth System Sci.*, 11, 2835–2846.

3.5 Heraklion, Crete Island

3.5.1 Description of the site

Crete occupies the central part in the Hellenic Arc which is the most active seismotectonic structure in the Mediterranean. The test-site of Heraklion, the capital city of Crete, is situated to the central-eastern side of the north coast of the island facing the South Aegean Sea. The study area includes the western part of Heraklion city and a larger part of the adjacent Malevion municipality. For reasons of brevity we call it “Gazion” due to the name given by local people. The study area of Gazion, which is located about 6 km to the west of Heraklion down-town, has a permanent population of about 8,000, which, however, during the summer vacation period nearly doubles. Our study area is about 500 m in length and 200 m in width. The area is of importance as it provides various activities such as the Pancriatio Stadium (Fig.3.5.1 and 3.5.2), the well-known Ammoudara Beach (Fig.3.5.3), which is very crowded during summer time, a large waterpark, large super markets and many small hotels, restaurants, cafeterias and pubs by the sea. At the southern side of the study area the main road connecting Heraklion with the western part of Crete runs. In addition, the area is topographically flat and, therefore, highly prone to tsunami wave inundation. No protection infrastructure (e.g.. high walls) is in place in the study area.

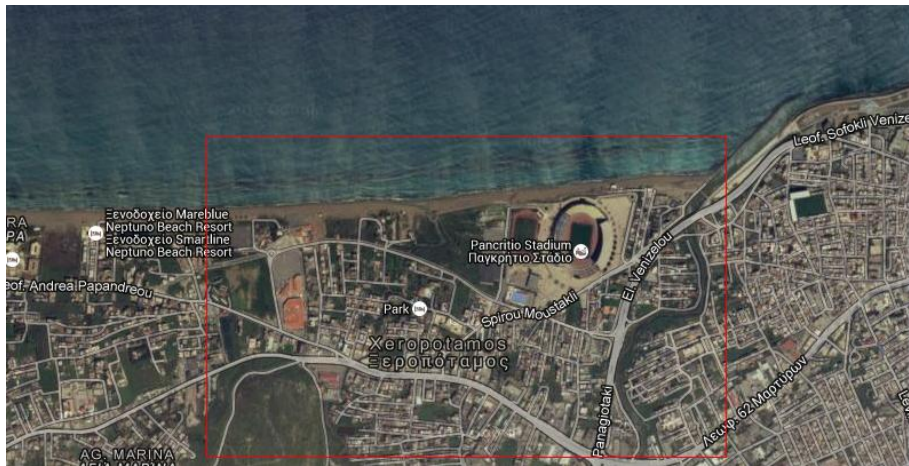


Figure 3.5.1. The coastal area of Gazion. Malevion, Crete, marked by red rectangular.



Figure 3.5.2. Airphoto of the Pancriatio Stadium in Gazion, Crete.



Figure 3.5.3. Typical picture of Ammoudara during summer in Gazion, Crete.

Brief tsunami history and previous studies

In pre-historical times, the largest tsunami in the area was produced by the giant Late Bronze Age (late 17th century BC) eruption of the Santorini (Thera) volcano situated about 120 km to the north of Heraklion. There is archaeological evidence that the so-called Minoan tsunami affected drastically the coastal zone in the area of modern Heraklion. Numerical simulations of the Minoan tsunami indicated wave heights up to ~25 m in north Crete (Novikova et al., 2011, Bruins et al., 2008). In the historical past, very large earthquakes produced equally large tsunamis that inundated the entire eastern Mediterranean basin (e.g. Papadopoulos et al., 2014). For example, the earthquake and tsunami destructive events of AD 21 July 365 and 8 August 1303 were among the largest ever reported in the Mediterranean region (Guidoboni et al., 1994, Ambraseys, 2009, Papadopoulos, 2011). The sources of these events were situated off the western and eastern Crete, respectively. There is no historical or other evidence on how Heraklion was likely affected by the 365 tsunami, but as regards the 1303 tsunami it is documented that it caused heavy damage and human deaths in Heraklion.

On 29th September 1650, after the paroxysmal phase of a strong eruption taking place in Kolumbo submarine volcanic edifice, lying outside of the Santorini caldera, a large tsunami was generated which inundated violently Heraklion and caused damage to vessels (Dominey-Howes et al., 2000). In the instrumental period, the 9 July 1956 tsunami, produced by a M7.5 tectonic earthquake in the South Aegean Sea, inundated the north coast of Crete and caused damage in Heraklion. Maximum observed wave heights up to ~15 m were reported in the near-field of the 1956 tsunami. In the north coast of Crete, including the Heraklion test-site, observed wave heights of 2-3 m were reported.

3.5.2 PTVA-3

One of the very first studies regarding tsunami risk assessment in the EM region, performed within the frame of the EU GITEC tsunami research project, was focused exactly in a coastal segment of Heraklion (Papadopoulos and Dermentzopoulos, 1998). Later, the so-called Papathoma Tsunami Vulnerability Assessment (PTVA) model was developed with testing and validation in Greek coastal zones, including Heraklion (Papathoma, 2003, Papathoma and Dominey-Howes, 2003, Papathoma et al., 2003). Dall'Osso et al. (2009), presented an enhanced version (PTVA-3) of the PTVA that takes into account a new understanding of the factors that influence building vulnerability. They introduced the use of the Analytic Hierarchy Process (AHP) for weighting the various attributes in order to limit concerns about subjective ranking of attributes in the original model. The authors successfully tested PTVA-3 using building data from Maroubra, Sydney, Australia. In the EM region the PTVA-3 model was applied in Stromboli (Dall'Osso et al., 2010).

The PTVA-3 model, however, is not applicable to Gazion test-site due to the lack of the following information per building:

- the vulnerability of building elements due to their contact with water
- the degree of protection which is provided to buildings by any barriers

3.5.3 SCHEMA

In the framework of the FP6 European Project SCHEMA (Scenarios for tsunami Hazard-induced Emergencies Management, www.schemaproject.org) new tsunami damage functions were developed to be used for quantifying the potential tsunami damage to buildings along the European-Mediterranean (EM) coasts. The method considers the distribution of a hazard parameter (inundation depth) and the building typology depending on the type of construction material. An ArcGIS tool has been developed (DamASCHE tool) in order to assess the level of damage on buildings using a damage matrix. The method has been tested and applied in Banda Aceh (Sumatra-Indonesia) (Valencia et al 2011), and in several EM test-sites selected for SCHEMA.

In the present study we selected tsunami scenarios for the South Aegean Sea, simulated numerically the tsunamis, calculated inundation depth in the test-site for each one of the scenarios and, finally applied the DamASCHE tool to a set of building data sets obtained by the Hellenic Statistical Authority.

Tsunami Hazard Assessment: scenarios selection

To perform tsunami hazard assessment for the Heraklion test-site we used two historical tsunami events with the aim to select realistic and worst case scenarios. The first event is the strong tsunami caused by the 9 July 1956 Amorgos tectonic earthquake of M7.5. Two tectonic and one landslide scenarios were selected as realistic scenarios. As a worst case scenario the Minoan large volcanic tsunami has been selected.

The realistic scenarios of 1956

The tectonic earthquake of magnitude 7.5 ruptured the back-arc region of the South Aegean Sea on July 9, 1956. This has been the largest crustal shock recorded in Greece in the last century or so. The submarine trough which is delineated by the islands of Amorgos, Santorini, Anafi and Astypalaea, has been considered as the rupture zone of the 1956 earthquake (Papadopoulos and Pavlides, 1992). A destructive tsunami was generated and inundated coastal zones of Cyclades islands and as far as north Crete. The 1956 tsunami is the largest one reported in the entire Mediterranean Sea after the equally large 1908 tsunami in Messina, South Italy. Two mechanisms have been proposed as a generation mechanism of Amorgos tsunami. The first involves co-seismic fault displacement while the second assumes submarine landslide caused by the earthquake. Two alternatives have been considered for the tectonic case while only one was tested for the landslide case.

Neotectonic observations (Papadopoulos and Pavlides, 1992) and submarine geophysical survey (Perissoratis and Papadopoulos, 2000) showed that the rupture zone of the 1956 earthquake is dominated by two main, antithetic normal faults striking NE-SW and dipping to SE and to NW (see below Table 4.5.1). Fault-plane solutions of the earthquake (e.g. Okal et al., 2009) are consistent with a normal fault striking NE-SW as well. However, numerical simulations performed so far by several authors underestimated drastically the observed wave heights. According to the submarine geophysical survey performed by Perissoratis and Papadopoulos (1999) a large-scale sediment landslide, very likely triggered by the 1956 earthquake, has been identified within the rupture zone. Initial tsunami reports (Galanopoulos, 1957, Ambraseys, 1960) considered the possibility that the tsunami was triggered by such a submarine landslide. However, using the parameters of the landslide determined by Perissoratis and Papadopoulos (1999), the numerical modeling failed again to explain the high tsunami amplitudes. Therefore, we run numerical modeling for a set of hypothetical landslide sources (paper at the final stage of preparation) and eventually, for the needs of the present study, we selected one landslide source with parameters given in Table 4.5.1.

The worst case scenario of Minoan tsunami

For the generation of the large Minoan eruption, several mechanisms have been considered such as caldera collapse, large earthquake, pyroclastic flow entering the sea. In the present study as a worst case scenario we selected a tsunami produced by massive pyroclastic flow entering the sea with given in Table 3.5.1.

Table 3.5.1. Parameters of pyroclastic flow

	Realistic scenarios				Worst case scenario	
	1956 seismic/landslide scenarios				Minoan Thira eruption	
	Source 1	Source 2	Source 3		Source 4	
	Fault with SE slip direction	Fault with NW slip direction	Underwater landslide		Pyroclastic flow	
Strike (deg.)	245	39	Length (km)	10	Pyroclastic debris flow volume (km ³)	60
Dip (deg)	67	25	Width (km)	6	Mean thickness (m)	≤50
Rake (deg)	281	246	Mean slope (deg)	20	Flow velocity (m/sec ²)	170
Centroid depth (km)	15	15	Thickness (m)	150	Flow duration (s)	≤500
Fault length (km)	100	100	Distance of slump motion (m)	≤ 1200	Run-out distance (km)	≤40
Fault width (km)	30	30	Longitude (deg)	26	Pyroclastic flow directivity (deg)	145
Seismic slip (m)	2	2	Latitude (deg)	36.8	Longitude (deg)	25.43
Longitude (deg)	26.3	25.86			Latitude (deg)	36.27
Latitude (deg)	36.7	36.7				

3.5.3.1 Description of the data sources and computational domain

As a first stage the bathymetric grid was built up using two sources: SRTM30 database (30-arcsec resolution) for the whole Aegean Sea region and EMODnet (300 m resolution) for the Heraklion test site. The digital elevation model (DEM) of Heraklion test-site was produced by NOA in an ARCGIS (<http://www.esri.com/software/arcgis>) Windows environment. The DEM was created by elevation data from cartographic maps with scale 1:5000 and elevation contour at 4 m interval, provided by the Hellenic Military Geographical Service (HMGS, <http://web.gys.gr/>). The maps were digitized, georeferenced, stitched to form a mosaic covering the coastal area of Heraklion. A grid interpolation was applied in order to construct the image file. The horizontal grid spacing of the DEM is 5.0 m in latitude and longitude and the spatial reference is WGS84. The DEM provides 32-bit floating data in a simple binary raster file. WGS84 is described at http://www.unoosa.org/pdf/icg/2012/template/WGS_84.pdf

3.5.3.2 *Description of the employed numerical techniques*

In this study we performed numerical simulations with the employment of the GEOWAVE software package (Watts et al., 2003), which is a combination of TOPICS (Tsunami Open and Progressive Initial Conditions System) and FUNWAVE. TOPICS uses a variety of curve fitting techniques and was designed (Grilli & Watts 1999) as an approximate simulation tool that provides surface elevations and water velocities as initial conditions for the tsunami propagation model. FUNWAVE (Wei & Kirby, 1995; Wei et al., 1995) performs wave propagation simulation, based on Boussinesq equations for the description of fully non-linear and dispersive waves, thus allowing us to obtain accurate runup and inundation at the same time. FUNWAVE includes also well-calibrated dissipation models for wave breaking and bottom friction (Wei and Kirby, 1995; Wei et. al., 1995; Chen et. al., 2000; Kennedy et. al., 2000).

The inclusion of both nonlinear and dispersive terms in Boussinesq models eliminates the excessive shallow water steepening and the corresponding early offshore wave breaking and dissipation that take place in non-linear shallow water wave models, such as TUNAMI-N2 or MOST. The frequency dispersion in the model is also necessary to account for the shorter wavelengths of submarine mass failure tsunamis, which have horizontal water velocity profiles that vary with depth.

The use of GEOWAVE for tsunami simulations has been previously well validated with case studies of tsunamis generated by earthquakes (Day et al., 2005; Grilli et al., 2007; Ioualalen et al., 2006, 2007), pyroclastic flows (Waythomas & Watts, 2003; Novikova et al., 2011), underwater landslides (Watts et al., 2003; Day et al., 2005; Greene et al., 2005), caldera collapse (Novikova et al., 2011) and debris flow (Walder et al., 2005).

3.5.3.3 *Tsunami generated by the 1956: tectonic and landslide scenarios*

The fault displacement in the 1956 tsunamigenic earthquake source was described by the standard half-plane solution for an elastic dislocation with maximum slip Δ (Okada 1985). The normal fault of the 1956 earthquake, being of horizontal length L and width W , with centroid located at latitude-longitude (x_0, y_0) and depth d of the earthquake at the centroid (Table 3.5.1), was discretized into many small trapezoids. The vertical coseismic displacement of the ocean floor surrounding the fault was calculated by summing up the contributions of point source elastic solutions, based on the actual depth of each one trapezoid. Okada's solution was implemented by the TOPICS software tool that provides as outputs the vertical coseismic displacements as well as a characteristic tsunami wavelength, λ_0 , which is smaller than the fault dimensions L and W , and a characteristic tsunami period, T_0 . TOPICS allowed also for the superposition of multiple fault planes, which can be assembled into complex fault structures or slip distributions.

Regarding submarine mass failure, according to the formalism introduced by Watts et al. (2003) the mechanics of moving and deforming bodies is often considered as a "relative motion", which decomposes the moving body into the motion of its center mass, and into the motion and/or deformation of the body about the same center of mass. Based on this framework, a deforming submarine mass failure has a center of mass motion with a given position and velocity.

The submarine mass failure was modeled as a rigid body sliding at small angle Δ_ϕ along a circular failure plane, subject to external moments from added mass, buoyancy, gravity, and shear stress summed up over the failure plane. Thus, the center of mass motion is governed by the following equation:

$$RV(\rho_b + C_m \rho_0) \frac{d^2 \phi}{dt^2} \approx -(\rho_b - \rho_0) V g \phi - w b S_u \quad (1)$$

where R is the radius of curvature, V is the slump volume, ρ_b is the bulk density, and ρ_w is the water density. The sediment residual shear strength S_u retards slump motion at all times (Bardet, 1997). Mass coefficient C_m assumed to be equal to 1 (Batchelor, 1967, Watts et al., 2003).

Deformation of the slump during its motion has only a second-order effect on water wave generation, and thus can be neglected.

3.5.3.4 Tsunami generated by pyroclastic flow during Minoan Thira eruption

For calculating pyroclastic flows as tsunami source mechanisms, following the suggestions of Watts & Waythomas (2003) and Walder et al. (2003), we used a pyroclastic flow with bulk density ρ_b with physical dimensions of width W , thickness T and length L , entering water of density ρ_w and constant depth. The flow is represented as a solid block that slowly decelerates as it travels along a horizontal surface with a given initial velocity. The differential equation governing the centre of mass motion along x axis with its origin at the shoreline is approximated by:

$$WTL(\rho_b + C_m \rho_w) \frac{d^2 x}{dt^2} = -WTL(\rho_b - \rho_w) g C_n - WT \frac{1}{2} \rho_w \left(\frac{dx}{dt} \right)^2 C_d \quad (2)$$

where C_m is the added mass coefficient, C_n is the Coulomb friction coefficient, and C_d is the form drag coefficient. The quantity WTL represents the pyroclastic debris flow volume while its projected area in the direction of motion is represented by WT . Following the suggestion of Watts & Waythomas (2003), which is based on experimental results, we choose the values of dynamic coefficients as follows: $C_m = 1.0$, $C_d = 1.0$, $C_n = 0.05$. The characteristic distance, time and velocity of motion are defined as:

$$s_0 = \frac{2L(\gamma + C_m)}{C_d}; t_0 = (\gamma + C_m) \sqrt{\frac{2L}{(\gamma - 1)gC_n C_d}}; u_0 = \sqrt{\frac{2L(\gamma - 1)gC_n}{C_d}} \quad (3)$$

$$\gamma = \frac{\rho_b}{\rho_w}$$

respectively, where $\frac{\rho_b}{\rho_w}$ is the specific density of the debris flow. Further, given the initial condition $x(0)=0$, the position of debris flow center of mass for as long as motion lasts is given by:

$$x(t) = Ut - s_0 \ln \left(\left| \sec \left(\frac{t}{t_0} \right) \right| \right) \quad (4)$$

where U is an impact flow velocity at shoreline. Solution is obtained for the point of time $t=t^*$ when the velocity vanishes to get an expression for the duration of the center of mass motion

$$t^* = t_0 \tan^{-1} \left(\frac{U}{u_0} \right) \quad (5)$$

which governs the tsunami wavelength. Then, by substituting t by t^* the distance traveled by the center of mass becomes:

$$x(t^*) = x^* = Ut^* - s_0 \ln \left(\left| \sec \left(\frac{t^*}{t_0} \right) \right| \right) \quad (6)$$

When a pyroclastic or debris flow enters water it generates a single, coherent wave profile (Walder et al. 2003). Deformation of the pyroclastic/debris flow during transformation and subaqueous translation is assumed to have minimal effect on tsunami generation and as a result it can be neglected Watts et al. (2003). Only the submerged portion of the pyroclastic flow is considered in our calculation, assuming that a density separation of the flow would occur at a short distance from the shoreline if not within the splash zone. However, the tsunami is produced by the submerged portion which is the largest part of the initial flow.

3.5.3.5 Description of the results of the numerical simulations

Realistic scenarios

The realistic case scenario of 1956 event apparently does not generate waves with significant amplitude and inundation inland (Figure 3.5.4.). The estimated run-up at the Heraklion location is about 1.2 m for tsunami generated by the landslide source and about 0.34m for tsunami generated by faults. Therefore, the inundation maps depict nearly invisible flooded zone for both the seismic fault and landslide sources. One reason is that because of the absence of finer bathymetric sources we used quite coarse bathymetry one with resolution of 300m. We expect to improve the final results after employing better resolution bathymetric source.

Worst case scenario

The results for the case of the worst scenario are illustrated in Figure 3.5.5. One may observe that in this case the inundation is significant. For the low land area of western part of the Heraklion coast, that is in the “Gazion” area, where our interest is mainly focused in this study, the inundation depth is more than 25 m which indicates that the coast is flooded remarkably. Moving to the eastern part of Heraklion coast, where the historical port is located, the presence of higher topography combined with a breaking wall of about 4 m high reduce the inundation depth value to 10-13 m, but it is still drastically affected by the tsunami wave.

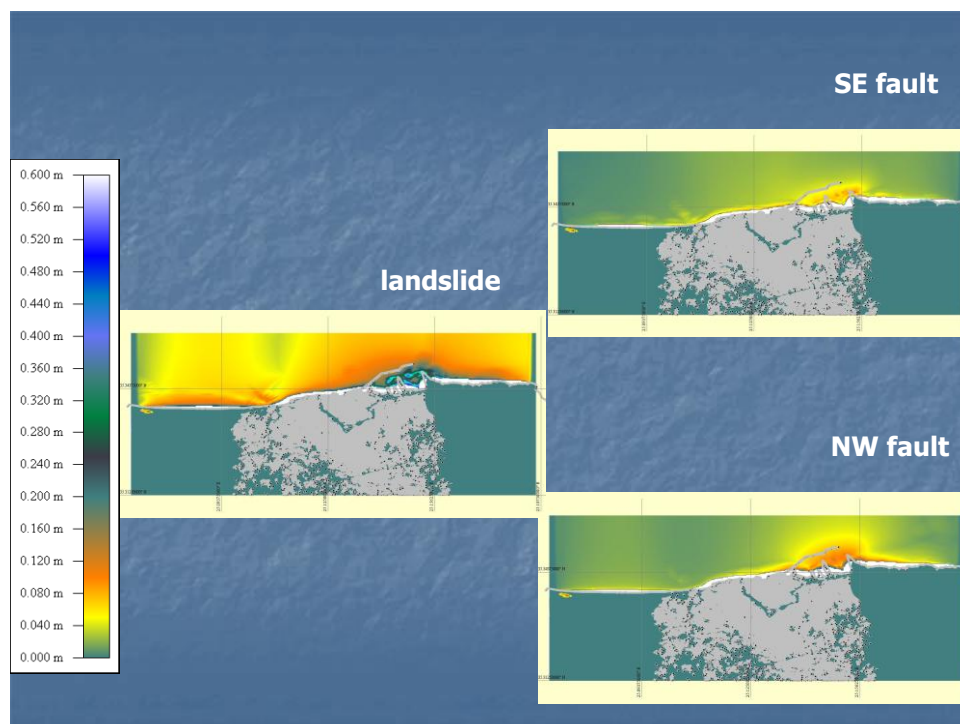


Figure 3.5.4. Crete Inundation depth for the realistic scenario

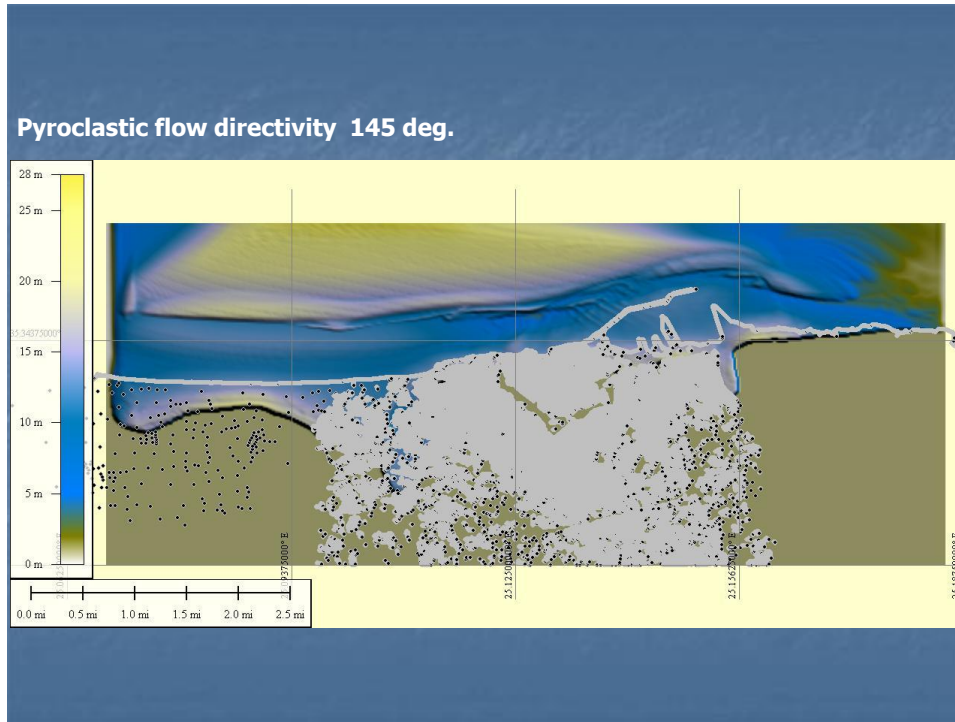


Figure 3.5.5. Inundation depth for the worst scenario

3.5.3.6 Building Classification

The amplitude of tsunami wave associated with the realistic scenarios of the 1956 event is very low, so we have decided to apply the DamASCHE tool taking into account only the worst case scenario. For the application of DamASCHE tool, the following vulnerability building classification was taken into account (Leone et al 2010) (Table 3.5.2).

Table 3.5.2. Building Vulnerability classification (Leone et al 2010.)

Building Class (Leone et al 2006)	Type of buildings
A	light constructions on wood or timber without any design
B	Brick not reinforced masonry
C	Brick with reinforced column and masonry filling
D	collective buildings, concrete not reinforced
E	well designed buildings, made of reinforced concrete with columns and infill walls

The Hellenic Statistical Authority (EL.STAT.) has provided us with the data set of building blocks of the area of Gazon and Heraklion city as well the corresponding GIS polygon shapefile. Concerning the structural material, the information available from EL.STAT. was per building block but not per building. In order to overcome the difficulty imposed, we have grouped the Building Vulnerability class into two general categories: The weak buildings (A) containing the buildings made of wood, bricks and cement tiles and the Strong Buildings (E) containing the ones made of concrete, metal and stone. Then for each building block the next normalization factor was introduced:

$$\Sigma = [A + 0.5 * E] / [A + E] \quad (7)$$

From (7) it results that Σ , varying between 0.5 and 1.0, is an expression of the average “weakness” or “strengthness” of buildings and, therefore, a measure of the buildings vulnerability. For $\Sigma \geq 0.74$ the building category is weak (A), while for $\Sigma < 0.74$ it is strong (E). In the test-site of Gazon and with given building data set the majority is classified as strong buildings (E).

Based on this building classification the results obtained are illustrated in Figures 3.5.6 and 3.5.7 where the special distribution of buildings' blocks as well as the number of buildings' blocks according to different vulnerability classes are illustrated.

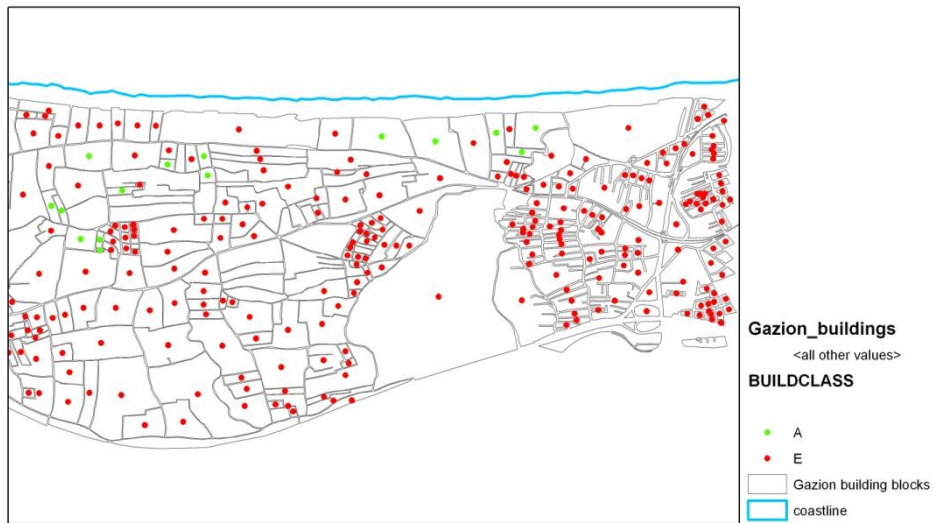


Figure 3.5.6. Spatial distribution of building blocks vulnerability classes A and E at Gazion, Heraklion area.

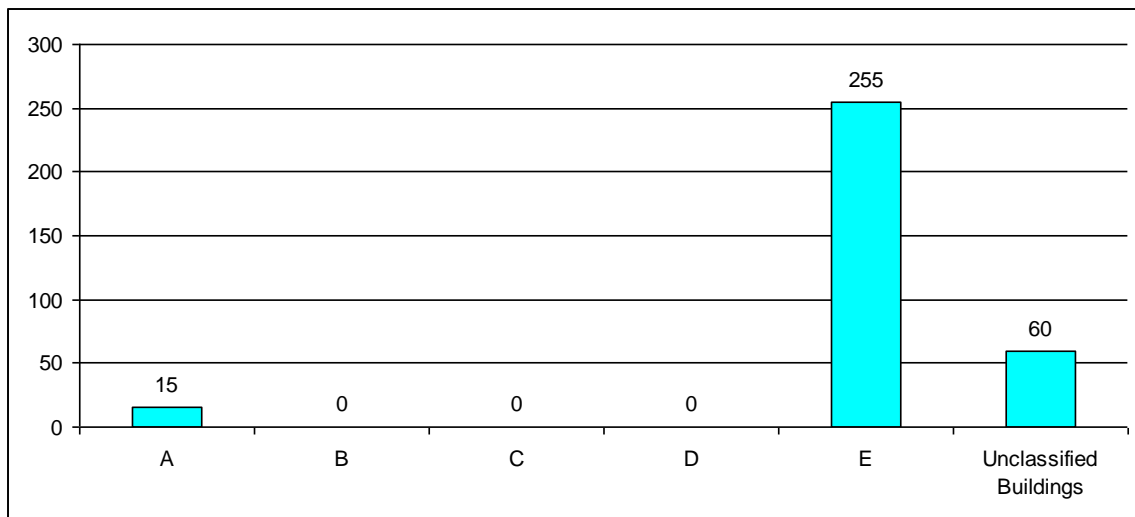


Figure 3.5.7. Distribution of building blocks vulnerability classes.

3.5.3.7 Application of the DamASCHE tool

The grid of water inundation depth and the building shapefile are inserted in ArcMap and the DamASCHE tool allocates to each point of the building layer the value of the hazard grid cell at the same location. The matrix table developed for this allocation is the one shown in Table 3.5.3. (SCHEMA Report D2.1). An automatic classification is obtained for the shapefile layer of blocks/ buildings (see Figures 3.5.8. and 3.5.9.)

Table 3.5.3. Expected Damage Level depending on Building Vulnerability Class and inundation depth (SCHEMA report D2.1)

Damage level		Class A	Class B	Class C	Class D	Class E
No damage	D ₀	0 m	0 m	0 m	0 m	0 m
Light damage	D ₁	0 – 1.8 m	0 – 2 m	0 – 2.5 m	0 – 2 m	0 – 3 m
Important damage	D ₂	1.8 – 2.2 m	2 – 3 m	2.5 – 4 m	2 – 4.5 m	3 – 6 m
Heavy damage	D ₃	2.2 – 2.6 m	3 – 4 m	4 – 6 m	4.5 – 6.5 m	6 – 9.5 m
Partial collapse	D ₄	2.6 – 3.8 m	4 – 5 m	6 – 8 m	6.5 – 9 m	9.5 – 12.5 m
Total collapse	D ₅	> 3.8 m	> 5 m	> 8 m	> 9 m	> 12.5 m

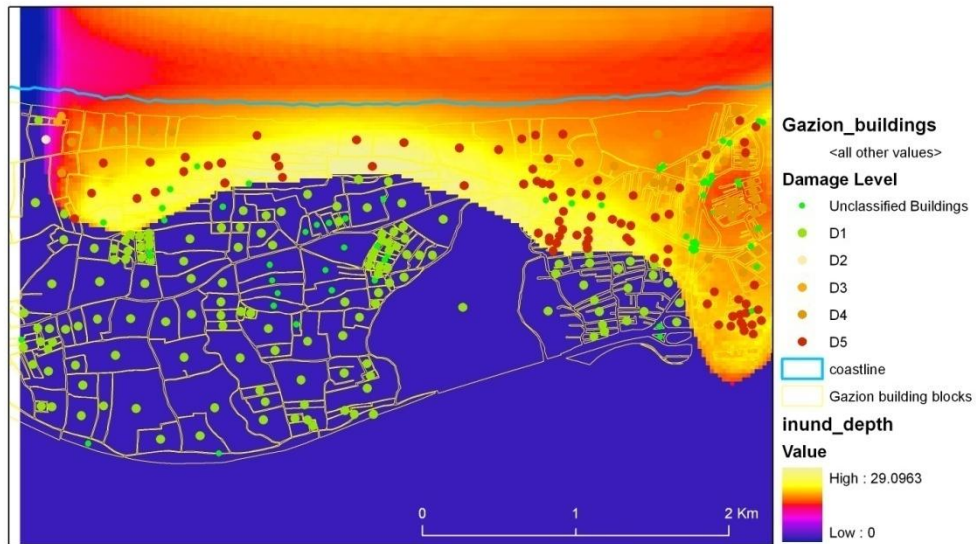


Figure 3.5.8. Spacial distribution of buildings' blocks damage level at Gazion, Crete caused by the Minoan eruption and grid of inundation depth.



Figure 3.5.9. Spatial distribution of buildings' blocks damage level at Gazion, Crete caused by pyroclastic flow of the 17th century BC.

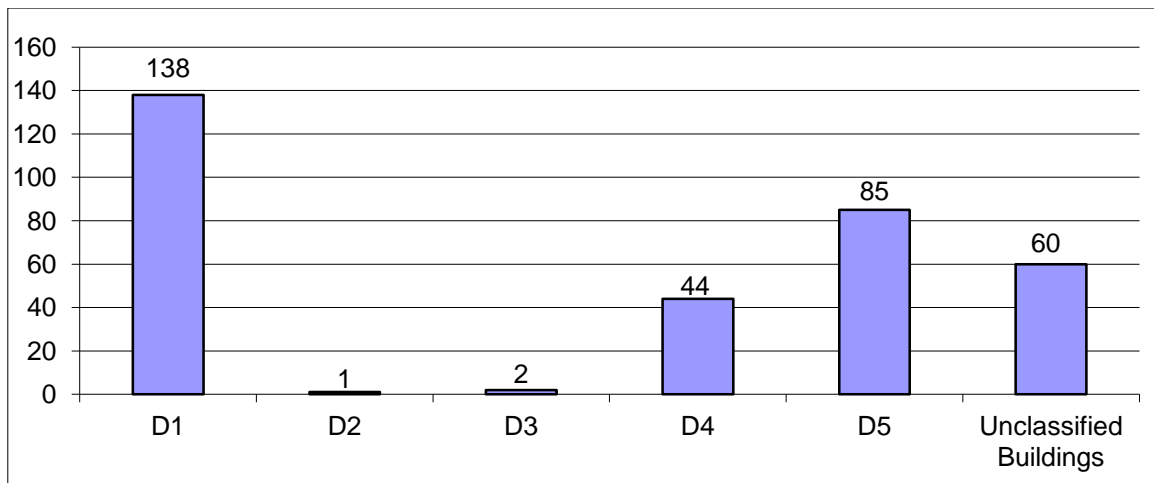


Figure 3.5.10. Number of buildings' blocks according to different damage level for the pyroclastic flow of the 17th century BC

3.5.4 Comparison of the results

In the present work, we assess the tsunami vulnerability of the buildings' blocks in the area of Gazion, Crete. From a total of 330 building blocks, 77.3% is of vulnerability building class E, 4.5% of vulnerability building class A and 18.2% of the blocks is unclassified (no information on the structural material). The results are produced by applying the DamASCHE tool developed in the framework of the European Scenarios for tsunami Hazard-induced Emergencies Management (SCHEMA) project (www.schemaproject.org). The only limitation in the application of the DamASCHE tool is the lack of structural type information per building. This investigation requires a future field survey in the area of Gazion in order to develop an inventory of all the buildings and their structural material, number of stores and the examination of satellite imagery for developing more detailed maps.

3.5.5 References

- Ambraseys N.N., 1960. The seismic sea-wave of July 1956 in the Greek Archipelago. *Journal Geophysical Research*, 65 (4), 1257-1265.
- Ambraseys N.N., 2009. Earthquakes in the Mediterranean and Middle East, A Multidisciplinary Study of Seismicity up to 1900. Cambridge Univ. Press, Cambridge, UK, 947pp.
- Atillah A., El Hadani D., Moudni H., Lesne O., Renou C., Mangin A., Rouffi, 2011. Tsunami vulnerability and damage assessment in the coastal area of Rabat and Sale, Morocco. *Nat Hazards Earth Syst Sci.*, 11, 3397–3414.
- Bardet, J.P., 1997, Experimental Soil Mechanics. Prentice Hall, Upper Saddle River, New Jersey.
- Batchelor, G.K., 1967. An Introduction to Fluid Dynamics. Cambridge University Press, Cambridge, UK.
- Bruins H.J., MacGillivra J.A., Synolokis C.E., Benjamini C., Keller J., Kisch H.J., Klugel A., van der Plicht J., 2008. Geoarchaeological tsunami deposits at Palaikastro (Crete) and the Late Minoan IA eruption of Santorini, *Jour. Arch. Sci.*, 35, 191-212.
- Chen, Q., Kirby, J. T., Dalrymple, R. A., Kennedy, A. B., & Chawla, A., 2000. Boussinesq modelling of wave transformation, breaking and run up. II: 2D, J., *Wtrwy, Port, Coast, and Oc. Engrg.*, ASCE, 126 (1), 48-56.
- Dall'Osso F., Gonella M, Gabbianelli G., Withycombe G., Dominey-Howes D., 2009. A revised (PTVA) model for assessing the vulnerability of buildings to tsunami damage. *Nat. Hazards Earth Syst. Sci.*, 9, 1557-1565.
- Dall'Osso F., Maramai A., Graziani L., Brizuela B., Cavalletti A., Gonella M. and Tinti S., 2010. Applying and validating the PTVA-3 Model at the Aeolian Islands, Italy: assessment of the vulnerability of buildings to tsunamis, *Nat. Hazards Earth Syst. Sci.*, 10, 1547-1562.
- Day S., Watts Ph., Grilli St., J. Kirby, 2005. Mechanical models of the 1975 Kalapana, Hawaii earthquake and tsunami, *Marine Geology*, 215, 59-92.
- Dominey-Howes, D., Papadopoulos, G.A., Dawson A.G., 2000. Geological and historical investigation of the 1650 Mt. Columbo (Thera Island) eruption and tsunamis, Aegean Sea, Greece. *Natural Hazards*, 21, 83-96.
- Greene H. G., Murai L.Y., Watts P., Maher N.A., Fisher M. A., Paull C. E., Eichhuble, P., 2005. Submarine landslides of the Sanat Barbara Basin: Potential tsunami generators, *Nat. Hazards Earth Syst. Sci.*, 6, 63-98.
- Hellenic Statistical Authority EL.STAT. <http://www.statistics.gr/portal/page/portal/ESYE>
- Galanopoulos A.G., 1957. The seismic sea-wave of 9 Iouliou 1956. *Praktika Academy Athens* 32, 90-101 (in Greek with Engl. abstr.).
- Grilli S.T., Watts Ph., 1999. Modelling of waves generated by a moving submerged body: Applications to underwater landslides, *Engrg. Analysis with Boundary Elements*, 23(8), 645-656.
- Grilli, S.T., M. Ioualalen, J. Asavanant, F. Shi, J. T. Kirby, & Watts, Ph., 2007. Source constraints and model simulation of the December 26, 2004 Indian Ocean tsunami, *J. Waterw. Port Coastal Ocean Eng.*, in press.
- Guidoboni E., Comastri A., Traina G., 1994. Catalogue of ancient earthquakes in the Mediterranean area up to the 10th Century. ING-SGA, Rome-Bologna, Italy, 504.
- Hellenic Military Geographical Service (HMGS <http://web.gys.gr/>).

- Ioualalen, M., Pelletier B., Regnier M., Watts, Ph., 2006. Numerical modelling of the 26th November 1999 Vanuatu tsunam, J. Geophys. Res., 1111, C06030, doi: 10.1029/2005JC003249
- Ioualalen, M., Asavanant J., Shi F., Kirby J.T., Watts, Ph., 2007. Modeling the 26 December 2004 Indian Ocean tsunami: Case study of impact in Thailand, J. Geophys. Res., 112, C07024, doi: 10.1029/2006JC003850.
- Kennedy, A.B., Chen Q., Kirby J.T., Dalrymple, R.A., 2000. Boussinesq modelling of wave transformation, breaking, and run-up I: 1D, J. Wtrwy, Port, Coast, and Oc. Engrg., ASCE, 126 (1), 39-47.
- Leone F., Lavigne F., Paris R., Denain Jc., Vinet F., 2010. A spatial analysis of the December 26th, 2004 tsunami-induced damages: lessons learned for a better risk assessment integrating buildings vulnerability. Appl Geogr., 31, 363–375.
- Novikova T., Papadopoulos G.A., McCoy F.W., 2011. Modeling of Tsunami Generated by the Giant Late Bronze Age Eruption of Thera, South Aegean Sea, Greece. *Geophysical Journal International*, doi: 10.1111/j.1365-246X. 2011. 05062.x.
- Okada S. (1985), Surface displacement due to shear and tensile faults in a a half-space, Bull. Seismol. Soc. Am., 75, 1135-1154.
- Papadopoulos, G. A., 2011. A Seismic History of Crete: Earthquakes and Tsunamis, 2000 B.C. – A.D. 2010, Ocelotos Publ., Athens, 415 pp.
- Papadopoulos, G.A., Dermentzopoulos, Th., 1998. A Tsunami Risk Management Pilot Study in Heraklion, Crete, *Natural Hazards*, 18, 91–118
- Papadopoulos, G.A., Pavlides, B.S., 1992. The large 1956 earthquake in the south Aegean: Macroseismic field configuration, faulting, and neotectonics of Amorgos Island. Earth Planet. Sci. Lett. 113, 383–396.
- Papadopoulos G.A., Gràcia E., Urgeles R., Sallares V., Marco De Martini P., Pantosti D., González M., Yalciner A.C., Mascle J., Sakellariou D., Salamon A., Tinti S., Karastathis V., Fokaefs A., Camerlenghi A., Novikova T., Papageorgiou A., 2014. Historical and pre-historical tsunamis in the Mediterranean and its connected seas: Geological signatures, generation mechanisms and coastal IMPACTS, *Marine Geology*, 354, 81-109, <http://dx.doi.org/10.1016/j.margeo.2014.04.014>.
- Papathoma Thesis, 2003. Tsunami vulnerability assessment using a Geographical Information System with special reference to Greece, PhD Thesis, Voventry University, March 2003, pp. 289.
- Papathoma M., Dominey-Howes D., 2003. Tsunami vulnerability assessment and its implications for coastal hazard analysis and disaster management planning, Gulf of Corinth, Greece. Nat. Hazards Earth Syst. Sci., 3, 733-747.
- Papathoma M., Dominey-Howes D., Zong Y., Smith D., 2003. Assessing tsunami vulnerability, an example from Herakleio, Crete. Nat. Hazards Earth Syst. Sci., 3, 377-389.
- Perissoratis C., Papadopoulos G.A., 2000. Sediment instability and slumping in the southern Aegean Sea and the case history of the 1956 tsunami. *Marine Geology*, 161, 287-305.
- Scenarios for tsunami Hazard-induced Emergencies Management (SCHEMA) project (www.schemaproject.org) deliverable 2.1, 2007. www.schemaproject.org
- Scenarios for tsunami Hazard-induced Emergencies Management (SCHEMA) project (www.schemaproject.org) deliverable 4.2, 2007. www.schemaproject.org
- Walder J., Watts Ph., Sorensen O., Janssen K., 2005. Tsunamis generated by subaerial mass flows, J. Geophys. Res., 108, NB5, 1-19.
- Ward S., & Day C., 2008. Tsunami Balls: a granular approach to tsunami runup and inundation, *Communication in Computational Physics*, 3, 1, 222-249.

Watts, P., Waythomas, C., 2003. Theoretical analysis of tsunami generation by pyroclastic flows, *J. Geophys. Res.*, 108, B12, 1-19.

Watts P., Grilli S.T., Kirby, Fryer G.J., Tappin D.R., 2003. Landslide tsunami case studies using a Boussinesq model and a fully nonlinear tsunami generation model, *Nat. Hazards. and Earth Syst. Sci.*, 3(5), 391-402.

Wei G., Kirby J.T., 1995. Time-dependent numerical code for extended Boussinesq equations, *J. Wtrwy, Port, Coast, and Oc. Engrg.*, ASCE, 121 (5), 251-261.

Wei G., Kirby J.T., Grilli S.T., Subramanya R., 1995. A fully nonlinear Boussinesq model for free surface waves. Part 1: highly nonlinear unsteady waves, *J. Fluid Mech.*, 294, 71-92.

Valencia N., Gardi A., Gauraz A., Leone F., Guillande R., 2011. New tsunami damage functions developed in the framework of SCHEMA project: application to European-Mediterranean coasts, *Nat. Hazards Earth Syst. Sci.*, 11, 2835–2846.

3.6 Haydarpasa

3.6.1 Description of the site

Tsunami Vulnerability study using Multi Criteria Decision Making Analysis (MCDA) is applied to Yenikapi region of Istanbul. The complete study has been performed by Ms. Ceren Cankaya as the MSc thesis in METU Department of Geological Engineering (Cankaya, 2015). A research paper is at the submission stage (Cankaya et al., 2015). Therefore, only a brief summary is given in this deliverable which, however, is still quite useful for reasons of comparison of the MCDA methodology with the methodologies applied in other ASTARTE test-sites.

3.6.1.1 Description of the site: the Sea of Marmara and the Yenikapi Port Text

According to numerous studies (e.g. Yalciner et al., 2002; Altinok et al., 2003, 2011; Altinok, 2006), there is tsunami risk in the Sea of Marmara. One of the most powerful tsunamis affecting the Sea of Marmara, especially the city of Istanbul, occurred in 1509 (Yalciner et al., 2002). The maximum height of the tsunami run-up in coastal areas of Istanbul in 1509 has been reported to be 6 m. Tsunami inundation was observed in several coastal areas. The 1894 earthquake triggered also a tsunami wave with about 4.5 m run-up height (Altinok et al., 2011).

Following the destructive, lethal earthquake of 17 August 1999 measuring magnitude of 7.4 and causing a death toll of 18850 people, the so-called Izmit Bay tsunami was observed (Alpar and Yaltirak, 2000; Altinok et al., 2011). After this event the awareness as regards the potential tsunami risk in Marmara Sea increased among the population and the governmental bodies. This led the government to put more emphasis on tsunamis as a serious natural hazard along with earthquakes in Turkey's agenda of disaster management strategies. There have been several projects aimed at the identification of the tsunami generation mechanisms, their occurrences, modeling and hazard analysis, and risk assessment in the Marmara Sea region. One of those related to vulnerability was "Simulation and Vulnerability Analysis of Tsunamis Affecting the Istanbul Coasts" which was performed by OYO Int. Co. Japan, under the microzonation project granted by Istanbul Metropolitan Municipality-IMM (IMM- OYO Report, 2008).

Due to the economic importance of Istanbul, the city possess several commercial ports (Derince port, Haydarpasa port, Yenikapi port, Ambarli port). Among those Haydarpasa and Derince ports are used for cargo handling and passenger terminal, Yenikapi port is used for fishery and passenger terminal, while Ambarli port serves for cargo handling. In ASTARTE, Haydarpasa port is selected as one of the test-sites to perform tsunami hazard, vulnerability and risk analysis.

In this study a GIS-based tsunami vulnerability analysis method is developed and applied to Yenikapi port and environs which is situated in the Fatih district of Istanbul. Figure 3.6.1 shows the location of the Yenikapi region in the Marmara Sea. It should be also noted that according to historical documents this region has been attacked by the 1509 tsunami (Altinok et al., 2011). The tsunami numerical model NAMI DANCE is used for the simulation and assessment of tsunami inundation and tsunami interaction with the structures. The vulnerability analysis carried out is based on the Multicriteria Decision Making Analysis (MCDA) approach. The vulnerability parameters are classified into two groups: vulnerability parameters related to the location and vulnerability parameters related to the evacuation procedure. The parameters and their weights according to the MCDA have been given in Cankaya (2015). In locational vulnerability, the parameters are (a) metropolitan use, (b) geology, (c) elevation and (d) distance from the shoreline. On the other hand, the vulnerability due to evacuation considers (a) the distance to buildings, (b) the slope, (c) the distance to road network and (d) the distance within flat area.

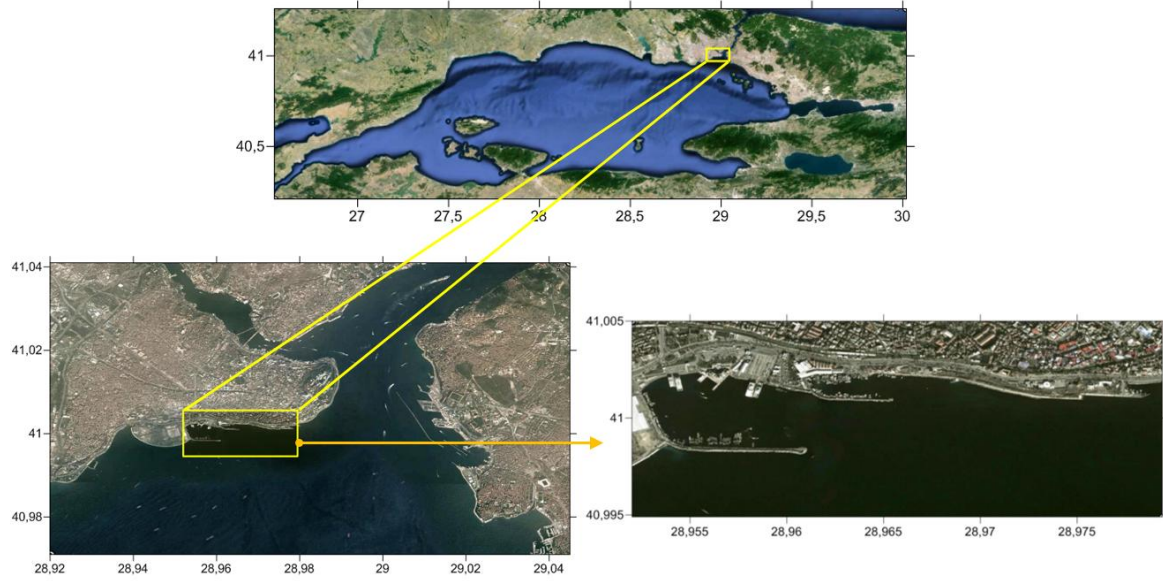


Figure 3.6.1. The study area: Yenikapi, Istanbul.

The level of tsunami hazard is determined from the plot of inundation (flow depth) which is one of the outputs of the simulation of selected critical tsunami scenarios related to the source (Figure 3.6.2) at Yalova region (east of Marmara). The tsunami numerical model NAMI DANCE (developed by Profs Andrey Zaytsev, Ahmet Yalciner, Anton Chernov, EfimPelinovsky and Andrey Kurkin) is used. Theinundation (flow depth) map of the source YAN, shown in Figure 3.6.2, is used in the current tsunami vulnerability analysis.

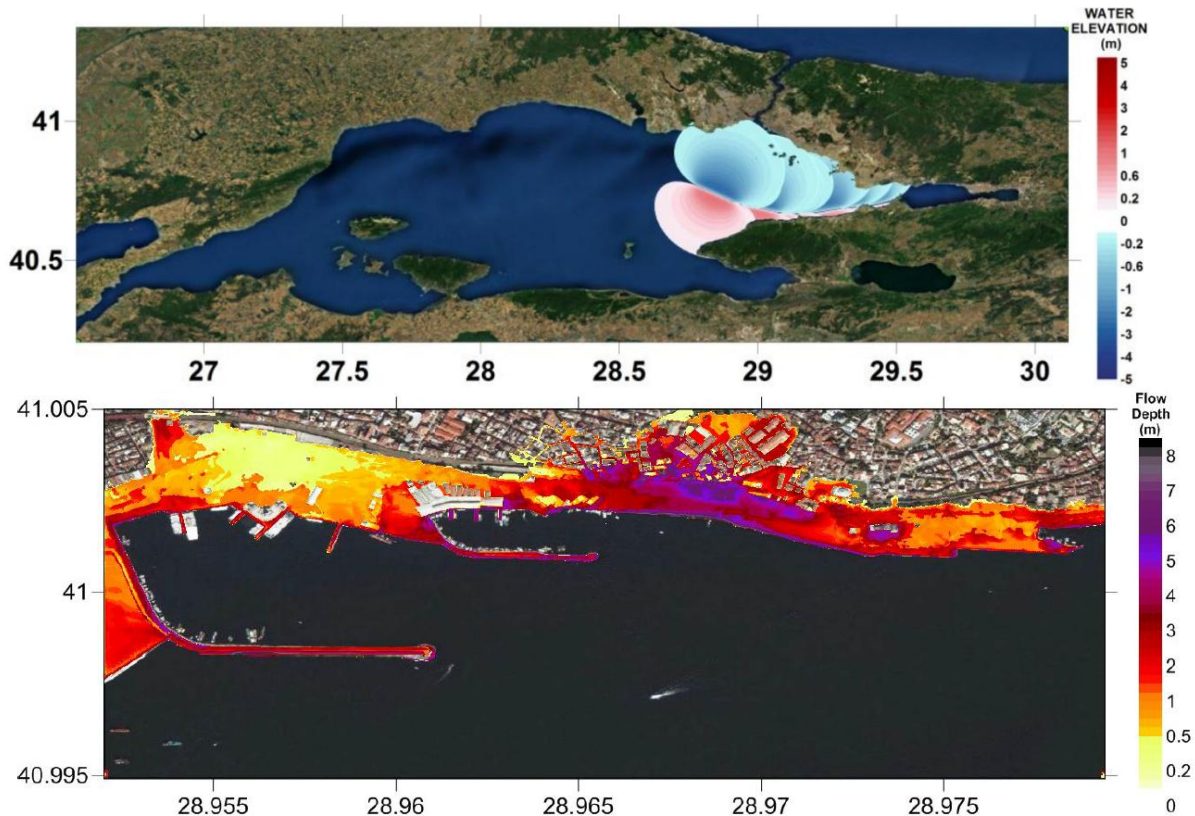


Figure 3.6.2. The tsunami source YAN (top) (Ayca, 2012) and the resulting inundation (flow depth) map (bottom) (Cankaya, 2015).

The resulting maps for locational and evacuation vulnerability is given in Figures 4.6.3 and 4.6.4, respectively. In these maps, the vulnerability increases with darker red color. These maps can be a valuable source of guidance not only for the determination of vulnerability of the individual locations

and planning of relevant evacuation in the region but also for the development of national tsunami guidelines.

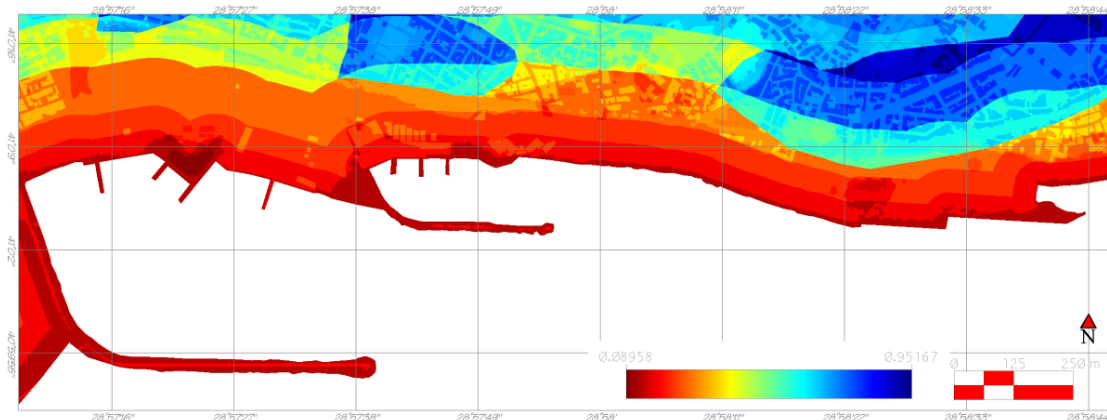


Figure 3.6.3. The final map of the locational vulnerability.

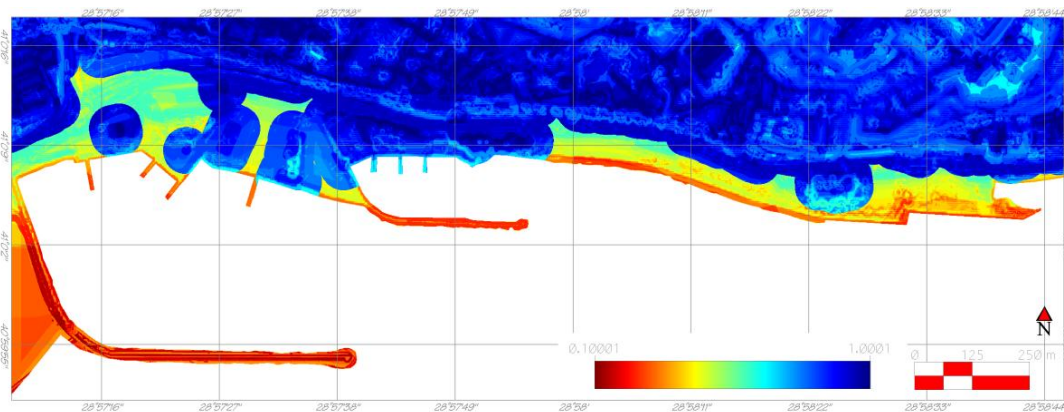


Figure 3.6.4. The final map of the evacuation vulnerability.

3.6.2 References

- Alpar, B., Yaltirak, C., 2000. Tectonic setting of the Marmara Sea. NATO Advanced Research Seminar, Integration of Earth Sciences on the 1999 Turkish and Greek Earthquakes and Needs for Future Cooperative Research, Abstracts, 14-17 May 2000. Istanbul, pp. 9-10.
- Altinok Y., Alpar B., Yaltirak C., 2003. Sarkoy-Murefte 1912 Earthquake's Tsunami, extension of the associated faulting in the Marmara Sea, Turkey. *Journal of Seismology* 7, 329-346.
- Altinok Y., 2006. *Turkiye ve Cevresinde Tarihsel Tsunamiler*. *Turkiye Muhendislik Haberleri*, 25-32.
- Altinok Y., Alpar B., Ozer N., Aykurt H., 2011. Revision of the tsunami catalogue affecting Turkish coasts and surrounding regions. *Natural Hazards and Earth System Science*, 11(2), 273–291.
- Ayca A., 2012. Development of A Web GIS-Based Tsunami Inundation Mapping Service; A Case Study For Marmara Sea Region. M.S. Thesis METU, Ankara, Turkey.
- Cankaya C., 2015. High Resolution Tsunami Vulnerability Assessment by GIS based Multi-Criteria Decision Analysis at Yenikapi, in Istanbul. M.S. Thesis METU, Ankara, Turkey.
- Cankaya C., Suzen L., Kolat C., Yalciner A. C., 2015. High Resolution Tsunami Vulnerability Assessment by GIS based Multi-Criteria Decision Analysis at Yenikapi, in Istanbul. (Manuscript in preparation)

IMM, O., 2008. Project report on simulation and vulnerability analysis of Tsunamis affecting the İstanbul Coasts. İstanbul: OYO Int. Co. (Japan) for İstanbul Metropolitan Municipality (IMM)

Yalciner A. C., Alpar B., Altinok Y., Ozbay I., Imamur, F., 2002. Tsunamis in The Sea of Marmara Historical Documents for The Past Models for The Future. *Marine Geology*, 190, 445–463.

4. Guidelines for tsunami vulnerability assessment in the NEAM region

For reasons explained below in the Conclusions section it is of interest to standardize and harmonize the several methods/models/approaches which are available for the assessment of the vulnerability of buildings and infrastructures to tsunamis in the North East Atlantic and the Mediterranean (NEAM) region. During the WP8 ASTARTE meeting of 17-18 February 2015 at NOA's premises in Athens, it was discussed that it is not only desirable but also absolutely realistic to elaborate a set of relevant recommendations. NOA being responsible of the Task 8.2 already started to organize a draft of recommendations. However, there is need for a wide discussion between ASTARTE partners before such recommendations will be concluded. In the Annual ASTARTE Meeting scheduled to take place in October 2015 in the Heraklion test-site it is expected to exchange ideas before the production by the end of the year of a final separate report/handbook containing recommendations for the assessment of the vulnerability of buildings and infrastructures to tsunamis in the NEAM region.

5. Conclusions

The tsunami history in the NEAM region clearly indicates that coastal communities of the region are vulnerable to tsunamis. However, the assessment of the vulnerability to tsunamis is a complicated procedure which depends on a variety of factors. In this document the vulnerability of buildings and infrastructures to tsunamis was examined in a number of test-sites selected within the ASTARTE project. A variety of models/methods were used to perform such an assessment. In some occasions more than one models were tested in the same test-site and the comparison of the results was discussed. However, other types of vulnerabilities were not examined at this stage, such as population or individuals vulnerabilities and their time/season dependence, indoor and outdoor vulnerabilities etc.

The fact that not a unique model/method was applied is due exactly to the many different factors that affect the assessment procedure. From the experience gained in the test-sites examined it comes out that such factors include: characterization of the tsunami sources (seismic, landslide, volcanic), selection of tsunami scenarios (e.g. realistic scenarios or worst case scenarios), tsunami simulation models used, resolution of the bathymetric and DEM data sets available, data regarding buildings and their classification according to their different types and construction materials. As regards the last, building data may come either from field inspection by the study team or from the official statistical surveys. However, official statistics provides either detailed data per building or data only per building block. In the last case it may be better to collect data from field inspection.

The variety of factors that are involved in a procedure for the assessment of tsunami vulnerability of buildings stresses the need for the production of relevant recommendations for the use by people (authorities, decision makers etc.) that would like to proceed with such an assessment for operational applications. As explained in the previous section the ASTARTE partners will work together under the lead of NOA for the production of a relevant handbook by the end of 2015.